Using Remote Sensing to assess the effect of Time of Day on the spatial and temporal variation of LST in Urban Areas

Thesis submitted for the degree of

Doctor of Philosophy at

The University of Leicester

By

Akram Abdulla

School of Geography, Geology and Environment

University of Leicester

2020

Abstract

This thesis seeks to add to the study of the relationship between land surface temperature (LST) and urban land cover by presenting a method to project Landsat LST data from the satellite overpass time (9:40 am) to a local peak of temperature (estimated to be around 1:15 pm locally), to investigate the impact of the time of image acquisition on modelling the spatial and temporal variations of LST. Additionally, it would also verify the effects of extreme temperature to reach more representative seasonal images.

The study uses remote sensing data extracted from Landsat 5 and 8 (30 m resolution) and the Spinning Enhanced Visible and Infrared Imager LST products (SEVIRI 3 km resolution), in addition to LST-based measurements collected from the ground. The study presented a method to convert Landsat images to be estimated during local peaks in LST with an accuracy of: standard error of 1.7°C and an R of 0.82 in comparison with actual ground-based measurements. This allowed an investigation of the effects of time of day on the spatial and temporal variation of LST, where it was found that this factor has clearly affected the relationship between LST and urban land cover. Similarly, the time of day has caused differences in estimating LST change over several years. It is also found that the extreme values of temperature can affect the trend of LST temporal variation, and which can be minimized by using the images in the form of the average of seasonal images for each year rather than images being used in a standalone manner. This study contributes to the improved study of LST by minimizing the uncertainty that can occur because of the angle of the sun and associated factors such as shadows, which has long been a controversial issue among researches due to the lack of appropriate satellite data.

Dedication

I dedicate this work to my parents, my wife, my children, my brothers, and my sisters.

Acknowledgements

I would like to express my sincere appreciation to my supervisors, Professor Kevin Tansey and Doctor Kirsten Barrett, for their unlimited fantastic support and the right guidance throughout the study years to complete this thesis. I would also like to acknowledge the panel, Professor Heiko Balzter and Doctor Jörg Kaduk, for their valuable feedback during their follow-up to the stages of the research. I acknowledge the support from the department of physics, University of Leicester, and I especially thank Professor John Remedios, Dr Mike Perry and Dr Darren Ghent for their help and valuable advices. Equally, I appreciate the help and encouragement of my colleagues at the department of geography and the centre for landscape and climate research (CLCR) as well as my friends. I also would thank all the staff at the School of Geography, Geology and the Environment and I especially mention the secretary, Charlotte Longley, who has always been very helpful and kind. Finally, I would like to conclude my acknowledgments by extending my thanks to all the officials of the University for providing this excellent environment for study.

Table of contents

List of figures

List of tables

Chaper 1. Introduction

This part of the research presents an overview of the existing knowledge of land surface temperature (LST) to provide readers with a reasonable background about the topic and set its importance in context. This begins with definition of the scientific area under study, the rationale for studying LST, earth surface heat budget, the relationship between the angle of solar radiation and LST, the impact of a changing LST on the environment, remote sensing and LST measurement and, finally, a description of the thesis structure.

1.1. Definition of Land Surface Temperature (LST)

The study of land surface temperature has become one of the contemporary environmental issues that has experienced a recent, and considerable, increase in scientific interest. In recent decades, many cities around the world have witnessed rapid developmental transitions, especially cities in developing countries, which have recently begun to achieve urban growth rates that are several times greater than those of cities of developed countries (López *et al*., 2001). Changes in land use, especially in urban areas, have contributed significantly to subsequent changes in the original characteristics of local environments, perhaps one of the most important of which is the increase in land surface temperature (LST) (Deng and Wu, 2013). Remote sensing can quantify the average surface temperature of the image pixel that, for succinctness, can be referred to as the land surface temperature (LST). LST has been described as being at least partially responsible for regulating the air temperature in the lower layer of the atmosphere, and it is the main factor in defining surface radiation and the weather (Weng, 2009). The LST is an important indicator that allows one to understand and interpret various other issues associated with environmental degradation, with some scholars accordingly describing it as the 'earth's skin temperature' (Weng *et al*., 2014). Other studies describe LST in cities as an 'artificial temperature' due to the impact of human activities that result in artificially induced increases in LST (Chakraborty *et al.*, 2015). Land surface temperature LST has been shown to be useful for agricultural applications, such as estimating the extent of frost damage in orange groves, and has become a key variable in monitoring the intensity and spread of UHIs (Peng *et al*., 2012). The sensitivity of LST to soil moisture and vegetation has been used as a sensitive means of detecting land cover changes, such as the tendency towards desertification (Sobrino and Raissouni, 2000). LST is applied to a number of ice-related studies such as mapping snow and its melt rate and the depth to which permafrost is thawing (Westermann *et al*., 2011). Additionally, the long-term climatology of accurate LST products could be used as an identifier of climate trends, as has been done with sea surface temperature (SST) climatologies (Veal *et al*., 2013).

Over land, LST is the primary driver of radiative heat loss into the atmosphere and the rate of evaporation, such that the LST-air temperature relationship plays a highly significant role in atmospheric convection currents (Bastiaanssen, *et al*., 1998). Furthermore, LST itself is heavily dependent on the absorption of incident energy by the surface and the rate at which that surface subsequently dissipates energy (Liang, *et al*., 1999). Therefore, precise observations of LST are required for a number of earth-system applications such as Numerical Weather Prediction (NWP), long-term climate models, and ecological/hydrological models (Ghent *et al*., 2011).

1.2. The Impact of Increase in Urban LST.

Due to a lack of proper planning in land use for sustainable development, rapid population growth has been a major cause of problems related to the ecosystem, especially with regard to LST and ambient air temperature.

1.2.1. Increased Energy Consumption

An increase in LST can result in serious negative environmental impacts, not only on urban environments but also on the ecosystem in a given area (Arrau and Pena, 2010), as it is known that higher summertime temperatures in cities often result in the need for increased energy consumption due to a higher demand for air conditioning. This, in turn, often requires increased use of fossil fuel-powered plants, increasing emissions of greenhouse gases such as carbon dioxide (CO_2) into the atmosphere. In addition, urban electricity demands are known to be rising (Santana, 2007; EPA, 2009).

1.2.2. Air Quality

The increase in energy demand associated with elevated summer temperatures also often results in higher levels of air pollution as fossil fuel-powered plants (which currently provide about 66% of global electricity) emit nitrogen oxides (NO_x), mercury (Hg), carbon monoxide (CO), sulphur dioxide (SO_2), and particulate matter (PM) into the atmosphere. These pollutants are known to have a detrimental effect on air quality, contributing to acid rain and as well as global warming (EPA, 2009a; WWF, 2010).

1.2.3. Human Health

Since UHIs tend to exacerbate the impact of heat waves, heat-related fatalities are another consequence of increased urban temperatures. High night-time temperatures during heat waves are associated with increased mortality, even more so than high daytime temperatures since there is no break from the heat, giving people no significant relief at any time (Kalkstein, 1991). In addition to heat-related mortality, increased urban temperatures may also contribute to heat cramps, exhaustion, non-fatal heat stroke, and general discomfort (EPA, 2009).

Urbanisation is considered one of the key reasons for the relative difference in the temperature of cities compared to their surrounding areas in LST, the so-called urban heat island (UHI) phenomenon (Weng and Fu, 2014). There are different categories of UHIs, which are as follows.

1.2.4. Surface Urban Heat Island (SUHI):

A SUHI is defined by the higher temperatures of urban surfaces compared to their (rural) surrounding surfaces. Studies of SUHI generally use LST images that are obtained from airborne and satellite thermal infrared remote sensing (Srivanit and Hokao, 2012). In contrast with Atmospheric Urban Heat Islands (AUHIs), SUHIs are at their greatest during the day when solar inputs are at their greatest, and lowest at night when long-wave losses occur (Roth *et al*, 1989). As a result of the variation in the sun's intensity, land cover and weather, the intensity of SUHIs changes with the seasons and is typically, and somewhat unsurprisingly, greatest in the summer (EPA, 2009)

1.2.5. Canopy Layer Urban Heat Island (CLUHI):

A CLUHI is defined by the higher the air temperature of the urban canopy layer compared to its (rural) surroundings. CLUHI refers to the air near the surface, which expands to approximately the height of buildings (Voogt, 2004). Patterns of air temperature inside the city are strongly correlated with the latter's development (Roth *et al.*, 1989).

1.2.6. Boundary Layer Urban Heat Island (BLUHI):

A BLUHI is defined by a higher air temperature of the urban boundary layer compared to its (rural) surroundings. This is another type of AUHI and is located above the CLUHI. During the day, its thickness can reach 1 km or more, while it shrinks to only 100 m or less during the night (Voogt, 2004). This type of UHI is potentially more visible at night. It can be measured and observed using specific remote sensing platforms such as long towers, radiosonde, balloons, and aircraft (Voogt and Oke, 2003).

1.2.7. Surface Urban Cool Island (SUCI):

In some cases, and perhaps somewhat counterintuitively, LST tends to be lower in cites than their surroundings due to the presence of a dry desert environment, which can make urban areas somewhat cool relative to their surroundings; indeed, the same applies when comparing the LST for a body of water to its surroundings, such as oases in desert areas (Rasul *et al.*, 2015)

1.3. Earth Surface Heat Budget

The exchange of heat energy with the earth is important to our understanding of its short-term effects on weather and climate (NASA, 2009). The sun provides virtually all of the energy received by the earth, where it drives biophysical and geophysical processes such as photosynthesis, evaporation and heat exchange between the earth's surface and the atmosphere. This exchange of energy is widely known as the surface energy balance (Figure 1-1).

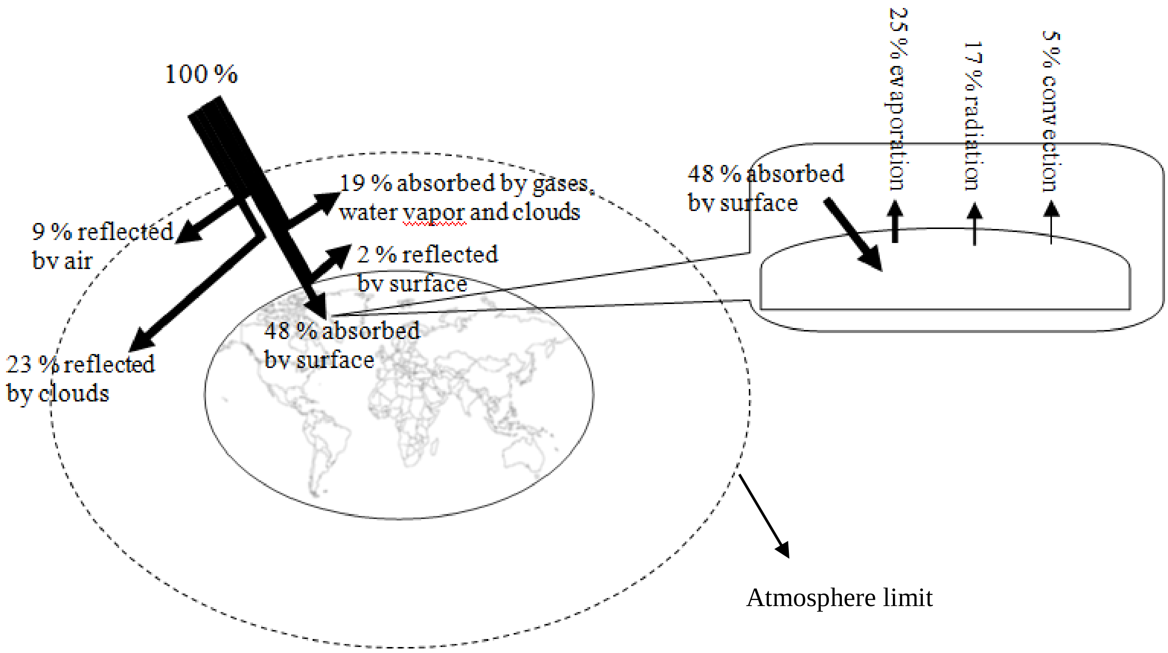

Figure 1-1: The earth's heat budget and how incident energy is processed by the earth's surface (Trenberth et al., 2009).

In general, approximately 48% of the shortwave energy incoming from space passes through the atmosphere to reach the earth's surface as incident energy. When this radiant energy is incident on some given body (or bodies), then three different scenarios can occur: reflection, absorption, and transmission, as depending on the properties of the surface(s) in question. At the same time, the earth's surface dissipates the absorbed energy back into the atmosphere through three principle mechanisms: convection, evaporation, and long-wave radiation, where all of these processes vary depending on the properties of the surfaces on the earth, which are themselves determined by the bodies' constituents. The physical properties of objects are therefore responsible for determining their behaviour (reflectivity, transmissivity, absorptivity, and emissivity), which in turn control the spatial distribution of the energy exchange process and, accordingly, the spatial variation of the LST.

1.3.1. Reflectivity

Reflectivity is the ratio of reflected radiation to incident radiation, which takes values as per the following expression.

$0 \leq \text{reflectivity} \leq 1$.

1.3.2. Transmissivity

Transmissivity is defined as the transparency of an object, where radiation can also be transmitted by bodies that are transparent; only an opaque material has a surface response that shows no transmission such that it takes the following values:

$0 \leq \text{transmissivity} \leq 1$

1.3.3. Absorptivity

The part of the incoming radiation absorbed by a surface defines that object's absorptivity, and is mathematically the ratio of absorbed energy to incident radiation, and thus takes the following values:

$0 \leq \text{absorptivity} \leq 1$

1.3.4. Emissivity

It is defined as the amount of the energy radiated from an object's surface to that radiated from a black body (a perfect emitter), and thus takes values defined by:

$0 \leq \text{emissivity} \leq 1$

1.4. The Electromagnetic Spectrum

The electromagnetic spectrum (EM) can be categorized into different wavelength regions known as ‘optical’ and ‘microwave’ (amongst others). The optical remote sensing detects waves reflected and emitted by surfaces, which ranges between 0.4 and 14 mm. Microwave remote sensing targets much longer wavelengths, between 1 mm and 1 m, as per Figure (1-3) (Woody *et al.*, 2003).

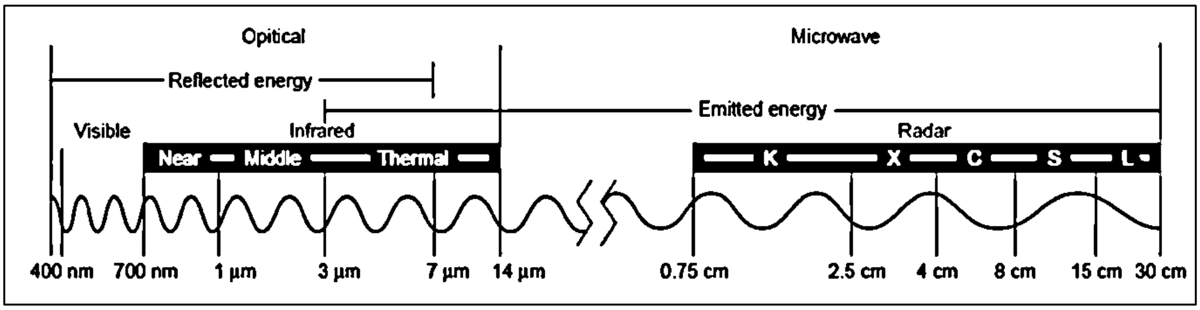

Figure 1-3: Diagram showing the electromagnetic spectrum (Woody et al., 2003).

The electromagnetic spectrum (EM) describes the complete set of wavelengths of light, which commences from the shortest wavelengths (gamma rays and X-rays) to the longest wavelengths that are used in telecommunications (microwaves). There is a series of terms that are commonly used in remote sensing to label the various spectral regions (Chuvieco and Huete, 2010).

Normally, the names and spectral ranges are as follows:

The visible radiation (VIS) region ranges approximately from 0.4 to 0.7 μm. This spectral region corresponds to the small fraction of electromagnetic radiation that can be detected by the human eye. It includes the three main colours, blue from 0.4 to 0.5 μm, green from 0.5 to 0.6 μm and red from 0.6 to 0.7 μm (Chuvieco and Huete, 2010).

The near infrared (NIR) region ranges approximately from 0.7 to 1.2 μm. This part of the spectrum is just beyond the region apparent to the human eye, but its ability to discriminate green vegetation results in it being of spatial interest. In this region, healthy vegetation has a high reflectance that decreases with plant-related disease and its associated damage (Tempfli *et al.*, 2009).

The mid-infrared (MIR) region ranges approximately from 1.2 to 8 μm. The MIR is situated between the NIR and thermal infrared regions. The range between 1.2 to 3 μm is referred to as the shortwave infrared (SWIR) region. The region from 1.3 to 2.5 μm is mainly useful for estimating soil and vegetation moisture content, while the 3 to 5 μm range is useful for perceiving high-temperature sources (Tempfli *et al*., 2009).

The thermal infrared (TIR) region typically ranges from 8 to 14 μm. This region characterizes the energy emitted from the earth's surface, which is useful when mapping surface temperatures. The peak wavelength of thermal emission from the land surface at 300 K is situated at around 10 μm. Indeed, the human body releases 'heat energy' with a maximum at $\lambda \approx 10$ μm. The thermal region is useful in the detection of vegetation stress and clouds, and in the assessment of environmental contamination (Tempfli *et al,* 2009; Chuvieco and Huete, 2010).

The microwave region (> 1 mm) is a relatively long wavelength region which can passes cloud cover. It is useful in the analyses of soil moisture and surface roughness (Chuvieco and Huete, 2010).

1.5. Satellite Observations of LST

Remote sensing refers to the detection of different electromagnetic radiations from using different platforms such as aircraft or satellites, as per Figure (1-4) (Gibson and Power, 2000). The advantages of using remote sensing are that it is possible to cover large areas in relatively little time, and of course that it is relatively cheap compared to field measurements (Song *et al*., 2002). Recently, the employment of multispectral image data to the detection and monitoring of change is an effective and powerful method for the detection and analysis of such changes (Dewidar, 2004).

Satellites offer a convenient platform from which to observe LST consistently and regularly over large regions. Over the last few decades, satellite observations of LST have become increasingly prominent. These developments were largely driven by the success of satellite-retrieved products.

To meet end-user requirements, a number of space-borne sensors have been developed that allow for observations of LST (and indeed SST) as their primary objective. These instruments make use of top-of-atmosphere (TOA) radiances in the infrared (IR) or microwave (MW) bands of the electromagnetic (EM) spectrum. The basic principal is to correct TOA radiances, or Planck function equivalent Brightness Temperatures (BTs), for the effects of the atmosphere and the non-unity of the earth's surface's emissivity such that an estimate of LST (or SST) can be made (Dash *et al*., 2002).

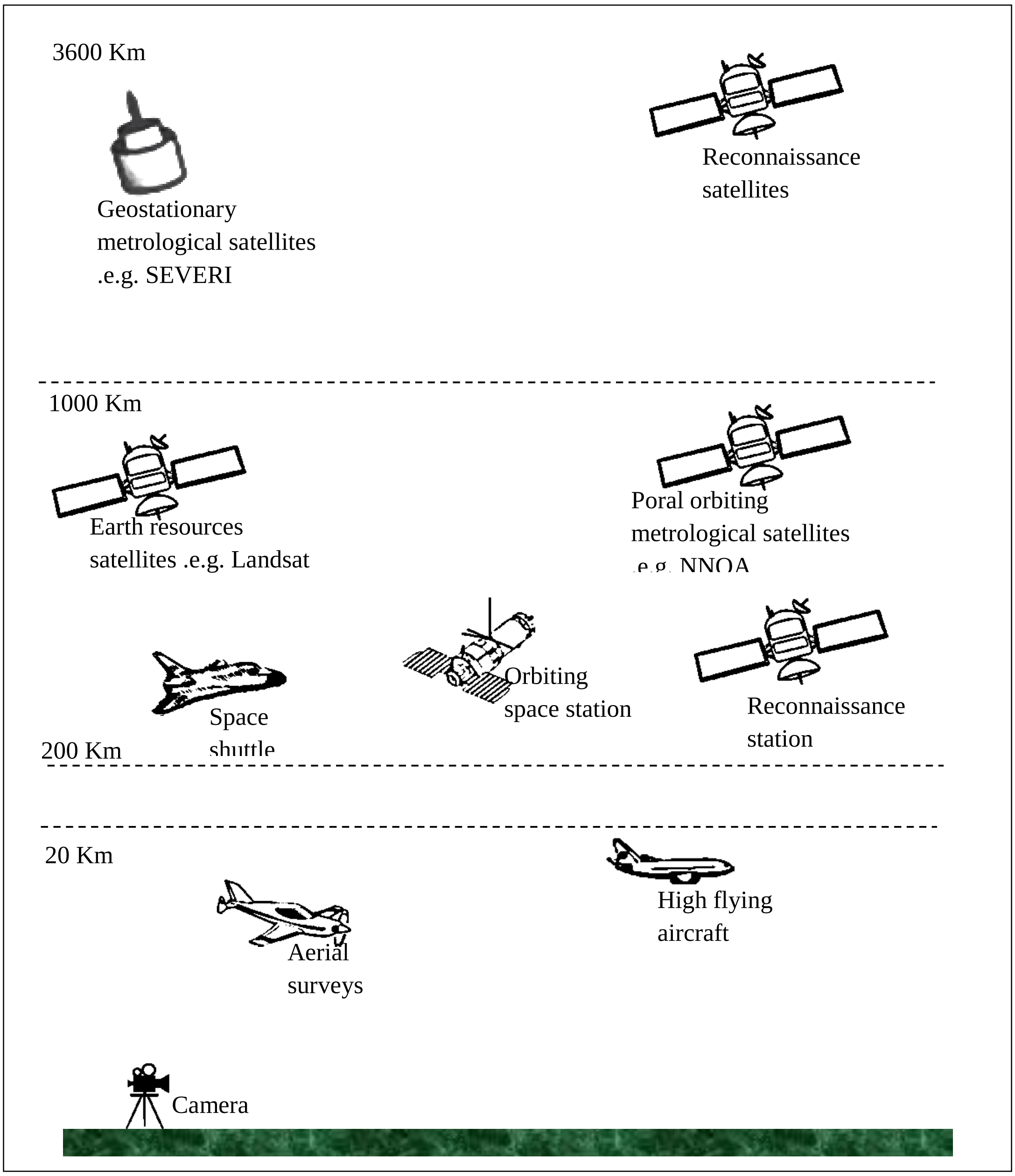

Figure 1-4: The different remote sensing platforms and the various heights at which they operate (modified from Gibson and Power, 2000).

IR sensors are generally preferred to MW sensors as the earth emits radiance peaks in the IR, as per Figure 1.1. In addition, IR signal is more sensitive to changes in the earth's temperature. Both of these features are a result of the Planck function component of the RT process. As a result, MW sensors struggle to match the accuracy achievable by IR sensors (Dash *et al*., 2002). Furthermore, MW sensors have a comparatively poorer spatial resolution than IR sensors, i.e., 25-50 km for MW sensors and 60 m – 5 km for IR sensors (Noyes, 2005). One advantage of MW sensors is that, unlike IR signal, MW signal penetrates clouds and hence MW sensors provide a more continuous LST dataset.

There are a number of satellite instruments which provide IR datasets suitable for LST retrieval. In a broader sense, these instruments can be split into two types based on their satellite platform, namely polar orbiting platforms and geostationary platforms.

Instruments on board polar orbiting satellites, which are generally sun-synchronous, give vast amounts of global data specific to the overpass time of the satellite such as:

Landsat: since the early 1970s, Landsat has continuously and consistently archived images of the earth. The Landsat programme has collected spectral information from Earth, creating a historical archive that gives scientist the ability to assess changes in the earth's landscape. Landsat sensors record reflected and emitted energy from the earth for various wavelengths of the electromagnetic spectrum. The electromagnetic spectrum includes all forms of radiated energy, from tiny gamma rays and X-rays all the way to huge radio waves, whilst Landsat sensors record blue, green, and red light in the visible spectrum as well as wavelengths in the near-infrared, mid-infrared, and thermal-infrared at a resolution of 30 m. Landsat 4 and 5 carried both the Multispectral Scanner (MSS) and Thematic Mapper (TM) instruments. Landsat 7 uses the Enhanced Thematic Mapper (ETM+) scanner. Landsat 8 uses two instruments, the Operational Land Imager (OLI) for optical bands and the Thermal Infrared Sensor (TIRS) for thermal bands, the satellites travelling on the descending (daytime) node from north to south cross the equator at 10:00 am ± 30 minutes mean local time on each pass. To provide maximum illumination, they cross every point on earth once every 16 days (http://www.usgs.gov/landsat).

The Advanced Very High Resolution Radiometer (AVHRR): AVHRR uses the upper surfaces of clouds or the surfaces of water bodies to remotely monitor the surface of the earth with a four- or five-channel scanner, sensing in the visible, near-infrared, and thermal infrared regions of the electromagnetic spectrum. This sensor is run by the National Oceanic and Atmospheric Administration's (NOAA's) Polar Orbiting Environmental Satellites (POES). There are three variants of this satellite, which were launched between 1978 and 1998. The highest ground resolution that can be obtained from the current AVHRR instruments is 1.1 km. The AVHRR's orbit allows two views per day for any point on the earth, using two AVHRR satellites, one with a morning/evening overpass and one with an afternoon/night-time overpass, with a view that is obtained approximately every six hours (AVHRR Level 1b Product Guide 2011).

The Moderate Resolution Imaging Spectroradiometer (MODIS) is one of the principal instruments aboard the Terra (originally known as EOS AM-1) and Aqua (originally known as EOS PM-1) satellites. Terra's orbit around the earth is timed so that it passes from north to south across the equator in the morning, while Aqua passes south to north over the equator in the afternoon. Terra MODIS and Aqua MODIS thus image the entire earth's surface every 1 to 2 days, acquiring data across 36 spectral bands with spatial resolutions between 250 m for the shortwave to 1000 m for the longwave (250 m for bands 1-2, 500 m for bands 3-7, and 1000 m for bands 8-36) (http://www.modis.gsfc.nasa.gov).

Advanced Spaceborne Thermal Emission and Reflection Radiometer (ASTER) imagery has been available since 2000 from the NASA Terra satellite. This sensor is a joint venture by NASA and the Japanese Ministry of Economy, Trade, and Industry (METI). ASTER covers a wide spectral region with 14 bands ranging across the visible to the thermal infrared with high spatial, spectral, and radiometric resolution (visible and infrared 15 to 30 m, thermal imagery 90 m). The orbit is sun-synchronous with a local time of 10:30 am and with a recurrent cycle of 16 days (ASTER User Handbook).

The Advanced Along-Track Scanning Radiometer (AATSR)

AATSR was one of the instruments on the European Space Agency's (ESA's) environmental satellite, ENVISAT (ESA, 2007). AATSR provided global TOA-BTs which could be used for LST and SST estimation with a spatial resolution of 1 km corresponding to a local overpass time of 10:00/22:00. Furthermore, AATSR provided unmatched levels of radiometric precision (< 0.1 K) such that AATSR measurements have provided SST datasets with accuracies of around $\pm$ 0.1 K (Veal *et al.*, 2013). AATSR makes observations at two specific local times (10:00 and 22:00) and at equatorial latitudes may observe a location as infrequently as once every three days, or worse in the instance of pixel contamination, such as in the instance of cloud contamination or channel saturation (ESA, 2007). This infrequent snapshot-type data is of only limited use, and which generally requires a sub-day temporal resolution at the threshold level.

The Spinning Enhanced Visible Infrared Imager (SEVIRI) on board the geostationary Meteosat Second Generation (MSG) satellites. These sensors can provide vast amounts of data, throughout the day and night. For the fixed earth image it observes SEVIRI provides

3712×3712 pixel images encompassing the earth's disk visible from the MSG geostationary position at 0^0 longitude every 15 minutes, hence it captures the diurnal cycle of LST. However, the disk image only covers ~40% of the earth's surface with a sampling distance 3.1 km (9 km^2) at nadir, which degrades to 12 km (40-140 km^2) at the rim of the observable disk (Merchant *et al*., 2009)

1.6. The Approach used to Extract LST from Satellite Data

Remote sensing can quantify the average surface temperature of the pixel that, for succinctness, can be referred to as the land surface temperature (LST). Table (1-1) gives an illustration of typical infrared sensors. There are three main LST retrieval methods: the single-channel algorithm, the split-window algorithm, and the multichannel algorithm.

1.6.1. The Single-Channel Algorithm

A single-window algorithm was proposed by Qin *et al.* (2001) to retrieve the LST from a TM image. The upward and downward radiance was expressed in an approximate manner by introducing the average atmospheric temperature. From the linear approximation of the Planck function, it is possible to calculate this at room temperature assuming that the average temperature of the atmospheric upward radiance and downward radiance are equal (Liang *et al.*, 2012)

1.6.2. Generalised Single-Channel Algorithms

A generalised single-channel algorithm was proposed by Jiménez-Muñoz and Sobrino (2003). The advantage of this approach is it can be used with any thermal infrared data to retrieve the LST.

Table 1-1: Different satellite sensors with the ideal algorithm for estimating LST (Rasul et al, 2015).

Satellite		**Typical Algorithm**
Landsat	8	Split-window algorithm
	7	Split-window algorithm
	4-5	Split-window algorithm
AVHRR/NOAA		Split-window algorithm TISI algorithm
MODIS/Aqua;Terra		Split-window algorithm Day/night algorithm
ASTER/Aqua		TES algorithm
AATSR/ENVISAT		Split-window algorithm
SLSTR/Sentinel-3		Split-window algorithm
ABI/GOES-R		Split-window algorithm
SEVIRI/MSG		Split-window algorithm
IRMSS/CBRES-1		Single-channel algorithm
MERSI/FY-3		Single-channel algorithm
IRMSS/HJ-1B		Multi-channel algorithm
S-VISSR/FY-2		Split-window algorithm
VIRR/FY-3		Split-window algorithm TISI algorithm

1.6.3. Split-Window Algorithms

The split-window algorithm was first proposed by McMillin (1975) for estimating sea surface temperature. The influence of the atmosphere is removed through the combination of brightness temperature from two channels (McMillin, 1975).

1.6.4. Multichannel Algorithms

Multichannel algorithms can estimate LST and LSE from sensors with multiple thermal infrared channels such as MODIS, ASTER, AVHRR and Landsat 8. These approach algorithms are capable of retrieving LSE and LST concurrently.

1.6.5. Temperature-Independent Spectral Index Method

Temperature-independent spectral indices (TISI), as defined by Becker, can be used to retrieve LST and LSE from the day and night data from channels 3, 4, 5 of NOAA AVHRR Li (Becker and Li, 1990).

1.6.6. MODIS Day/Night Algorithm

A physical algorithm was proposed by Wan and Li (1997) to retrieve LST and LSE from MODIS day and night data. Based on day/night observations of the seven infrared MODIS channels, in order to gain the solutions for land-surface and atmospheric parameters, 14 equations are created from which LST and LSE can be ultimately derived. Geometric corrections are necessary to reference the two scenes in the day and night observations (Liang *et al.*, 2012).

1.6.7. Integrated Retrieval Algorithm

An integrated retrieval or the two-step retrieval algorithm was proposed by Ma *et al.* (2000) for the MODIS airborne simulator (MAS), and was then applied to MODIS data (Ma *et al.*, 2002). In the first step, the values of various parameters are derived using a regression method; in the second step, the initial values of the above are adjusted using Tikhonov's regularised method (Hansen, 1998).

Landsat and SEVIRI products, in addition to ground-based measurements are the remotely sensed data used in this study to prepare the images that are required for the analysis and presenting the results.

LST has long been a topic of interest among scholars. Although remote sensing techniques have facilitated the study of LST, the fact that high spatial resolution thermal data is only normally acquired at a specific time of the morning such as the data provided by Landsat. This may in turn affect the accuracy in estimating the variation in the spatial domain of LST,

1.7. The Main Aim of the Study

This study aims to find a method to covert Landsat LST images to be estimated during a local peak of temperature rather than being in the morning, which would improve the investigation of the relationship between LST and urban land cover by minimizing uncertainties that can be caused by shadow. This can be shown in detail in terms of the following objectives.

1.8. Objectives

1. Using SEVIRI LST products and properties of pixels to convert Landsat LST data from being representative of morning (satellite overpass time) to a local peak of the temperature.
2. Apply a comparative study of the effect of urban land cover on the variation of LST between morning time and during a local peak of temperature to investigate the role of time of day in terms of its influence on this relationship.
3. To improve the representation of the data when studying changes in LST over the years (multi-temporal images).
4. To investigate how the temporal variation in LST can be affected by time of day

1.9. Thesis Structure

This thesis consists of seven chapters. The chapters can be generally categorised into five main parts. The first part includes Chapters 1 to 3 which give appropriate context and background information to the study. The second part focusses on the main chapters of the thesis which include the data analyses and present the results. The third part provides a discussion and conclusions, as shown below.

- Background which includes:
  Introduction, Literature review and the study area chapters
- Chapter 4- Converting Landsat LST data from morning to a local peak of the temperature (9:40 am to 1: 15 pm)
- Chapter 5- Assessing the effect of the time of day on the spatial variation of LST
- Chapter 6- Assessment and enhancement of analysing the temporal variation of LST over a time series

- Chapter 7- Discussion and conclusions

Chapter 1: presents general information about land surface temperature (LST) and describes the thesis structure as an introduction to the research, and includes the definition of LST, the rationale for studying LST, earth surface heat budget, the relationship between the angle of solar radiation and LST, the impact of LST change on the environment, remote sensing and LST measurement, and the thesis structure.

Chapter 2: presents a literature review of LST, which discusses the findings of previous studies in this field as an initial step to act as a basis or starting point for this research, which can contribute to improving or addressing certain aspects of these studies. The chapter concludes by describing the current gaps in knowledge in the literature, and the objectives and research questions of the study.

Chapter 3: defines the geographical features of the study area including the location, topography, soil type, and climatic elements of the city including temperature, air pressure, wind, relative humidity, cloud cover, demography, and population.

Chapter 4: improves Landsat LST measurement time using SEVIRI data. This chapter presents a technique which can be used to convert LST data derived from Landsat from morning time (Landsat overpass time) to during the zenith (peak temperature) using a combination of ground measurements and SEVIRI data.

Chapter 5: investigates how the relationship between LST and urban land cover can be affected by the time of day. By obtaining an estimate of LST data at zenith for Landsat data with a resolution of 30 m as shown in chapter 4, this part of the study investigates whether the relationship between LST and urban land cover is influenced between the morning and at zenith, and how significant this is through the difference in the relationship between these two periods.

Chapter 6: improves the analyses of the comparisons of the multitemporal LST images. This chapter seeks to reduce the probability of monthly and daily thermal extremes when analysing trends in LST over a number of years.

Chapter 7: this final section of the study presents a summary of and conclusions for the results found in this study.

Chaper 2.　Literature review

2.1. Introduction

Cities are environments where most of the landscape has been replaced with anthropogenic elements which can reflect a picture of the extent of the impact of human activities on the ecological balance. Previously, urban areas differed from the surroundings and countryside due to various human-related characteristics, such as population density, human activities, and land use patterns. However, recently some differences in natural features have also been constructed in many cities as a result of urbanisation.

In recent years, scientists have begun to witness noticeable changes in worldwide temperatures as a result of various human activities, which are increasing rapidly (Jiang and Tian, 2010). Until the beginning of the nineteenth century, urban growth was characterised by gradual changes and simple global transformations, both in terms of population growth, or the development of the means of production, and the consumption of raw materials (Seto, *et al*, 2012). However, compared with the past few decades, this picture has dramatically changed to the point where many countries in the world have started to witness excessive population growth, particularly in urban areas. This has resulted in increased pressure on the land use and the weakened ability of the environment to accommodate these developments (Zhang *et al.*, 2013). This increase in population has also resulted in widespread changes in patterns of land use, where many existing cities have been extended and many villages have turned into cities as a result of the phenomenon of urbanisation. Studies have indicated that the urban population at the beginning of the twentieth century was only around 10% of the total world population. Now, at the beginning of the twenty-first century, the urban population represents more than the half of the world’s population, and because of this this century has been described as a century of urbanisation (Zhou, *et al*, 2011). In this urbanised world, the urban land surface temperature has started to gradually rise, mainly as a result of urbanisation processes. According to Dewan and Yamaguchi (2009), urban zones are the biggest source of factors affecting ecological balance, and indeed are simultaneously the most affected by it. The constant urban consumption of natural resources and the continuing changing of the natural features of the Earth’s surface have resulted in cities’ environmental conditions differing from the surrounding areas, especially in terms of the temperature As a product of the energy exchange process carried out by surfaces, which can be appeared more affected in light of rapid urban growth in the absence of good urban planning, as is the case in many cities of the developing world. Therefore, the earth surface need to be monitored frequently to detect the extent of the impact of land cover changes on the environmental elements.

2.2. Relationship between LST and Land Cover

In recent decades, many cities around the world have experienced dramatic urban growth, especially in the cities of developing countries which have recently been developing several times faster than cities in developed countries (López *et al.*, 2001). As a result of land use changes, which are more concentrated in urban areas, LST has become increasingly high, whereby it has been estimated that the average global LST rose by about 0.8ºC between 1950 and 1993 (Jones *et al.*, 1999). The simultaneous removal of natural land cover and the introduction of urban materials changed the surface energy balance, with a consequent increase in heat flux (Lo *et al.*, 2010). This is consistent with Kalnay and Cai (2003), who concluded that the land surface temperature in the USA between 1980 and 1990 increased by 0.31°C for urban sites compared to only 0.13°C in more rural areas. Changing the absorption function of the land surfaces and decreasing its reflectivity as a result of urban expansion can led to different effects such as less sunlight being reflected into space, which has an effect on the global climate, and regional atmospheric conditions can occur, creating so-called local climate (heat and cool islands) (Brian *et al*, 2005). Land cover changes are a major concern in many countries, regardless of whether in developed or developing countries. The rapid change in urban land cover is mainly the result of economic development, population growth and urbanization (Fan *et al*, 2007). In some countries, accelerated economic development and a rapidly increasing population has caused, or requires, abrupt changes in land cover. Urban sprawl, expressing its stresses on the environment has, of late, been witnessed in developing countries in particular (Kumar *et al*, 2009).

Peng (2012) states that from a worldwide report of 419 cities with more than a million residents, the increase of urban temperature compared with the surroundings has become increasingly evident with an average of about 2.3°C in North America, 2.0°C in Europe, and 0.9°C in Africa. This illustrates how cities of the world are becoming sources for generating heat, which in turn exacerbates global warming. Which is supported by Kalnay and Cai (2003), who has observed that the land surface temperature in some cities in the USA over the ten years between 1980 and 1990 increased significantly compared to the rural areas.

Several studies confirmed that areas that are covered by natural landscapes have not experienced an increase in LST over time, unlike those subjected to land cover changes resulting from anthropogenic activities. Oke (1982), cited by Weng *et al.*, (2004), noted that the greatest levels of latent heat exchange are found where there is greater vegetation cover, while the sensible heat exchange is increasingly active with lower vegetation density as in built-up areas. When the majority of the surface cover within a certain area is more homogenized, the LST values will become less spatially varied due to the similarity of land surface behaviour for processing the incoming and outgoing heat energy (Xiao *et al.*, 2007).

According to Weng and Lu (2008), urbanization has resulted in an adverse relationship between impervious and vegetation regions, and because of LST correlations with both impervious and vegetation coverage, new LST patterns have been created. Xiong *et al.* (2012) concluded that the highest temperatures in Guangzhou, China were positively associated with built-up areas, whereby the hot spots or UHI distributions mainly followed the expansion of built-up areas during the study period. In the same context, city temperatures were generally higher than in the suburbs, which promotes the role of urban vegetation coverage as to whether trees or grasses can be used to mitigate the city's temperature in order to maintain temperatures at around those of the local environment. According to Wu *et al.* (2014), the variation in LST in cities depends on the distribution of land use patterns, which might explain the increase in LST in the direction of suburbs to city centres; however, this is not in keeping with the findings of Feyisa *et al.* (2016), who indicated that there is no considerable difference in LST between Addis Ababa city, the capital of Ethiopia, and its surrounding areas across the study years, as per Figure (2-1), where most of the suburbs of the city have been almost barren soil for long seasons, taking on a similar thermal behaviour between the urban and the surrounding land cover, which shows the importance of vegetation in minimizing excessive increases in LST. As Maimaitiyiming *et al.* (2014) claimed, even the planting of trees on the edges of roads in cities would have a role in reducing the rise of local LSTs. This was also found by Chakraborty, Kant and Mitra (2015), in that the highest LSTs in the city of Delhi were recorded over its barren land area, industrial, and built-up areas, respectively, as well as no clear temporal changes being shown between the years 2000 and 2010.

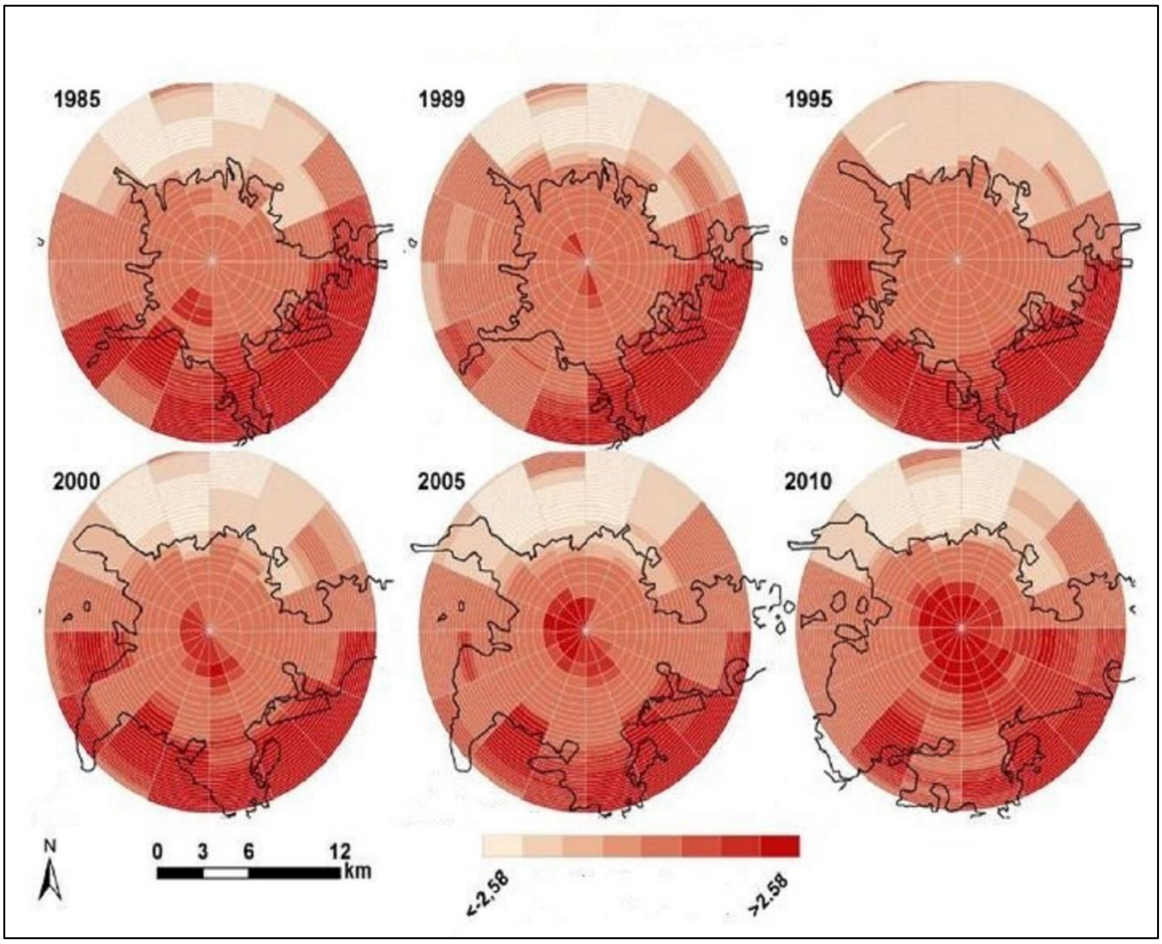

Figure 2-1: The spatial variation of land surface temperature intensity between the city of Addis Ababa and its surroundings during different years between 1985 and 2010 (Feyisa et al., 2016).

In other cities where the land cover is more diverse, the variation of LST can be effected significantly, with the difference reaching about 35°C in some tropical dry regions (for example in Tehran, Iran), as water bodies represented the lowest temperatures, while the highest appeared above barren surfaces (Bokaie *et al.*, 2016). In contrast, when applying this variation in different areas which are more moderate and abundant in rainfall and vegetation cover, it was revealed that the variation in LST was much lower and did not exceed 13°C among the different land use patterns (Rotem-Mindali *et al.*, 2015). These indicators could lead to one major factor behind the effects (different land use) on LST, which is the evaporation factor. It was found that the impact of this factor on reducing air temperature can be as much as 5°C in some dry regions (Bokaie *et al.*, 2016). However, this is not considered a fixed value, as it is possible that it can be influenced by the quantity and type of evaporation sources. This view is supported by Guo *et al.* (2015), who found that the relationship between

LST and the vegetation index is a negative one, while it appeared to be positive for the built-up index. Thus, the relationship between LST and air temperature is a positive one, where an increase in LST means that the air temperatures will be increased, and vice versa. This depends on a number of factors, the most important of which are geographical location and the availability of evaporation sources, such as vegetation cover and bodies of water. The difference between surface temperature and air temperature is not usually as big, typically ranging between 5°C – 6°C (Shen *et al.*, 2015). The relationship between LST and land use is not only an effected relationship, but also an affected relationship, where LST can affect the land surface in some areas through its influence on soil moisture. In this respect, it was found that areas with high LSTs are characterised by a lack of soil moisture (Cai *et al.* 2016; Jiang, Fu and Weng, 2015). In contrast, wetter lands are characterised by a stronger impact in terms of reducing LST (Cai *et al.*, 2016). The relationship between surface moisture and LST can be an inverse one through the role played by evaporation in reducing temperatures, as supported by Rasul *et al.* (2015). Thus, estimating LST during the rainy seasons can result in greater uncertainty than in other seasons; indeed, this same reasoning also applies between morning and zenith, whereby the morning hours are wetter than at around noon.

According to Morabito *et al.* (2016), there is a link between built-up areas and an increase in LST, where it was found that the highest LST indicators were generally noted in areas that were known to have a high percentage of impervious surfaces. Therefore, it appears that the expansion in urban areas can lead to an increase in LST whether in terms of values or breadth. This is in line with the view of Fu and Weng (2016), according to which any changes of any kind of land pattern to built-up cover can contribute to an increase in LST. This is supported by Chaudhuri and Mishra (2016), who noted that pre-existing urban areas during their study time experienced a stable LST index, while areas that had recently been converted to build-up areas registered a noticeable increase in LST within the study area. Impervious surfaces, such as buildings and paved roads in cities, represent the highest LSTs, but these surfaces differ in terms of the possibility of heat reflection.

As Connors *et al.* (2012) have shown, industrial and commercial areas within cities generated the highest LSTs compared to other urban areas, such as residential areas. In the same context, vegetation type also varies in its impact on LST, especially with regard to plants' seasonal greenness, where the vegetation cover's impact on LST is almost non-existent during these seasons. This could be the reason for the high temperatures in the suburbs of the city of Erbil, the capital of Iraq's Kurdistan region, compared to the city centre during the summer season (Rasul *et al*, 2015).

The reflectance spectra of natural and artificial surfaces are highly variable. Dry leaves can be clearly differentiated from green leaves, for instance. The absorption of the healthy vegetation cover is particularly strong in visible range, though less intense in the green (~550 nm). In the red, it increases again but toward 670 nm decreases (Tupin *et al*., 2014). The spectral signature of soil depends on surface conditions because, in contrast to vegetation, only a small amount of electromagnetic energy is transmitted from the soil (Chuvieco and Huete, 2010). Soil that is wet and contains a large amount of humus is dark. From the blue to the red, the reflectance of soil increases only very slowly, and in the NIR region attains a plateau. Several white soils and artificial materials, such as concrete and asphalt, have a higher reflectance in the blue range (Tupin *et al*., 2014).

2.3. The Use of Satellite Thermal Data in the Study of LST

Remote sensing technology provides a unique way to detect the thermal characteristics of land surface rather than relying on ground-based measurements, especially in geographical and environmental studies, where it acts as a record of visible data of areas that are covered by images during a certain time (Jones *et al.*, 1999). Employing this technology in environmental studies has enabled an increase in the flow of related data and the ability to monitor different variables, including in inaccessible places and for invisible phenomena. An increasing awareness is being experienced among scholars with regard to the fact that remote sensing can play a role in providing the data needed to identify ecosystem conditions and to detect changes on spatial scales (Avdan and Jovanovska, 2016). Through the development of satellite technologies and the availability of satellite data with a high spatial resolution, remotely sensed data remains the most effective means that can be adopted to measure LST over wide areas with sufficient spatial resolution and that is completely spatially averaged rather than giving point values (Isaya and Avdan, 2016). This has helped the study of LST become a fertile field for research aiming to obtain a much greater understanding of its characteristics (Voogt and Oke, 2003). NOAA AVHRR satellite data are the primary source for studying LST (Weng *et al.*, 2004). The first urban temperature observations (from satellite) were reported by Rao (1972), since when a series of sensor-platform combinations (satellite, aircraft, ground-based) have been applied (Weng *et al*, 2004). At present, there are a number of satellites that can be used to monitor geographical variables with various high-resolution sensors, some of them obtaining a less than 50 cm/pixel resolution, such as the

Worldview satellites. However, in spite of this, a few of these satellites have a thermal infrared bands which provide the ability to detect thermal electromagnetic spectrum (Earth radiation) that can be used to measure changes in LST. The Landsat thermal data are the most commonly used as a means of studying LST, where the literature review survey found that most of the research on LST has used Landsat data as a method of detecting the change in this variable. According to Zhang *et al.* (2013), Landsat sensors can produce more persuasive findings for studying LST and with much greater accuracy in comparison to other satellite thermal infrared data, such as AVHRR and MODIS.As Chakraborty, Kant and Mitra (2015) found over 10 years of studies (2000 to 2010 in Delhi), the average change in LST found by Landsat was 1.4°C, while for MODIS data this same change was 3.7^{o}C, where the LST values estimated by Landsat had a standard error of ± 2°C, whilst those of MODIS had a standard error of ± 3°C which gives preference to the results obtained by the Landsat data.

Both infrared and microwave sensors have been used to detect LST. Infrared thermal sensors provide high spatial resolution, such as 30 m for Landsat, but are limited in the sense that they are only capable of imaging under transparent sky situations. In contrast, passive microwave sensors provide lower spatial resolutions and lower precisions while being capable of use in all-weather situations because they are only slightly affected by atmospheric influences. Since the size of atmospheric particulates such as smoke and biomass burned aerosols are usually smaller than microwave or infrared wavelengths, the atmospheric effects of small particles in this region are generally relatively insignificant (Chuvieco and Huete, 2010). However, the 1 km retrieval precision that is required in practical applications cannot be attained by any one of these sensor types. The most reliable LST data are from MODIS, which can only attain this precision for homogeneous surfaces such as water surfaces and sandy areas of land, while in reality 1 km of homogeneous land surface is quite a rare occurrence (Liang *et al*, 2012). The spatial resolution of satellite thermal images can differ depending on the sensor that takes the image of the earth's surface with different sizes of pixels, which in turn determines the resolution and the details of a scene. At present, only a few space-borne sensors can provide the relatively high-resolution thermal data that is required to identify urban LST, such as with the Landsat and ASTER data. However, these satellite sensors typically have low temporal resolutions due to the long-repeat cycle of these satellites. Thus, researchers have also used LST data from TIR sensors with low spatial resolution but can provide high temporal resolutions from geostationary platforms such as MODIS and SEVIRI. The use of high-resolution satellite images is important to a further understanding of the LST and in allowing researchers to gain more accurate results (Biro *et al.*, 2013). The sources of remote sensing in providing visible data with high resolution images are still not seen as an important development in terms of resolution (Rozenstein *et al.*, 2014) where the 30 m spatial resolution provided by the Landsat sensors is still the most detailed data compared with other satellites such as AVHRR (8 km), SEVIRI (3 km), MODIS (1 km), HJ-1B (Huan Jing) (300 m) or ASTER (90 m) (Zhang *et al.*, 2013) table (1). Landsat 8 Operational Land Imager (OLI) is different to the other previous Landsat sensors, where it has nine spectral bands and a Thermal Infrared Sensor (TIRS) with two thermal bands (10 and 11), though the National Aeronautics and Space Administration (NASA) recommend using band (10) for surface temperature retrieval (Zhu *et al.*, 2016).

Most thermal satellite data is regularly taken during the morning time, which is a relatively long time from the time at which maximum temperatures occur, normally at or around zenith. A number of authors (Guo *et al.*, 2015; Li *et al.*, 2016) favoured this view, and mentioned that the satellite overpass times for Landsat and ASTER do not coincide with peak surface temperature when surfaces can be at a maximum for generating heat, which can in turn affect the spatial variation of LST. While In contrast, the other satellites which can provide data during times of peak temperature cannot show sufficient details due to its spatial resolution, such as SEVIRI which provides data every 15 minutes with a 3,000 m resolution (Ghent *et al.*, 2010).

In contrast, the other satellites which can provide data during times of peak temperature cannot show sufficient detail due to its spatial resolution, such as SEVIRI which provides data every 15 minutes with a 3,000m resolution (Ghent *et al.*, 2010). According to Coops *et al.* (2007), who investigated the difference between the morning and afternoon MODIS thermal data to estimate the spatial variation of LST over a range of land cover classes, the results showed a statistically significant differences between the two sensors' data, considering that the afternoon MODIS data is more suitable due to it is more closer to the maximum daily LST than the other data acquired during the morning time.

Table 2-1: Specifications for the Infrared satellite sensors (Rasul et al*, 2015).*

Satellite		Channels or bands	Spectral range (μm)	Spatial Resolution (m)
Landsat	8	10 11	10.6-11.2	30
	7	6	11.5-12.5	30
	4-5	6	10.4-12.5	30
AVHRR/NOAA		3 4 5	3.55-3.93 10.30-11.30 11.50-12.50	1100 1100 1100
MODIS/Aqua;Terra		20 22 23 29 31 32 33	3.66-3.84 3.929-3.989 4.02-4.08 8.4-8.7 10.78-11.28 11.77-12.77 13.185-13.485	1000 1000 1000 1000 1000 1000 1000
ASTER/Aqua		10 11 12 13 14	8.125-8.475 8.475-8.82 8.925-9.275 10.25-10.95 10.95-11.65	90 90 90 90 90
AATSR/ENVISAT		6 7	Central wavelength: 10.85 & 12.0 Channel width: 0.9 & 1.0	1000 1000
SLSTR/Sentinel-3		S7 S8 S9	Central wavelength: 3.74, 10.85 & 12.0 Channel width: 0.38, 0.9 & 1.0	1000 1000 1000
ABI/GOES-R		14.15	Central wavelength: 11.2 & 12.3	2000
SEVIRI/MSG		9.10	Central wavelength: 10.8 & 12.0	3000
IRMSS/CBRES-1		9	10.4-12.5	300
MERSI/FY-3		5	Central wavelength: 11.25	1000
IRMSS/HJ-1B		4	10.5-12.5	300
S-VISSR/FY-2		IR1 IR2	10.3-11.3 11.5-12.5	5000 5000
VIRR/FY-3		3 4 5	3.55-3.93 10.3-11.3 11.5-12.5	1100 1100 1100

Other research has been conducted to estimate the effects of the daily temperature cycle on the study of LST using ground-based measurements, as per Figure (2-2). This research found that the spatial distribution of LST is considerably affected by the time of day (Aneesh *et al*, 2018).

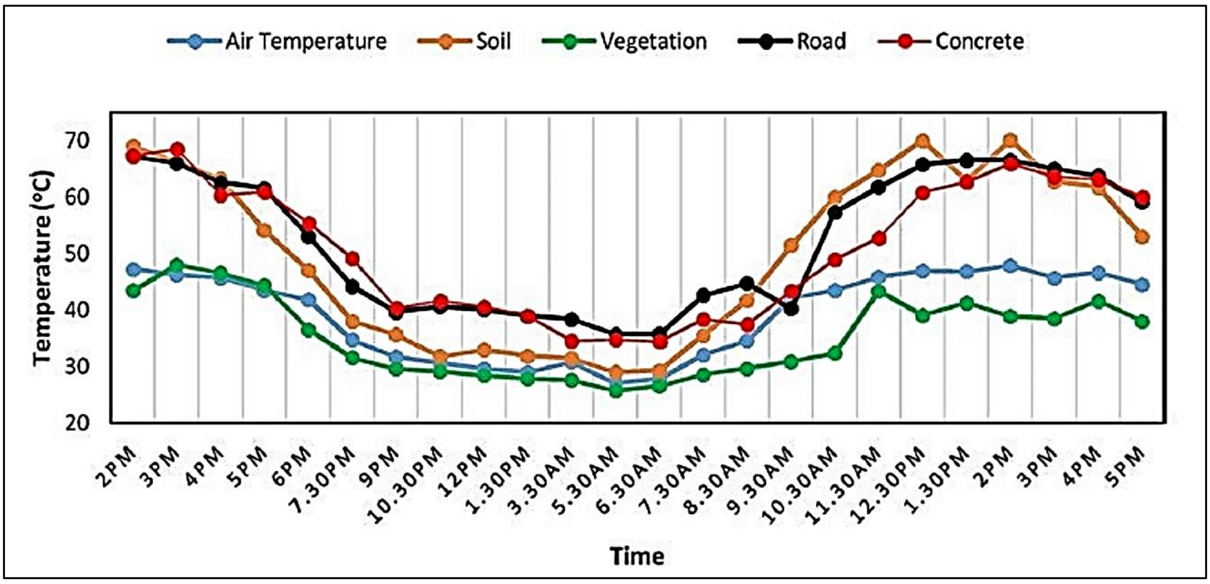

Figure 2-2: Shows daily spatial variations of LST over different land cover classes estimated by using ground-based measurements (Aneesh et al, 2018).

This is also supported by Petropoulos *et al.* (2009), who state that although the Landsat satellites provide higher resolution data, morning time is not ideal in terms of identifying the LST when the temperatures reach a maximum. Li *et al.* (2016) recommended future research examine other summer days and times, foremost during the noontime when maximum temperatures are typically achieved, as there is a link between maximum spatial variation of LST and solar insolation peak time.

Studying LST and analysing its relationship with urban land cover is an important aspect of understanding and monitoring a number of phenomena including evaporation, climate change, the hydrological cycle, vegetation monitoring, and urban climate. In addition, it has been found that LST is useful for environmental applications, as in monitoring plant damage and health, the dynamics of urban heat islands, and also those studies interested in ice cover (Weng, 2009). Urbanisation influences local climate and ecosystem functions, as well as biodiversity and quality of life through the expansion of increasingly impervious surfaces at the expense of the more natural landscapes. Vegetation and impervious surfaces are two key urban components; transpiration from plants plays an important role in mitigating the effects of built-up areas on increasing LST (Li *et al.*, 2011).

Despite the variety of findings that have been achieved when studying LST, the data available is not suitable either in terms of time, such as Landsat (morning time), or resolution, such as with SEVIRI, which provides data at a 3 km resolution every 15 minutes (Aminou, 2002).

It has been mentioned that the analysis of LST can provide more suitable results if the measurement is made when temperatures are at a maximum (midday) rather than during the morning (the satellite overpass time), where most urban land cover has a relatively similar thermal response and surface temperature differences are minimal (Mathew *et al.*, 2018; Zhou *et al.*, 2013). Other researchers have reported that the morning time is not appropriate for urban surfaces to absorb and generate the energy sufficient for use in recognising the relationship between LST and different urban classes (Coops *et al.*, 2007; Nichol, 1998). In addition, wet surfaces, as a result of the night dew and shade that are mostly prevalent in the morning time, can play an important role in reducing ground heat flux (Rinner and Hussain, 2011).

According to Guillevicababa *et al.* (2013), the angle of incoming solar radiation plays an important role in the spatial distribution of LST over a given location when the sun's radiation strikes the earth's surface more perpendicular to the ground (midday time) the incoming solar radiation becomes more focussed, and therefore more amount of incident energy per area unit, in contrast to when the sun is at a more inclined angle, will be reduced, thus resulting in lower temperatures, which will exposed to further decline in some spaces due to the shadows effect, as per Figure (2-3). The author motioned that, in a similar manner to this diurnal sun elevation, cites that are located at lower latitudes can show higher surface temperatures during a particular time of the day. It is frequently recommended that LST might better studied during times of peak solar insolation when temperature is normally at its greatest, so that the ability of surfaces to absorb and emit will be at a diurnal maximum, and hence the spatial variation of LST will be more recognisable during this period than others, or in other words the relationship between LST and different land cove will be stronger (Zhou *et al.*, 2011, 2013). This is in agreement with Weng *et al.* (2004) who argue that the spatial variation of LST can be greater around midday than in the morning, which means more opportunity for investigating the effect of land surface materials on LST.

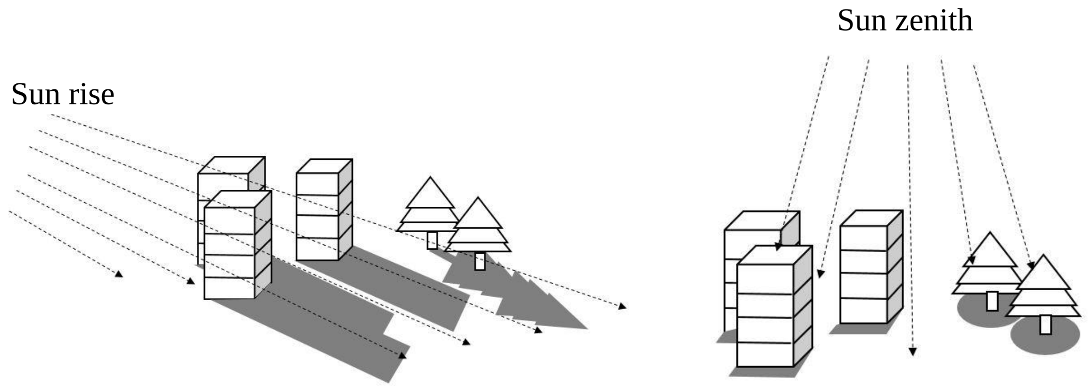

Figure 2-3: Schematic illustrating the effect of the sun elevation on the process of heating the surfaces through the difference in the concentration of the incident heat radiation and the intensity of the shadows.

It is noted that cities located within a dry region and surrounded by non-vegetated suburbs they are tend show lower LST values than its surrounding areas, this variation can be at the greatest during the sunrise time as a results of some factors related to the angle of the sun such as building shadows and the amount of the incident energy, while the opposite can be seen in those cities are surrounded by more vegetation cover because of the role of the vegetation for mitigating the temperature. This might be an important reason for the incompatible results between studies interested in LST, where it has been found that built-up areas can be cooler than the surrounding areas, leading to what is known as the urban cool island phenomenon (Rasul *et al*, 2015), whilst at the same time other studies have found that built-up areas have higher LSTs than their surroundings, resulting in urban heat islands (Imhoff *et al.*, 2010). As Frederic and Albert (2005) found, the reflected radiation from surfaces is clearly affected by the sun angle, where it was lower around zenith than during morning and sunset, which in turn determines the amount of the incoming irradiation from the total incident energy, see Figure (2-3). This means that the ability of a terrestrial surface to absorb and emit reaches its peak when the sun’s angle is more perpendicular to the ground, and vice versa (Lukeš *et al*, 2013).

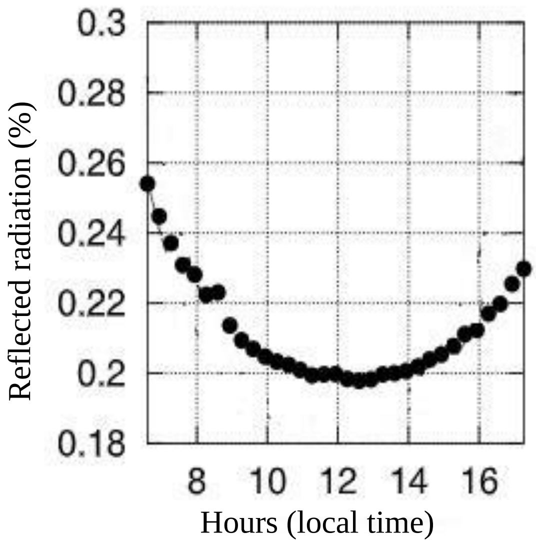

Figure 2-4: The effect of the sun angle on surface reflectivity using airborne data over a field (5 km²) located in the southeast of France (Frederic and Albert, 2005)

Studies have also shown that the use of different satellites to study LST does not give the same or similar values, which may reduce the credibility of the results reached. For example, Landsat and MODIS thermal images were applied to measure LST for the same area and over the same period, and it was found that LST, which was measured by MODIS, increased over the 10 years of the study by around five times that measured by Landsat. However, the results that were derived from Landsat remain more convincing given the difference in the resolution and the land cover changes that occurred during this period (Chakraborty *et al.*, 2015), and hence the clear preference for the use of Landsat thermal data in the study of LST.

Previous studies in this field have attempted to analyse the temporal variation of LST using remote sensing data with a different resolution. Shen *et al.* (2015) used five Landsat images to find the relationship between LST and ULUC over a 35-year study period. This resulted in certain difficulties in distinguishing between land patterns that have similar characteristics as a result of a relatively low accuracy of 70 to 75%. Landsat data may be useful in determining LST, however, in terms of finding the relationship between LST and ULUC, higher resolution data is needed in order to distinguish between the classes correctly and then to identify their impact on LST (Shen *et al.*, 2015). Other studies have used high-resolution satellites, such as IKONOS and QUICKBIRD, to classify urban land use and its relationship with LST as derived from thermal data. However, this was not sufficient to gain further insights into LST and ULUC because this high-precision data was not used for more than a year such as to coincide with the thermal data collected for LST. The high cost of such data makes it difficult to use. As such, many authors have admitted facing difficulties in accurately classifying ULUC in certain areas, which they referred to as a particular weakness of their studies (Jiang and Tian, 2010; Dewan and Yamaguchi, 2009; Biro *et al.*, 2013; Shen *et al.*, 2015). In line with the view of Dewan and Yamaguchi (2009), some of the classes were not categorised correctly, with certain residential areas being misclassified as landfill sites due to having similar spectral characteristics. Most studies recommend the use of higher resolution data to obtain a greater understanding of LST and its relationship with urban land use. However, this can also be achieved using a higher number of images, where multiple images can give a greater opportunity to follow variables of interest instead of relying on more disparate pieces of data. Previous research continued to follow the same approach in terms of the collection of satellite images. According to Fu and Weng (2016), two Landsat images (EM and ETM+) were taken in 1984 and 2011 to analyse the change in the LST over this period. A long period of time in such studies can be helpful to further understanding, but it is perhaps unreasonable to rely on such a small number of data points in terms of generating a valid representation. To follow the changes in LST in a certain area over a number of years requires enough data to at least represent the seasons. Another recent study, for instance, investigated the change in LST in the US Midwest between 2000 and 2006 using only two Landsat EM images (Jiang, *et al*, 2015).

Similarly, a study carried out to reveal the relationship between LST and urban vegetation cover using one satellite image (ETM+) concluded that the findings were consistent with the urban development in the study area and recommended further work that consisted of more than one area for comparative purposes (Asgarian *et al.*, 2014).

It is important to obtain the cloud-free data for standing LST. However, using only one single image to represent a certain season will be more vulnerable to unusual changes, such as extreme values of temperature or saturating buildings with moisture as a result of rain or fog or other weather fluctuations. In such cases, the thermal data can be significantly influenced by temporal variations in temperature. Hence, one cannot rely on one image to represent a certain season; the risk of misinterpretation of anomalous or erroneous results is far too significant to do so.

2.4. Knowledge gaps.

A review of the literature dealing with the issue currently under study shows that there are gaps in relation with high spatial resolution need further investigation and understanding, which in turn would help to improve the study of LST; these points will be the focus of this work.

1. Landsat LST data can be improved in terms of the measurement time being during times of peak temperature instead of morning time to minimize uncertainties associated with factors that can be more impactful in the morning period such as lower amount of incident irradiation and higher intensity of shadows.
2. There is a necessity to identify the relationship between urban land cover and LST during a local peak of temperature when LST spatial variation reaches the greatest, and how this relationship is affected by time of day.
3. The effect of time of day on the LST temporal variation across years has not been investigated.
4. Monthly variation in temperature is not normally taken into account, which can influence the representation of the seasons, especially for multitemporal studies which have previously relied on single seasonal datasets to represent each year.

2.5. Research Questions.

1. To what extent does the use of SEVIRI LST products (geostationary satellite) and properties of pixels have on converting LST data retrieved by Landsat during morning time on being more representative of that during a local zenith?
2. How is the relationship between LST and urban land cover influenced by time of day?
3. To what extent does using a seasonal (June, July, and August) average temperature, in terms of improving upon single data observations, constitute a more representative dataset?
4. To what extent does time of day affect the temporal variation of LST?

Chaper 3. Study Area

This chapter provides an overview of the features and characteristics of the study area for the purposes of giving a background on the nature of the area.

Study Area Selection

The characteristics of a study area can play an important role in reaching a more accurate understanding of the relationship between land cover and local LST. Areas within dry and hot regions are more suitable than those within cold and rainy regions, as they can help to obtain cloud-free satellite data and are less effected by soil moisture, as well as higher temperatures showing a greater spatial variation of LST. Equally important, the structure of an area containing a variety of land cover can show more homogeneous classes, such as built-up areas, vegetation cover and open barren land, which helps achieve a better understanding for the spatial variation of LST, especially when the spatial resolution of satellite data is not sufficient to detect the changes over a very small area.

The city of Tripoli has been chosen as a field of this study based on several considerations that make this city an ideal area for conducting this research, which can be summarized as follows:

- The city is characterised by high temperatures in the summer as well as low-speed winds which can led to broadening the spatial variations of LST over the different classes and thus can contribute reaching a clearer understanding of the relationship between LST and the land cover.
- The city is normally free of cloud cover that enables access clear thermal remotely sensed data especially in the summer where the weather is sunny most of the time.
- There will be minimal soil moisture impact, especially that resulting from rain, where this factor can have a significant effect on the relationship between LST and the urban land cover (Karnieli *et al.*, 2010).
- Shadow is minimised during the summer season due to the angle of the sun, especially during the local noon time.
- The high intensity of solar radiation in the summer as a result of the location of city within the low latitudes can led to maximizing the spatial variation of LST, which can facilitate the understanding of the relationship between LST and the land cover (Weng *et al*, 2004)

- As noted above, the landscape structure of the city helps to obtain the required data where it provides a range of homogenised classes such as vegetated areas and wide unused areas, as well as the presence of built-up areas with different densities, designs, and direction which can help to detect the effect of the shadows on LST.

The context below presents further descriptions of natural and human characteristics of the study area including the location, geological structure, soil, topography, climate, the structure of the city, and population.

3.1. Geographical Location

Tripoli is located between 32° 49' to 32° 55' north and between 13° 05' to 13° 22' to 13.05 east. On the geographical side, the city is situated in the north-western part of Libya at the top of the Jaffara plain, and it is bordered to the west by the junction of the highway with the Ghut al-Shaal road and the Karkarish road (Geyran), to the south is the Abu-Sleem, and to the east are the Souq al-Jum'ah and Tajoura districts, as per Figure (3-1). The city occupies an area of approximately 180 km^2 (Department of Surveying, Tripoli)

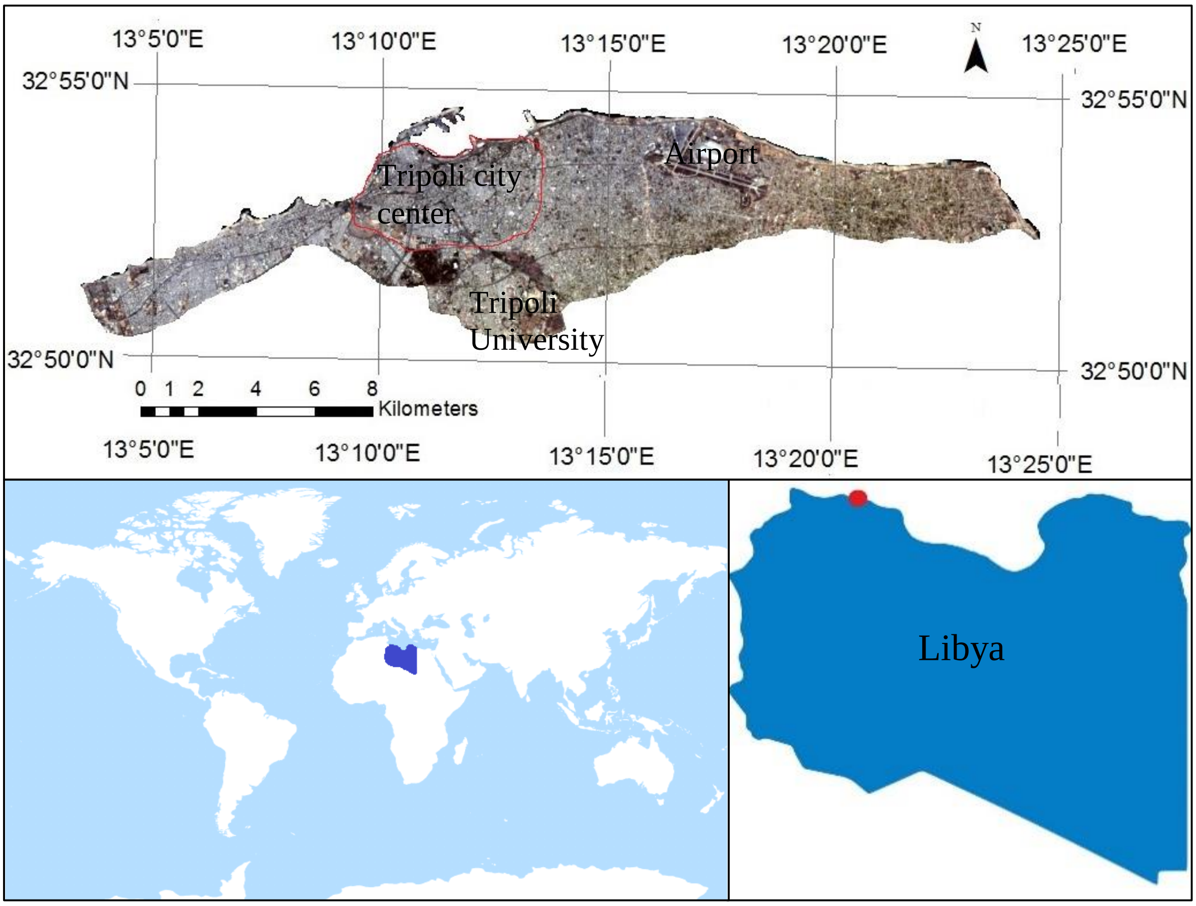

Figure3-1: The regional and global location of the study area (Tripoli, the capital of Libya)

3.2. Topographic area:

The city of Tripoli covers a plain that is generally characterised by a gradual decline from the southern direction of the sea in the north. However, from the analytical studies of the topography of Tripoli, there are some minor differences that lead to some of the residential neighbourhoods rising above sea level to a greater extent than other neighbourhoods, which range between 15 to 20 m above sea level (Centre for Industrial Research, Explanatory Book of the Tripoli Plate, Libya Geological Map, 1970)

3.3. The geological structure:

Tripoli is geologically an integral part of the sandstone plain, which extends from the coast to a distance of 10-20 km to the south. However, from a geological perspective, it appears that the formation of the inner Jaffara area differs slightly from that of the city of Tripoli. The southern region of the Jaffara plain is geologically older. This is due to the decline of the sea in the ancient geological ages from the southern region of the plain first and then to the lower part of the central region. The coastal area to which the city of Tripoli belongs is at a later stage, relatively speaking. As the geological studies indicate, the area of Tripoli began to emerge in the late second and third periods. This was reinforced by a study carried out by Hanis in 1962. It was found that the most recent marine sediments in the Hamada al-Hamra were deposited in the Pliocene era and, by the beginning of the Eocene era, a large part of Tripoli had become land (Jaudat, 1975).

The geological formations of Tripoli are the latest geological formations belonging to the fourth geological epoch, which is Pleistocene deposits with marine origin Miocene rocks, represented by the composition of Karkarach and the sediments of the Jaffara formation, in addition to the coastal sand dunes. The geological formations scattered in and around the study area are divided into two periods: the Pleistocene and the modern Holocene, as shown in Table (3-1) and Figure (3-2) (Jaudat, 1975).

These geological formations contain deposits of economic importance such as beach sand and igneous rocks which are used in concrete mixtures and in the stabilisation of building stones, and paving roads. The geological formation of the city has helped ensure the abundance of groundwater, throughout the previous historical periods, where the rocks of the Pleistocene and the other Mayosian marine and continental have the ability to retain groundwater and possibility allow its storage (Al-Hajjaji, 1989).

Table 1: The geological formations of the study area (Al – Hajjaji, 1989).

Age	Name	Type of geological formations
Pleistocene	Configuration of Jaffara	This covers the plain of the Jaffara and consists of sandy and silt deposits with different levels of igneous.
	The composition of Karkarash	They form beach slopes, such as granite, which are used on a wide scale for the extraction of building stones.
Holocene	Sedimentary deposits	These appear in the coastal area between the towns of Sabratha and Zuwara, which is a saline crust mixed with sand.
	Water sediments	These cover the lower parts of the Jaffara plain, which is soft sand.
	Sand dunes	The middle part of the Jaffara plain is covered, as it sometimes appears at the shoreline and consists of limestone sand.
	Sediments of modern valleys	This is gravel and soft sand.

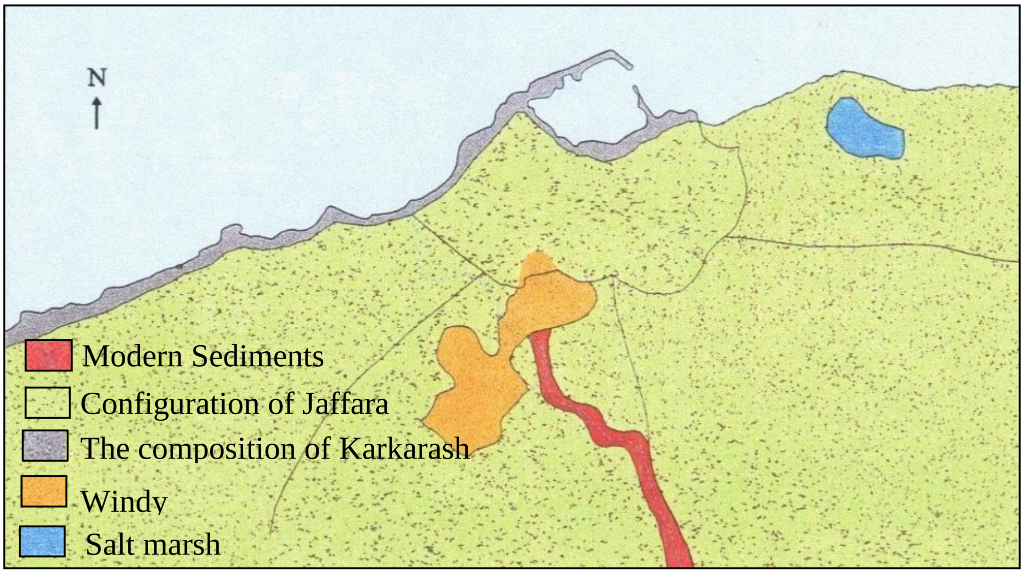

Figure 3-2: The distribution of geological formations of the study area (Al – Hajjaji, 1989).

3.4. Soil

Soil is the surface layer of the earth's crust that is formed and can be prepared for plant growth, each of which has a distinctive area to the physiological horizons, which differ from the original material that consists of morphological, natural, chemical and biological properties. It is the fragmented layer that allows plants to root, and whose fertility depends on its natural and chemical composition (Bin Mahmoud, 1995).

The soil in the city of Tripoli falls into five categories, which are as follows:

1. Sandy soil: This is a soil that has lost most of its natural properties because it is mixed with calcareous soils and is therefore brownish. It is generally poor in organic and non-organic matter and is based on marine limestone, this type of soil is found in the Old City (Ministry of Housing and Utilities: Tripoli Municipality in 100 years, Tripoli 1970).

2. Light sandy soil: The origin of this type of soil goes back to the wind sediments. The distinctive feature of this type of soil is that it is sandy; thus, it is poor in organic matter content and often contains more than 85% sand grains ranging in size from 0.5 to 2 mm. It does not exceed the proportion of clay to 10%, and the quality of ventilation is not good due to the widening of pores, which makes their ability to retain water weak as it is poor in the essential nutrients, such as nitrogen and phosphorus and potassium (1). However, the degree of interaction (PH) in alkaline ranges between 7 and 9 (2). This type of soil is found in the south and south-east of the city of Tripoli, and in large parts outside the Old City, including West Street and Abi Khair Street and Corner Street, as well as the Fashloum, Zawiya Dahmani and Manshiyeh areas (Bin Mahmoud, 1995).

3. Sedimentary soil: This type of soil consists of deposits of valleys and sediments from watercourses at successive intervals of time. The main feature of this soil is the presence of different sedimentary layers of different characteristics of the ages between the three, which is one of the most fertile types of agricultural soils in the city, including Wadi al-Majinin at the southern border of Tripoli, as well as in large areas of Ain Zara, Al-Hadbah al-Khadra, Bab al-Aziziyah, Bab al-Salam, and Abu Salim (Bin Mahmoud, 1995).

4. White sandy soil: This is a fragile and incoherent soil mixed with calcareous deposits and marine fossils. This soil spreads along the northern coast of Tripoli and in most of the resorts and beaches (Ministry of Housing and Utilities: Tripoli Municipality in 100 years, Tripoli 1970).

5. Red brown soil: This is composed of carbonate with a percentage of salts and gypsum, as it sometimes appears in the form of saline and surface gypsum crusts, which gives it a pH of 8.0 to 8.6 and is quite fertile. The red brown soil, which has a small percentage of phosphorus and iron, is widespread across the Al-Jaffara plain and parts of the area of the Janzour and east of Tripoli. In general, most of the soil in the city of Tripoli has lost its ability to act as agricultural soil, due to urban encroachment and its transformation into a residential land (Abu Lakma and Al-Qaziri, 1995)

3.5. The climate

Climate is the state of the atmosphere in a region over a long period of time, or in other words the average weather conditions in a particular place, which might be a for a season, a year, or a number of years. It is agreed that 35 years is the minimum time period to best describe climate (Mqaily, 1993).

It is known that climatic elements such as temperature, air pressure and wind are affected by a variety of factors, such as location, topography, land, and water distribution, etc. However, the climate is being severely affected by human activities that have recently led to changes in the radiative and thermal balance at both local and global levels, such as climate change, pollution, and global warming (Shehata, 1983).

Tripoli has a Mediterranean climate as a result of its location on the southern bank of this sea, which is generally hot and dry in the summer and rainy in the winter. Through the statistics and data available, one can identify the main features of the climate in the city of Tripoli as follows:

3.5.1. Temperature

Temperature is one of the most important elements of the climate through its direct and indirect influence on all other weather-related elements such as precipitation, evaporation, humidity, and atmospheric pressure, as well as all living organisms. Also, it has been found that whether it is high or low, temperature is affected by various factors such as the angle of solar radiation, the degree of transparency of the atmosphere, and the density of vegetation (Shehata, 1983). Figure (3-3) shows the average monthly maximum and minimum temperature between 1980 and 2010 distributed during the months of the year in Tripoli. There is a gradual rise in temperature at the beginning of the spring, with the quarterly average reaching 19.3°C, with the highest temperature in this season being observed during April and May. The reason for this is the low air pressure in the Mediterranean, which leads to the so called Alkebly winds. These are hot and dry winds that can lead to a significant increase in temperature, which then continues to increase gradually through the summer months, reaching its peak during July and August.

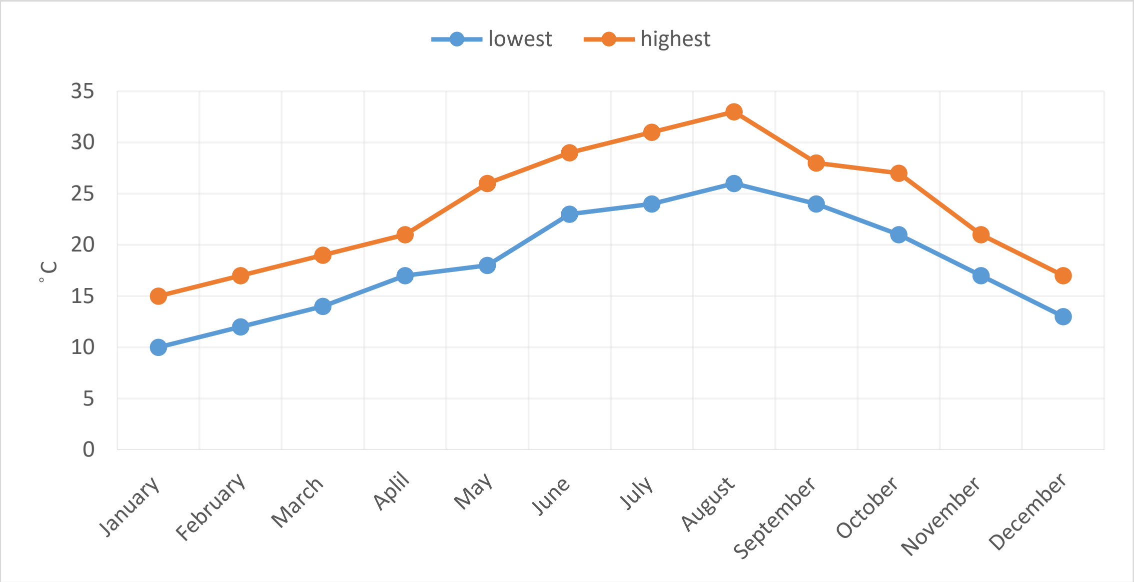

Figure 3-3: The average monthly maximum and minimum temperature between 1980 and 2010 distributed during the months of the year in Tripoli

The latter are the hottest months of the year in this city, with an average of about 30.9°C, and with a temperature that frequently exceeds 40°C. This can be explained by the angle of the sun, the clarity and dryness of the weather, as well as the length of the day (approximately 14 hours), resulting in the arrival of large amounts of highly concentrated solar energy on the land surface. The temperature rises in the early autumn, especially in September, because of the southern hot winds, with the average temperature in this season reaching about 22.2°C. Soon after, the temperature begins to decline gradually until reaching its lowest level in the winter, specifically in January, which is the coldest months of the year. This is ascribed to exposure to polar air masses, resulting in cold northern winds, with an average temperature in this season of 14.1°C (Abu Lakma and Al-Qaziri, 1995).

3.5.2. Air pressure

Air pressure is the weight of a column of air with a base area of 1 cm extending from the surface of the earth to the top of the atmosphere. This element is directly responsible for the formation of wind in terms of its direction, strength, duration, and distribution (Mqaily, 1993). In the winter, the sun is aligned above the southern hemisphere and thus the radiation reaches the study area at a slight angle causing the temperature to drop at the surface, which in turn leads to a pressure increase according to the climatic rule that states that the lower the temperature the higher the pressure of air, and vice versa. As the relationship between them is inverse in nature, accordingly most of the country will experience high pressure Azouri, which moves south by 5-10 degrees in latitude (Mqaily, 1993).

Figure (3-4) shows that air pressure increases in January to about 1,021.8 mbar, while the Mediterranean Sea is the centre of low pressure due to warm water and air humidity. By spring, the high-pressure zone shrinks to the north, while the low air pressure dominates over the Sahara Desert, causing the local hot winds known as Alkebly, with the average air pressure in this season ranging from 1014.5 to 1016.7 mbar. In the summer, the surface temperature begins to rise, while atmospheric pressure drops to 1014.7-1015.3 mbar in June and August, respectively. In the autumn, the difference between the characteristics of the air masses increases, resulting in low air drops on the Mediterranean moving from the west to the east (Abu Zeid, 1998). The data show the average pressure in the autumn varies between 1016.5 and 1018.0 mbar.

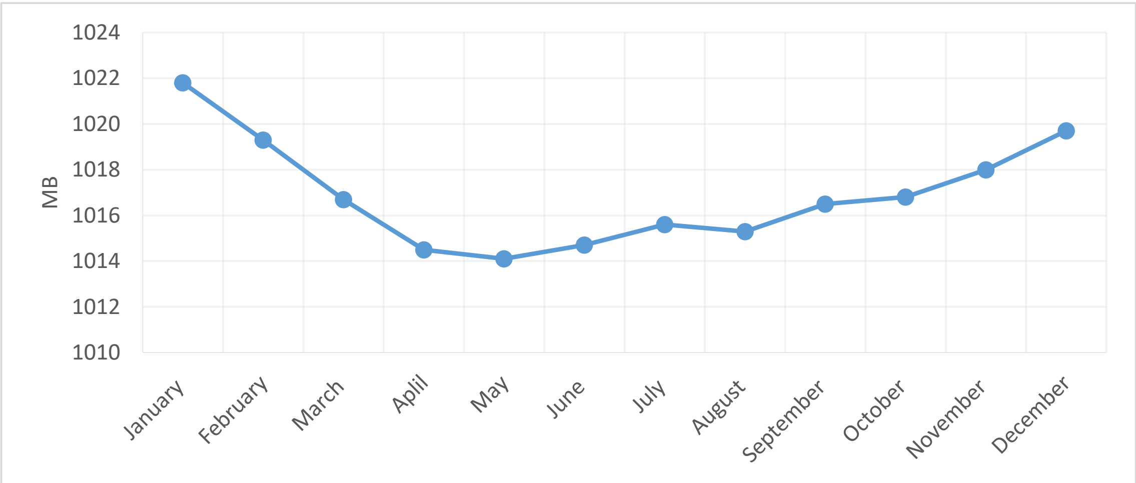

Figure 3-4: The average distribution of air pressure within the study area throughout the year.

3.5.3. Wind

Tripoli is characterized by low wind speeds as shown in Figure (3-5), where in the winter, especially in December, the southern and south-western winds increase due to the concentration of depressions in the Mediterranean Sea. When these winds are close to the cold, air masses change their direction due to low temperature and high atmospheric pressure, then their general trend is north and north-westerly (Abu Zeid, 1998). As these winds pass the Mediterranean Sea, they are saturated with moisture, resulting in rain during this season of the year. The average speed of these winds ranges from 7.2 to 7.9 knots in January and February, while the average season is 7.55 knots. During the summer, the north and north-eastern winds start to blow, with a seasonal average of 7.2 knots; and being dry helps to soften the temperature which reaches its impact to a latitude 18 north.

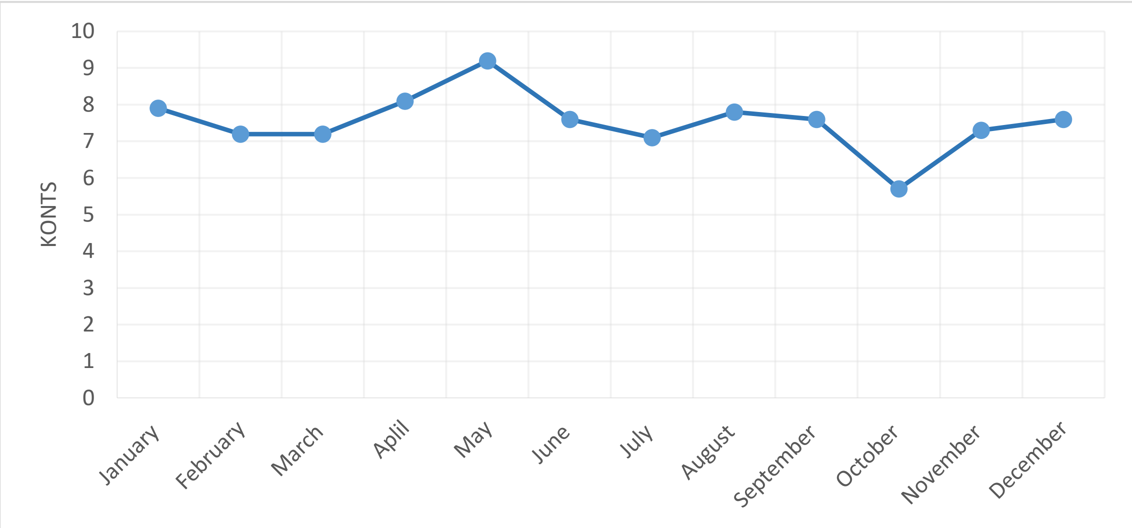

Figure 3-5: The average monthly wind speed in Tripoli

Consequently, this could increase the southern tribal wind, which is a strong wind laden with dust, causing an increase in the temperature accompanied by a relatively decreased and sudden humidity, with temperatures rising above 45°C. It also leads to dehydration of soil and crops, which affects air traffic and reduces visibility, as well as people’s psychological states (Abu Zeid, 1998). The average speed of these winds during the autumn season is about 6.6 knots, with the highest average being the month of September (about 7.6 knots). As for the exceptional records of wind speed in the city, wind speed was registered at 70 m/s in October 1966 and 66 knots in November 1987, causing the uprooting of a large number of trees, disruption to the electricity supply and communications, and various other physical damage (Abu Zeid, 1998).

3.5.4. Humidity

Tripoli is characterised by high relative humidity throughout the year due to high evaporation rates from the sea.

Figure (3-6) show that the overall humidity is 65.87%. In addition, the difference between the highest monthly rates and the lowest is not significant, at no more than 7%. In the winter, the relative humidity rises to a season average of 66.16% due to the low temperature, and the humidity rises in the summer due to the high rate of evaporation from the sea.

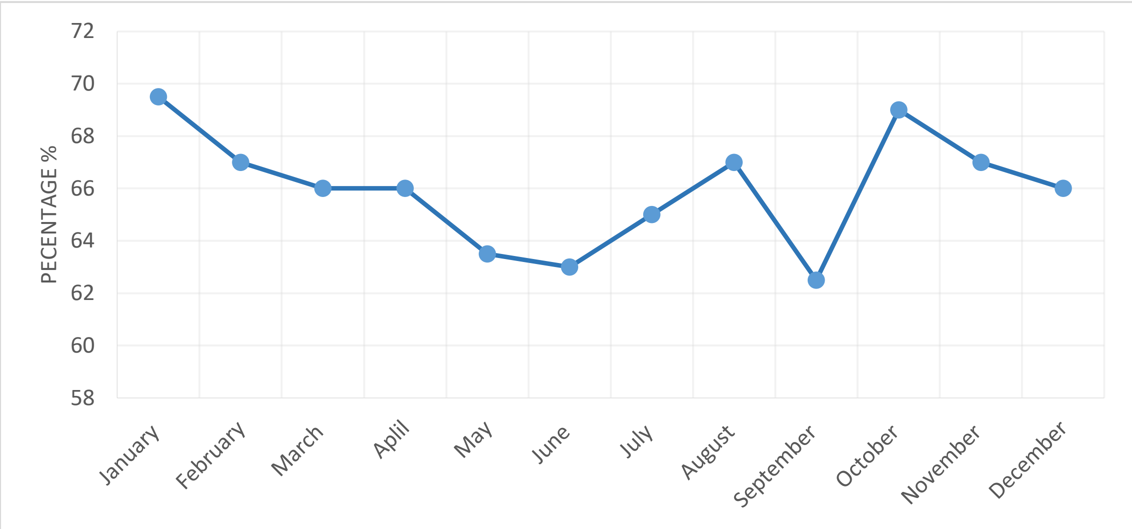

Figure 3-6: The average monthly humidity in Tripoli during the period between 1980- 2010

3.5.5. Rainfall

The amount of rain falling on Tripoli is affected to a large extent by only two factors, namely the shape of the coast and the recurrence of air depressions in the Mediterranean Sea.

1. Coastal form: This factor leads to the control of the amount of rain falling, as the coast of the region rises towards the north; therefore, the winds coming from the west collide with the coast and rain falls there to a greater extent than on the area located to the east of the city where the coast curves towards the south. Thus, the chances of rainfall are greater in Tripoli than its neighbouring cities.

2. The recurrence of depressions: The rain falling on Tripoli in general is of cyclical type, and these depressions arise from the convergence of two sets of air; one continental, coming from the Sahara, and the second polar, coming from the north. The rain is concentrated in very short periods where it does not fall regularly during the rainy season, but randomly for different periods of between one hour and a few hours or, sometimes,

continuously for days. This reduces their actual value and at the same time increases the risks to the environment. In 1985, the amount of rain falling on the city of Tripoli from a single storm was 115 mm, which is equivalent to one-third of the total annual rainfall, at 340 mm (Abu Lakma and Al-Qaziri, 1995).The estimated number of rainy days in Tripoli is between 55 and 60 days a year, which means that there are approximately 305 days in the year that are rain-free.

Distribution of rainfall during the year

Figure (3-7) shows the following results:

The rainy season starts in October and then the rain gradually increases until reaching the peak in December and January where the average rainfall during these two months is about 67.9 and 63.16 mm, respectively, while the winter amount is about 166.67 mm. The rainfall begins to decrease during the spring due to the emergence of spring air depressions, which often causes a little rainfall, especially in May. This month marks the end of the rainy season, where the average rainfall is about 50 mm of the total season (about 51.33 mm). On the other hand, the seasonal total of precipitation in the summer does not exceed 2.08 mm due to the high surface temperature, as well as the lack of difference between the air masses.

The total annual rainfall in Tripoli is approximately 342.65 mm. If this quantity is divided over the four seasons, the winter months would account for about 166.67 mm at 48.64%, while the autumn months would follow with 122.57 mm at 35.78%. As for the spring months, they average of around 51 mm is 14 % of the total, with the summer months contributing only 0.6% of the annual rainfall. However, these averages are not constant, but fluctuate from one year to another and from one month to another.

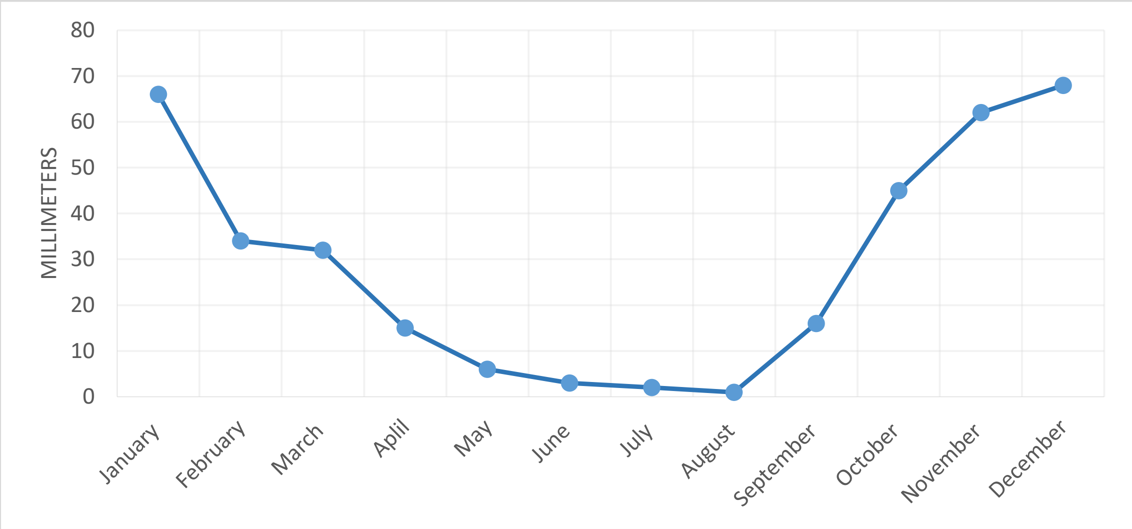

Figure 3-7: The average monthly distribution of rainfall in Tripoli during the period between 1980- 2010

3.5.6. Water sources

Tripoli is based entirely on groundwater to cover the city's water requirements, whether for household, agricultural, or other uses. As a result of the development of the city and the rapid population growth, especially after the discovery of oil, the city is experiencing a severe depletion of available water resources.

The following are the most important sources of water in the city:

First is surface water, which is water that appears on the surface in valleys and lakes, but which represents only a small proportion of the total water resources in the city because there is no constant flow. These are only seasonal at specific times depending on seasonal rainfall, such as Wadi al-Majinin, on which a dam was built in 1972 to protect the city from inundation, and to benefit from the associated water resources instead of it being lost to the sea. The dam is 75 km south of Tripoli, with a total area of 579 km². It has a storage capacity of about 58 million cubic metres per year.

Second is groundwater, on which Tripoli relies to meet its agricultural, domestic and industrial needs. Groundwater is the primary source of water for the entire region. This water is available in the layers of Mayssonian limestone rocks based on solid rocks, such as igneous base. Due to the rapid development of the city, especially in recent decades, there has been a rapid agricultural, urban, industrial, and population growth. In addition to the low annual rate of rainfall, the focus continued to be on groundwater, which accounts for 99% of water sources in Tripoli, resulting in severe depletion of water. Unfortunately, this situation is worsening by the day (Mqaily, etl, 1990).

3.6. The structure of the city

Tripoli enjoys a distinguished location, from many aspects administratively, economically, commercially, and industrially, with a growing land, sea, and air transportation infrastructure. The city consists of city centre and its branches in a number of suburbs, including Al-Andalus, Ain Zara, Souq Al-Jum'ah and Abu Salim, all of which are densely populated areas (Ministry of Housing and Utilities: Tripoli Municipality in 100 years, Tripoli 1970). It is considered the most densely populated of Libya's cities, inhabited by about a third of the country's population. It is generally composed of high percentage of buildings, most of which are for residential purposes, and which increase in density toward the city centre, as shown in figure (3-8). (This map was classified according to the main classes in the area: buildings, barren land and vegetation area using unsupervised classification-maximum likelihood reaching an accuracy of 0.91). The buildings in the city differ between the historical and the archaeological, which reflect the civilizational eras in which they were built, as well as modern constructions, but in general they are similar in terms of building materials, rocks and cement, as per figure (3-9), either on roads and streets, most of which are paved with asphalt. In terms of green areas, they range from gardens to parks with the largest vegetation area in the city being Annasr forest at about 1.5 km². (Ministry of Housing and Utilities: Tripoli Municipality in 100 years, Tripoli 1970).

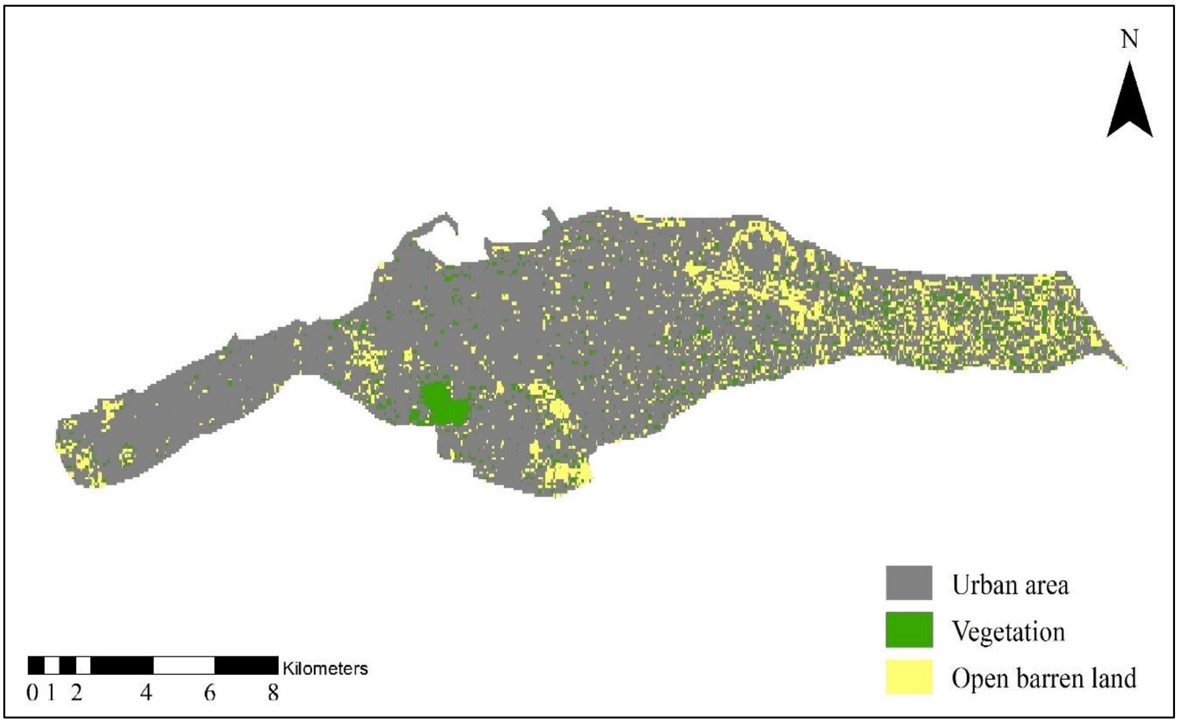

Figure 3-8: The main land cover classes in the study area

Figure 3-8: Some features of the structure of the city of Tripoli.

3.7. Population

Natural factors, especially the climate, as well as human factors, especially the economic factor, of the city of Tripoli have helped to make it the largest urban and service community in Libya. Since the beginning of population censuses, specifically in 1954, the population has significantly increased, as shown in Figure (3-9).

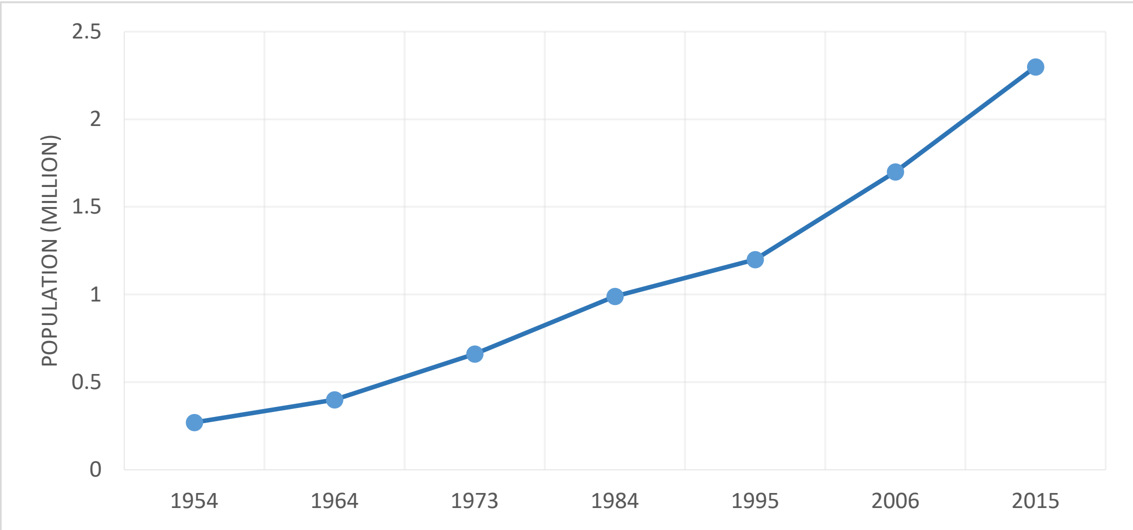

Figure 3-9: The population growth in Tripoli during the period between 1954- 2015

In 1954, the population was about 264,000. This figure had increased to about 405,000 people by 1964, meaning that the difference between the two censuses was 141,000 with an annual growth rate of about 3.5%. In the following census, 1974, the population jumped to 663,100 people at an annual growth rate of 14%, which was an unfamiliar increase at the time due possibly to the improvement in the city in many regards following the discovery of oil. The population growth continued to increase significantly until it reached about 1,183,762 people in 1995 from 994,100 in 1984, with an annual growth rate of about 3.4%. Then, the population continued to increase, but at a slower pace. For example, in 2006, the population was about 1,234,345 with an annual growth rate of about 3%. The population was estimated to be around 1,767,544 in 2016. This continued increase in the population of the city witnessed during recent decades was not only the result of the improvement of living conditions and economic activities, but migration has also played an important role as the city witnessed a significant influx of immigrants, both internal and external.

These various characteristics have played an important role in giving this city certain advantages that have historically made it an attractive area in which to settle. Recently, this city began to witness an increasing urban expansion that has made it a fertile and interesting field for various different fields of study.

Chaper 4. Converting Landsat LST data from morning to peak temperatures (9:40 am to 1:15 pm)

4.1. Introduction

The study of LST and its spatial variation with land cover characteristics has long been an interesting area of research. Remote sensing technology has increased the flow of data and enabled the estimation of LST more effectively, including various sensors and platforms. The Landsat satellite data, especially that provided by sensors 5, 7 and 8, are widely used in monitoring the changes on the earth's surface, including LST. These sensors provide high-resolution data with which to study the spatial distribution of LST and accompanying phenomena as a result of the impact of human activities, such as urban heat islands (UHIs). However, the lack of remotely sensed, high-resolution data measured in during a local peak of temperature has rendered the study of this variable an increasingly controversial issue. Through the literature review, it has become apparent that there is an urgent need to obtain LST images estimated when the temperature reaches a maximum in order to be able to investigate the effects that may occur because of the time of day and associated factors such as shadow on the spatial variation of LST, which is the rationale of this part of the study. The availability of a different number of satellites that include thermal bands with different features and specifications can provide the opportunity to compensate for this deficiency in this type of data by taking advantage of some of these characteristics offered by these satellites and integrating them.

This chapter examines and addresses the possibility of overcoming the issue of the unavailability of high-resolution satellite thermal data measured in conjunction with the period of a local peak of temperature. Thus, this chapter seeks to find a method to convert Landsat LST data from the satellite overpass time (9:40 am) to 1:15 pm as it was estimated in the study figure (4-1), by redistributing the ΔLST (increasing value of land surface temperature) based on the properties of the pixels for responding the incident energy. An evaluation will then be applied to test the accuracy of this conversion process.

4.2. Data preparation.

This chapter uses remotely sensed data collected from a summer season (10th of September 2017), where the date is predetermined to coincide with the overpass times of the Landsat satellite over the study area, with a preference for cloud-free data. This satellite data is represented in Landsat 8 (TIRS) at 9:40 am (Path 189, Row 37), pre-processed land surface temperature from SEVIRI produced at 9:40 am and 1:15 pm coinciding with the Landsat overpass time and a local peak temperature, in addition to LST ground-based measurements during the times specified above (around 9:40 am and 1:15 pm)

4.2.1. LST retrieval from Landsat 8

To retrieve LST from Landsat 8, there are a series of consecutive steps need to be followed (https://www.usgs.gov/land-resources/nli/landsat/using-usgs-landsat-level-1-data-product).

- The digital number DN value needs to be converted to spectral radiance using the following formula.

$$L_\lambda = M_L Q_{cal} + A_L \tag{1}$$

Where

L_λ = Spectral radiance (Watts/ (m^2sradμm))
M_L = Band-specific multiplicative rescaling factor from the metadata (RADIANCE_MULT_BAND_x, where x is the band number)
A_L = Band-specific additive rescaling factor from the metadata (RADIANCE_ADD_BAND_x, where x is the band number)
Q_{cal} = Quantized and calibrated standard product pixel values (DN).

- Converting spectral radiance to At-Satellite Brightness Temperature (TOA) using the following equation:

$$Tb = \frac{K_2}{1n\,(\frac{K^1}{L\lambda}+1)} \tag{2}$$

Where:

Tb = At-satellite brightness temperature (in Kelvin)
L_λ = Spectral radiance (Watts/ (m^2sradμm))
K_1 = Band-specific thermal conversion constant from the metadata (K_1 = 774.89)
K_2 = Band-specific thermal conversion constant from the metadata (K_2 = 1321.08)

- Land surface emissivity correction

After TOA has been processed the next step is the emissivity correction from which we obtain the final ground surface temperature correctly derived by Landsat

The land surface emissivity (LSE) or (ε) expresses the ratio of the radiating capacity of an object to that of a perfect black body. This correction process requires one to estimate LSE from the Landsat satellite using the NDVI method presented by Isaya and Avdan (2016), as per figure (4-1). The land surface emissivity LSE will also be used later in the equations to enable the conversion process.

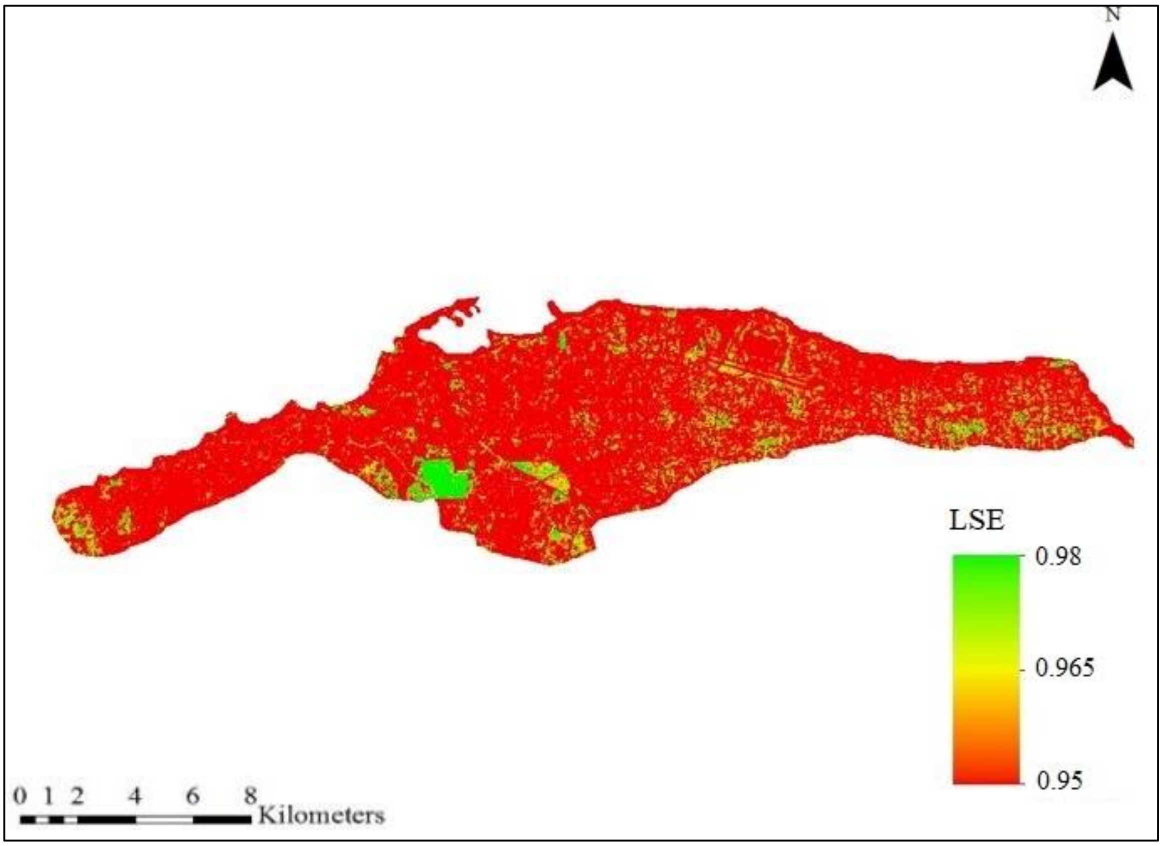

Figure 4-1: The land surface emissivity LSE retrieval for the study area to be used for both extracting LST from Landsat data and for the LST conversion process.

After preparing the earlier steps, equation (3) is used to retrieve the LST, which is the most commonly used formula for retrieving LST from Landsat (Isaya and Avdan, 2016):

$$\mathrm{LST} = \frac{\mathrm{Tb}}{1+\left(\lambda * \frac{\mathrm{Tb}}{\mathrm{p}}\right) 1n\varepsilon} - 273 \tag{3}$$

Where LST is the land surface temperature in degrees Celsius, as per figure (4-2), Tb is the At-satellite brightness temperature (in Kelvin), λ is the wavelength of emitted radiance (11.5 μm), P is a constant = 14380, ε is the surface emissivity and -273 is used to convert from Kelvin to Celsius

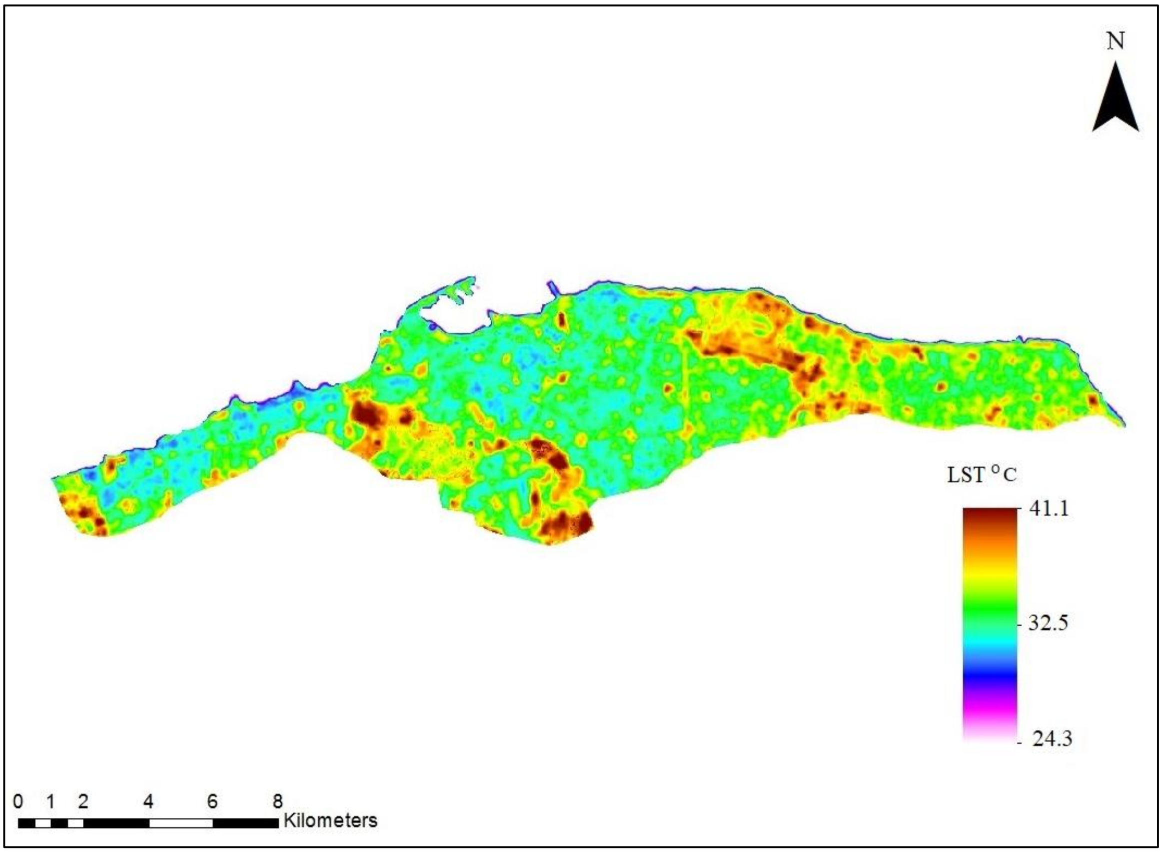

Figure 4-2: The LST image retrieval from Landsat 8 for the study area during the satellite overpass (10/9/2017 at 9:40 local time).

Besides the above Landsat images, the proportion of the vegetation (PV) and absorptivity LSA (1-abedo) images need to be prepared to be used later in the LST conversion process, which can be accounted for as follows.

According to Sobrino, Jiménez-Muñoz and Paolini (2004), the proportion of the vegetation (PV) can be estimated from Landsat data using the NDVI index which is a parameter that indicates the density of the vegetation cover within a certain area or pixel, as per the following expression.

NDVI ≤ 0.20 = non-vegetated, PV = 0

NDVI > 0.20 NDVI < 0.50 = partly vegetated PV= (NDVI- 0.20)/0.30

NDVI ≥ 0.50 = fully vegetated PV = 1, Figure (4-3).

The absorptivity (LSA) which is (1-albedo) can be obtained by Landsat 8 data using the following expression (Suherman *et al*, 2014).

((0.356×B2) + (0.130×B4) + (0.373×B5) + (0.085×B6) + (0.072×B7)-0.0018)) / 1.016

Where B represents the bands used**.**

After albedo has been obtained, (1-albedo) needs to be determined to get the land surface absorptivity Figure (4-4)

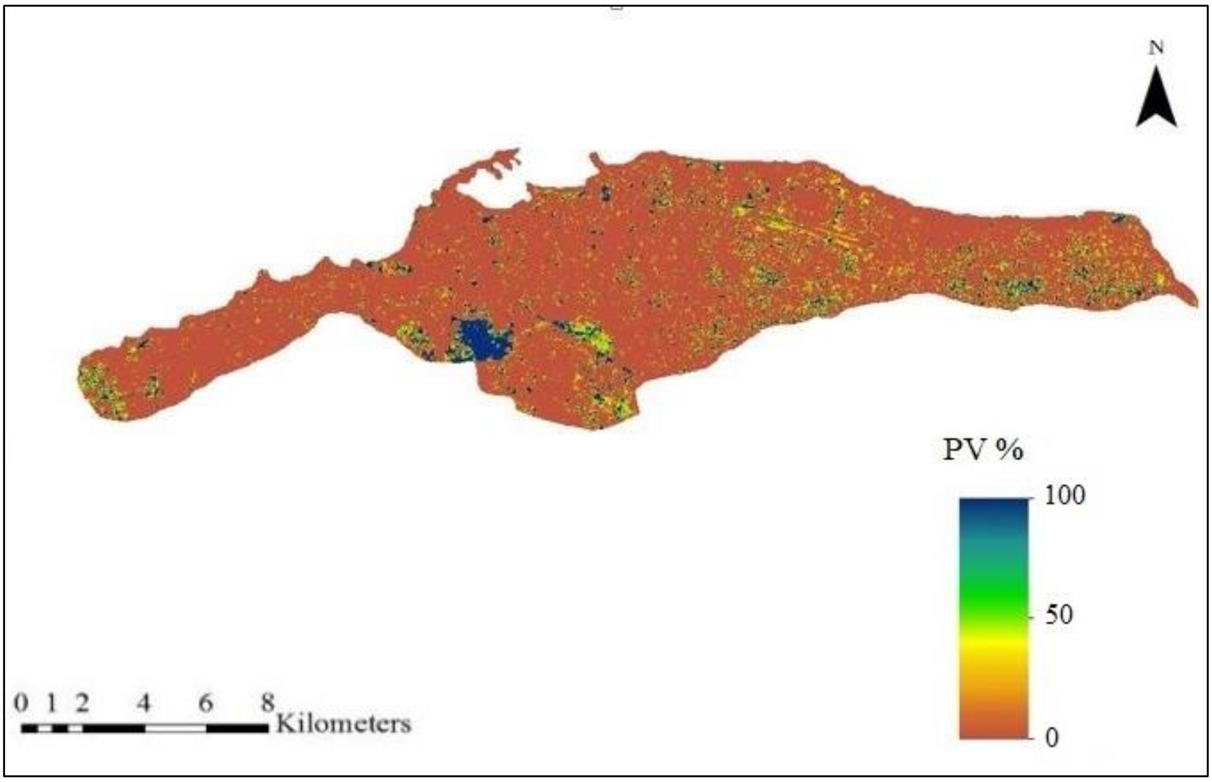

Figure 4-3: The proportion of the vegetation PV of the study area to be used later for converting Landsat LST from the morning to during peak temperature.

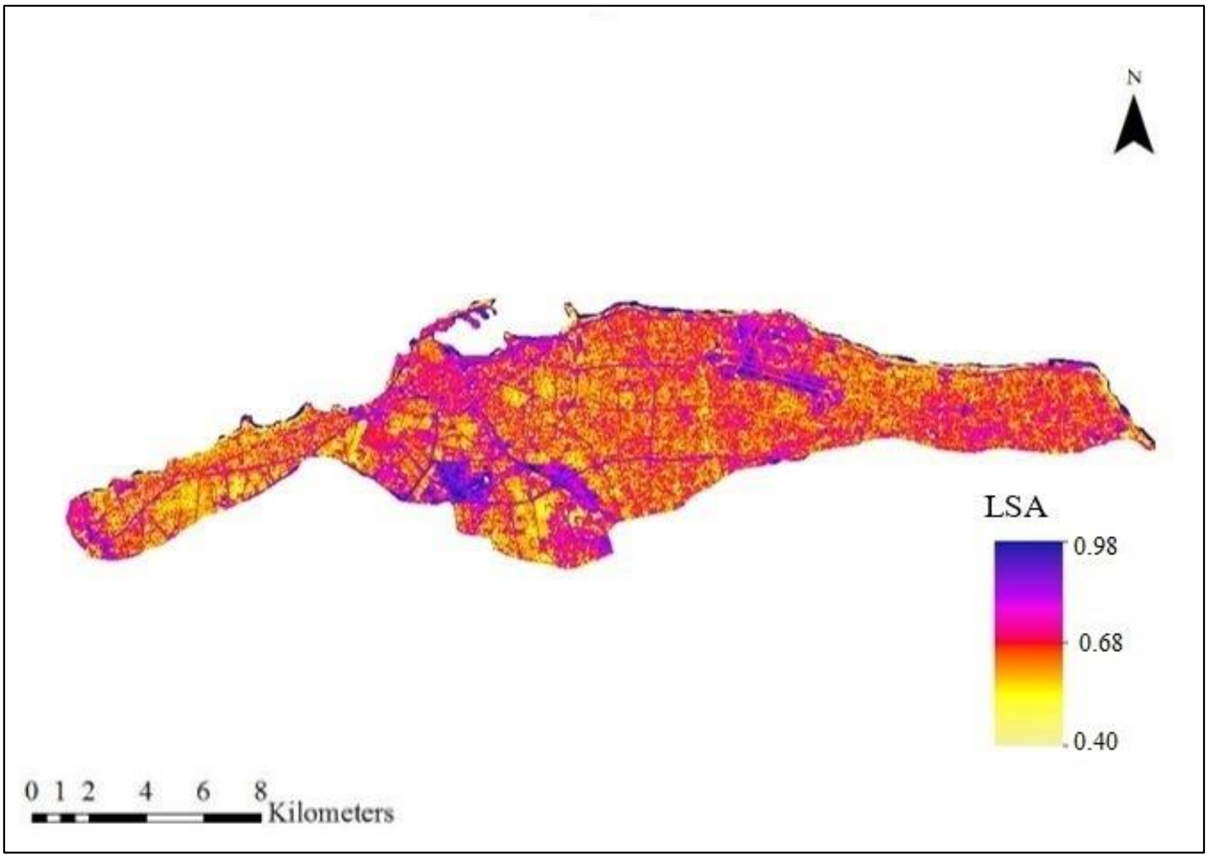

Figure 4-4: The absorptivity LSA (1- albedo) for the study area to be used later for converting Landsat LST from the morning to during peak temperature.

4.3. SEVIRI LST data

The Spinning Enhanced Visible and Infrared Imager (SEVIRI) sensor is on board the Meteosat Second Generation (MSG) geostationary satellite. This space-borne sensor provides 12 spectral channels, including image data in four visible and near-infrared (VNIR) channels and eight infrared (IR) bands with a baseline repeat cycle of 15 minutes (Aminou, 2002).

These data can be found in processed form through the LAND SAF website https://landsaf.ipma.pt/en/ which provides a variety of SEVERI products including LST covering the area of Africa, Europe, the western part of Asia, and part of eastern North America with a resolution of around 3000 m. The following images (4-5) shows the LST from SEVIRI for the area under study at 9:40 am and 1:15 pm local time. These images are used to estimate an average change in LST between 9:40 am and 1:15 pm using those pixels located within the land and excluding others that partly cover the water.

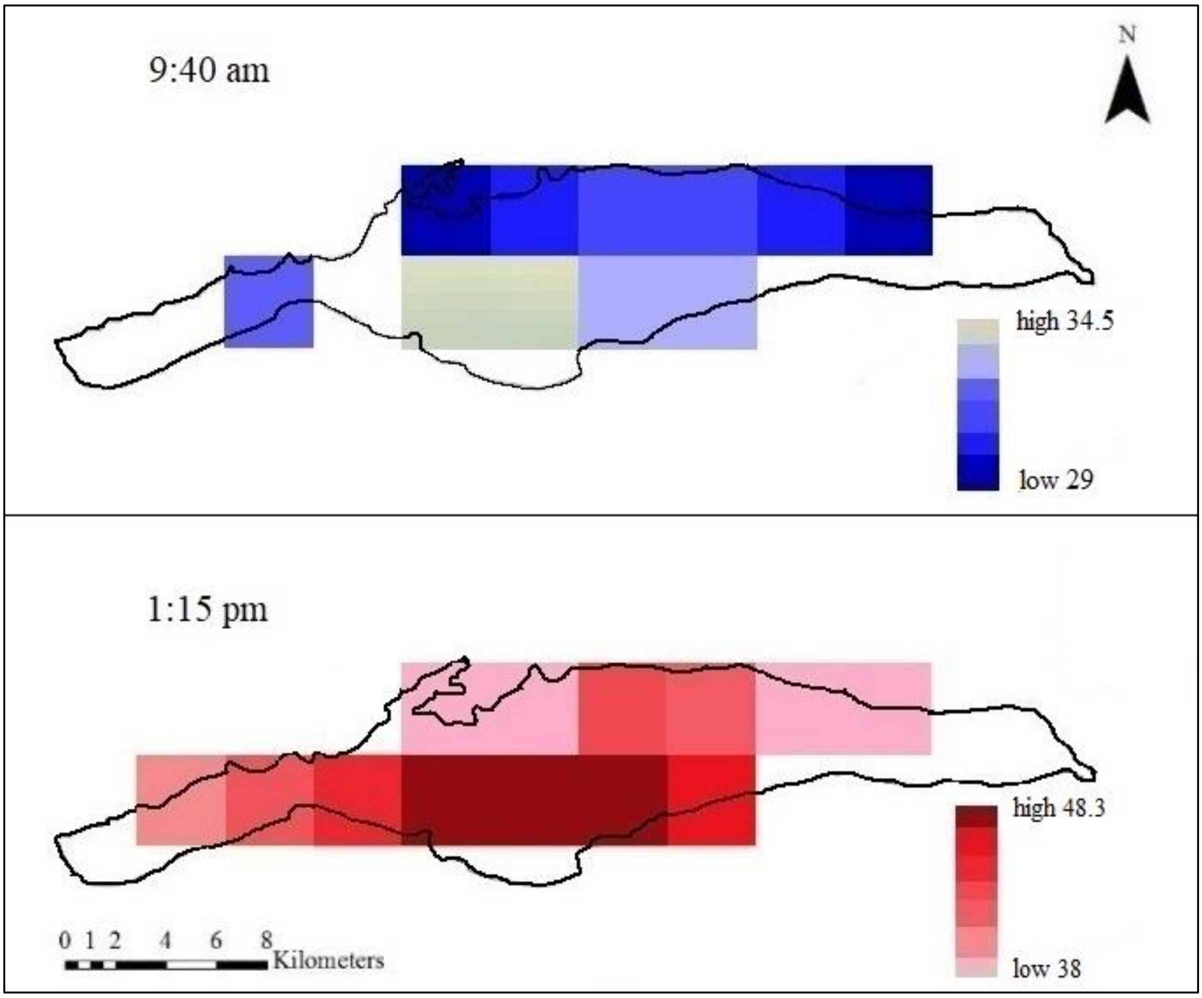

Figure 4-5: LST images from SEVIRI at 9:40 am and 1:15 pm local time for the study that will be used to obtain a sample, and which shows an increase between the two target periods.

4.4. Converting Landsat LST from Morning to Peak Time

As has already been found, land surface is heated through the balance of incoming and outgoing energy, where each object on the earth has a different response to generating heat from incident radiation (Trenberth *et al*, 2009). When radiation is incident on a surface it is distributed according to three different possibilities depending on the properties of the body; see figure (4-6): part is reflected by the surface depending on its albedo (a), which is the percentage of the reflected radiation to the total incident energy, another part is absorbed by the body and then emitted depending on the emissivity LSE, and the final part is transmitted, which occurs in transparent bodies that can allow light to pass through them such as glass, where for non-transparent surfaces this part is zero, such as soil (Hanks, 1965; Krenzinger and de Andrade, 2007). An object that can absorb all the incident energy (absorptivity LSA = 1 or albedo = 0) and emits all the absorbed energy (LSE = 1) with none transmitted, is referred to as a so-called perfect black body, which represents the maximum absorption and emission that can occur, and thus LST as well (Matsumoto *et al.*, 2013).

(Transparent body) (Non-transparent body) (Black body)

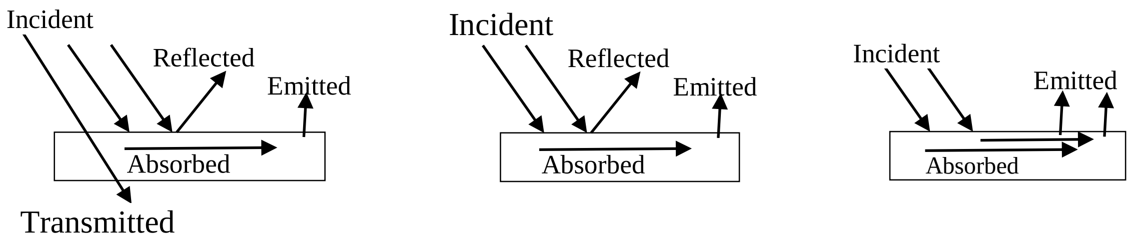

Figure 4-6: The three different possibilities that can occur at surfaces where there is incident radiation, as depending on the properties of the bodies themselves.

LST studies show that homogenous surfaces or pixels normally record similar LST values over the same time and under the same conditions, and the opposite for heterogeneous pixels which vary depending on composition (Lin *et al.*, 2008). This means the pixel whose LST is increased by 10°C within a certain period, other pixels that have the same properties (absorption and emission power) and that are under the same conditions will show similar changes. Thus, the ability to absorb and emit energy (LSA and LSE) can be used to estimate the change (here, increase) in land surface temperature, ΔLST, from a pixel that has a longer time to absorb and emit energy to another which receives less as a result of being in the first object's shadow or the difference between the peak in temperature compared to some earlier time. This can be obtained by converting the ΔLST of a certain pixel to the equivalent of being a black body, ΔLSTb, by dividing it into the LSA and LSE for this pixel, where the output will then represents a maximum in LST in accordance with a particular case, and so another unknown LST increases associated with other pixels' ΔLSTs can be derived from this ΔLSTb value by multiplying it by LSE and LSA of these pixels.

$$\frac{\Delta LST \div LSE}{LSA} = \Delta LSTb \tag{4}$$

$$\Delta LSTb \times LSE \times LSA = \Delta LST \text{ of a pixel} \tag{5}$$

However, this is in relation to non-vegetated areas or the image under the conditions mentioned earlier. However if there is a certain proportion of vegetation (PV) in the pixels, the LST value will be negatively affected by the role of the transpiration process which contributes to a decrease in LST (Deng and Wu, 2013). Therefore, in order to take this factor into consideration, the difference in the dynamics of the LST between vegetated and non-vegetated classes between the morning (when the Landsat passes the area) and at midday (when the temperature reaches a maximum) must be observed to investigate the ability of the transpiration process to slow or reduce ΔLST for the vegetation that is assumed to be produced in the absence of this transpiration role.

This observation requires ground-based measurements for LST to monitor the dynamics of LST over a full vegetated and non-vegetated class for the purposes of estimating the role of transpiration in reducing ΔLST. These measurements were collected on different days in the summer of 2017 (dry weather conditions and free of clouds) including a Landsat overpass time 10/9/2017, the morning measurements were collected between 9:35 and 9:45 am (5 minutes before and after the Landsat overpass time) and in the early afternoon between 1:10 and 1:20 pm (5 minutes before and after the SEVIRI capture time), where the daily LST values are likely to be at the highest level during this time figure (4-7). These measurements were taken from green leaves to represent the vegetated class and open land (dry soil) to represent the non-vegetated area, taking into account the effect of the shadow, so these measurements were taken from the sides that had been exposed to the sun throughout the time between the morning and the midday measurements.

4.5. Results

The local peak in LST needs to be estimated as a first step in processing the method, which is the time that the Landsat data need to be converted to, which the results showed to be around 1:15 pm, as per figure (4-7). This was obtained by using a number of SEVIRI LST images to calculate the average LST for each daytime hour from a number of days collected randomly during the summer from the years under study (2005, 2009, 2013 and 2017).

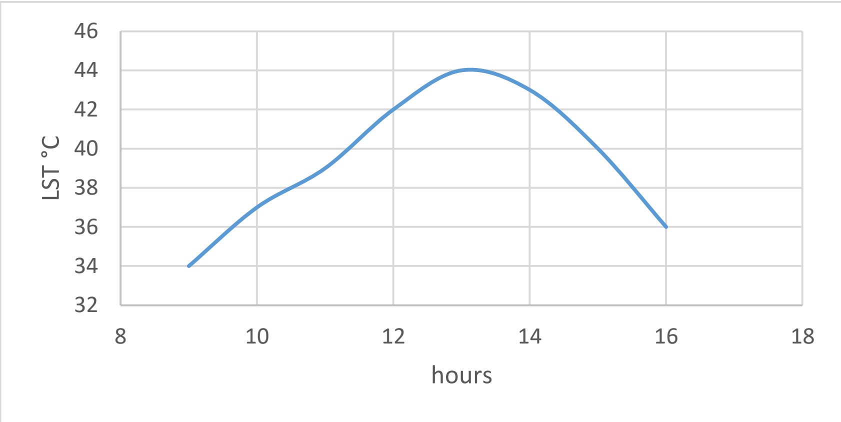

Figure 4-7: The time when the LST normally reaches a maximum during the a day in the study area determined using SEVIRI data as an average of a number of summer days collected from the years under study (2005, 2009, 2013 and 2017).

The difference in ΔLST between the vegetated and non-vegetated areas was estimated in the results shown in the following table (4-1), which presents a number of actual ΔLST between morning at 9:40 am and early afternoon at 1:15 pm for from different days (August and summer).

Table 4-1: Ground-based measurements for LST increase the ΔLST between 9:40 am and 1:15 pm, collected from hot and cloud-free days (summer 2017) to estimate the ΔLST between vegetated and non-vegetated classes (dry soil).

LST increase value ΔLST			$\frac{\Delta LSTn \div 0.95}{0.70}$	ΔLSTb ×0.985×0.87	$\frac{L - \Delta LSTv}{L}$	$\frac{L - \Delta LSTv}{\Delta LSTb}$
	ΔLSTv	ΔLSTn	ΔLSTb	L	PLV	P
Day 1	5.5	9.5	14.7	12	0.54	0.44
Day 2	6.5	10	15	12.8	0.49	0.42
Day 3	6.5	10.7	16	13.7	0.52	0.45
Day 4	5	8	12	10.2	0.50	0.43
					0.51	0.44

Where ΔLSTv and ΔLSTn are ΔLST of vegetated and non-vegetated (dry soil), respectively, and ΔLSTb is estimated as the ΔLST of a black body (LSE=1, LSA=1, PV=0), L is estimated ΔLST of the vegetation as there is no transpiration effect; PLV is an estimated ratio for the effect of transpiration on reducing the ΔLST of the vegetation, P represents a percentage of the transpiration effect on reducing the ΔLST of a ΔLSTb (black body increased LST value), The LSEs for the fully vegetated and non-vegetated pixels (dry soil) were 0.985 and 0.95, respectively, where 0.87 and 0.70 are the LSAs values for fully vegetated and non-vegetated pixels (dry soil), respectively, as provided by the Landsat data.

It was found that there are similar ratios for the role of the transpiration process in terms of reducing ΔLST over the period between the morning and the peak temperature on different days, which shows that there is a clear relationship between the increase in the vegetation ΔLSTv and the other value that would otherwise be produced by its LSE and LSA. The ΔLST of the vegetation is lower than the value generated by its LSE and LSA by around 51%, indicating the role of the transpiration process, which is also equivalent to around 44% of the value that would otherwise be produced by a perfect black body (LSE = 1, LSA = 1) over the same area, time and conditions. Therefore, to convert the ΔLST for a full or partly vegetated pixel to a value of a perfect black body which then can be redistributed to other pixels, the ΔLST needs to be estimated as it is supposed to be given by LSE and LSA by eliminating the effects of the property of the vegetation (transpiration) to reduce the ΔLST, as shown in figure (4-8).

According to the SEVIRI images (4-6), the mean ΔLST between 9:40 am and 1:15 pm is 11.5°C and its PV, LSE and LSA are 0.05, 0.96 and 0.78, respectively. In this case, in order to be able to redistribute this mean ΔLST value to the morning Landsat image (4-2), the following expressions (6, 7, 8 and 9) need to be applied.

- Eliminate the effect of the vegetation on reducing ΔLST.

$$\Delta LST \div (((1-(0.44 \div LSA \div (LSE))) \times PV) + (1 - PV)) = L1 \qquad (6)$$

$$11.5 \div (((1-(0.44 \div 0.78 \div (0.96))) \times 0.05) + (1-0.05)) = 11.85°C$$

The output of this expression (11.85°C) represents the ΔLST as it is supposed to be given by LSE and LSA as a non-vegetation pixel.

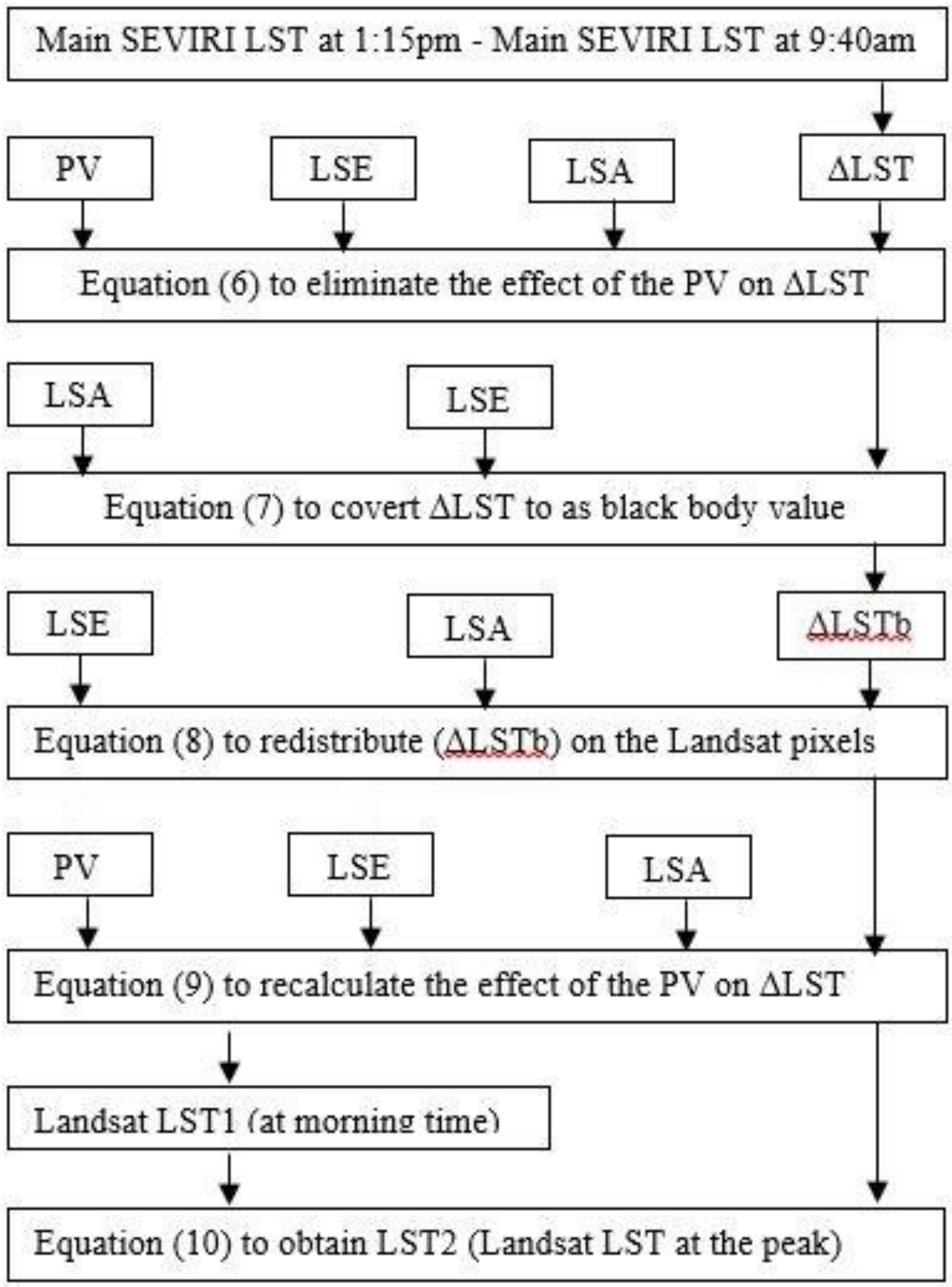

Figure 4-8: The main steps for converting LST from Landsat overpass time (9:40 am) to the time when the temperature reaches its peak (1:15 pm)

- Converting to as a perfect black body ($\Delta LSTb$).

$$L1 \div LSA \div LSE = \Delta LSTb \tag{7}$$

11.85°C ÷ 0.78 ÷ 0.96= 15.75°C

This output (15.75°C) represents the increase in LST of a perfect black body (ΔLSTb) for a part of the study area, which represents a key value for deriving the ΔLST of the Landsat pixels according to the properties of each pixel within the target area, so the next step is to redistribute this ΔLSTb across the Landsat pixels.

- Redistribute ΔLSTb across the Landsat pixels using as follows.

$$\Delta LSTb \times LSA \times LSE = L2 \tag{8}$$

$$15.75 \times LSA \times (LSE) = L2$$

The output here represents the ΔLST for each Landsat pixel as it is supposed to be given by the LSE and LSA of the pixel, where LSA and LSE are the absorptivity and emissivity images from Landsat.

- Recalculate the property of the vegetation to reduce the ΔLST using the following expression.

$$L2 \times (((1-(0.44 \div LSE \div (LSA))) \times PV) + (1 - PV)) = \Delta LST2 \tag{9}$$

The ΔLST2 image is the LST increase between 9:40 am and 1:15 pm in Landsat resolution, so to obtain the final image which represents Landsat LST estimated at a maximum of the temperature, this output (ΔLST2) need to be added to the morning Landsat image figure (4-8).

$$\Delta LST2 + LST1 \text{ (at 9:40 am)} = LST2 \text{ (at 1:15 pm)} \tag{10}$$

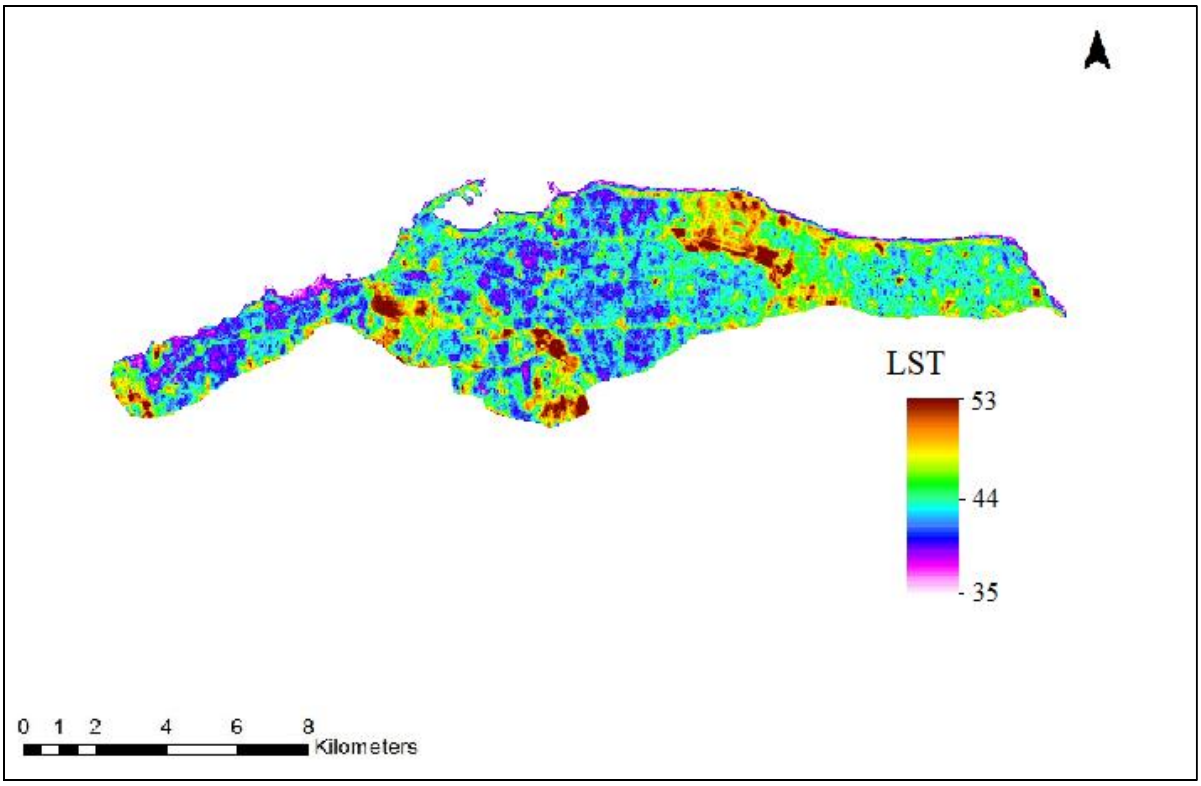

Figure 4-8: The estimated Landsat LST image over the peak of the temperature (1:15 pm) for the study area.

4.6. Accuracy assessment

As a results of the lack of actual data to be used to evaluate the accuracy of the different images are used in this method to generate both of LST images, the study evaluates the final images of the process which are the morning Landsat LST image and the converting LST image that represents a peak period of temperature. The two main LST validation approaches are through ground-based measurements or the determination of near-surface air temperature (Avdan and Jovanovska, 2016). This morning LST image and the final image converted to at a local peak of temperature are subjected to a validation via a number of LST ground based measurements for the same time in the study area.

Figure (4-9) shows a validation of the Landsat morning image by testing the standard error and R of the variability between a number of LST points or pixels from Landsat images and their counterparts from the actual points. It is shown that the standard error or uncertainty of these selected points is around 0.7°C and R = 0.88, while figure (4-10) shows a validation of the Landsat image converted to at a local peak of temperature. It is shown that the standard error of these selected points is around 1.7°C and R = 0.82, which is considered a reasonable result for this comparison and reflects high percentage acceptability (Avdan and Jovanovska, 2016).

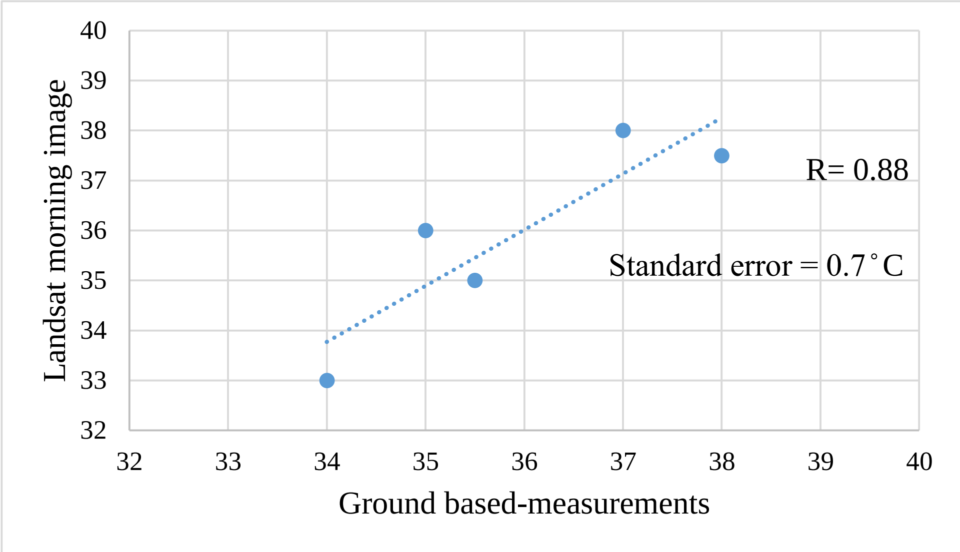

Figure 4-9: An accuracy assessment of the Landsat morning image 9:40 am, where it shows the standard error and R of the variability between points from this image and their counterparts from the actual LST ground measurements.

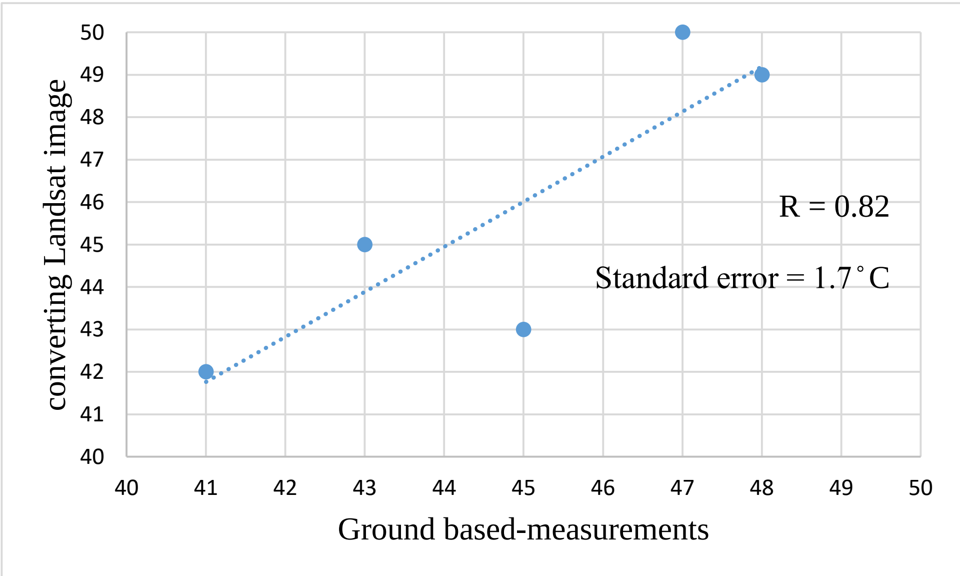

Figure 4-10: An accuracy assessment of the Landsat morning image converted to at a local peak of temperature (1:15 pm) which shows the standard error and R of the variability between points from this image and their counterparts from the actual LST ground-based measurements

4.7. Discussion

This chapter seeks to improve the time measurement for LST derived by Landsat as an important aspect for studying this variable and analysing its relationship with the spatial structure of the urban landscape, where high-resolution thermal satellite data such as that extracted from Landsat is only normally acquired at a specific time of the morning when factors related to sun angle is more impactful such as the amount of incoming and the outgoing heat energy as well as the intensity of shadows of buildings, which in turn can affect the accuracy in estimating LST variation. This study addresses this controversial issue by providing a method to convert Landsat LST images to be estimated when the temperature reaches a maximum, rather than directly using data from the morning (the satellite overpass time) by distributing the increasing ΔLST between these two times using SEVIRI LST products (3 km resolution every 15 minutes) based on the properties for generating the heat of each pixel on the Landsat scene (absorptivity LSA, emissivity LSE and the property of the vegetation cover PV for reducing ΔLST due to transpiration, estimated by ground-based measurements) during the summer season in a semi-arid region.

By observing the increase in LST from morning to midday in different classes, it was found that in non-vegetated open areas under dry conditions the ΔLST is strongly controlled by LSE and LSA. In contrast, the vegetative cover behaviour is affected by the transpiration process which reduces the ΔLST that is assumed to be generated by the LSA and LSE of this vegetated class, which is consistent with arguments stated earlier in the literature review (Oke,1982), (Weng *et al*, (2004) and (Chakraborty *et al*, 2015). This difference was found to vary coincide with the change of the diurnal temperature, this difference was appeared with a similar ratio when it was applied for different days, where it showed that the actual ΔLST of a vegetated class is lower than that assumed to be generated by an object such in a black body properties (PV = 0, LSA = 1 and LSE = 1) between 0.42% and 0.45% (0.44% as an average), which represents the role of the vegetation for reducing the heat beside LSE and LSA when estimating the ΔLST for each Landsat pixel.

The presented method has allowed the estimation of an LST image during a local peak in temperature at a resolution of 30 m (Landsat), where it can be seen from the assessment of the accuracy using actual ground based measurements that the errors range between 1°C to 3°C, and the standard error or uncertainty of this converted image is 1.7°C and R = 0.82. This can be used as an alternative solution to addressing the issue of the lack of high-resolution thermal satellite data recorded simultaneously with the local peak in temperature, which would contribute to minimizing uncertainties when estimating LST and studying its relationship with urban land covers, and overcome the impasse caused by this issue which has long been recommended by many researchers interested in this field (Petropoulos *et al.*, 2009; Li *et al.*, 2016).

By obtaining this expression for converting Landsat LST time measurement, it would become possible to obtain more reasonable data for studying LST, which could pave the way to more profound studies in this field. This study recommends to improve the accuracy assessment method by allowing additional coverage to maximize the training points within the study area and not to be limited only in the final image, so that it can include the images used for processing the final image.

Chaper 5. Assessing the effect of the time of day on the spatial variation of LST.

5.1. Introduction

Studying the relationship between land surface temperature (LST) and urban land cover is an interesting topic in the field of remote sensing applications, where the use of satellite sensors with thermal bands has facilitated the associated data collection processes. Landsat products are widely used in this field due to the accessibility to relatively high spatial resolution thermal data, making this satellite more suitable for studying LST and its relationship with land cover than others. However, this remotely sensed data is not captured during times of local peak temperature to represent the greatest special variation of LST, which in turn has created a controversy among researchers due to the fact that morning time is not an ideal time to identify the relationship between LST and urban land cover. Similar to a number of previous research efforts (Zhou *et al*, 2011; Zhou *et al.*, 2013), the presented study hypothesizes that analysing the relationship between LST and urban land cover during periods other than those of a local peak of temperature, as when using Landsat data, can affect the reliability of the final results due to the presence of shadows and other effects associated with the angle of the sun, such as the intensity of the radiation being greater around the time of solar zenith.

This chapter seeks to investigate whether the time of day can affect the spatial variation of LST and to what extent this can affect the accuracy of the relationship between the LST and urban land cover over the study area, which in turn could provide the ideal time for conducting this study. This chapter uses Landsat 8 LST images from 10th of September 2017 and converted Landsat LST images estimated via the method suggested in the previous chapter for estimating LST during the peak the temperature at 1:15 pm; in addition, this chapter further suggests another method to obtain an LST image that can give an estimate of LST in the event that the maximum incident heat energy is evenly distributed across surfaces throughout the day.

5.2. Data Preparation.

This section uses different resolution Landsat LST images that represent different times and cases for the study area; a normal LST image at 9:40 am, converted Landsat images at 1:15 pm, and the LST estimated in the event that the maximum of the amount of incident heat energy is evenly distributed across surfaces throughout the day, in addition to land cover images representing vegetative and non-vegetative cover. The R programme (R Core Team, 2017) is used in this chapter to apply the scatterplot technique to determine the correlation, if any, between the above images.

5.3. The Morning Landsat LST image.

The Landsat LST image, as provided by the USGS website at the actual satellite overpass time, is shown in Figure (5-1). This image has already been processed in the previous chapter, which represents the LST in the morning time in the analysis provided in this chapter.

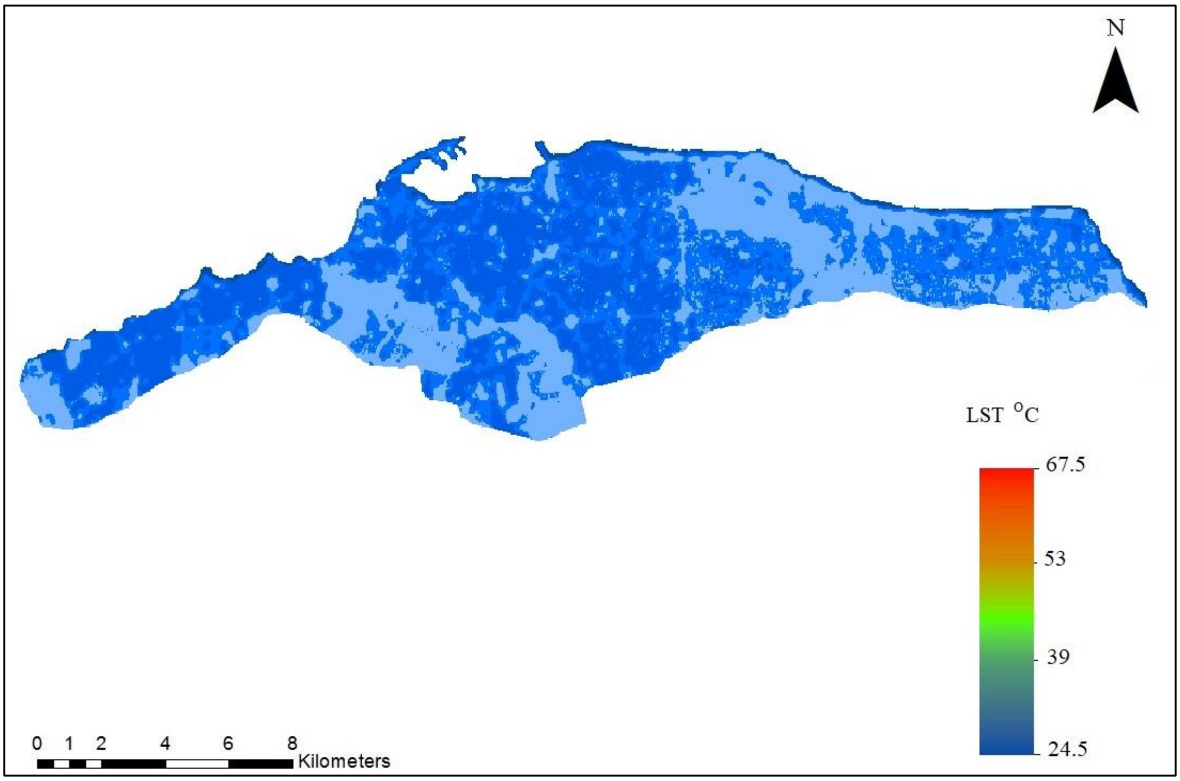

Figure 5-1: The LST retrieval from Landsat 8 for the study area during the morning time (10/9/2017 at 9:40 am local time).

5.4. Landsat LST during times of peak temperature (1:15 pm local time).

Figure (5-2) below shows a Landsat image from the satellite overpass time (9:40 am) that has been converted to represent times of peak temperature (1:15 pm) which has already been processed as per the previous chapter, and will be used to conduct the analyses for the effect of time of day on LST.

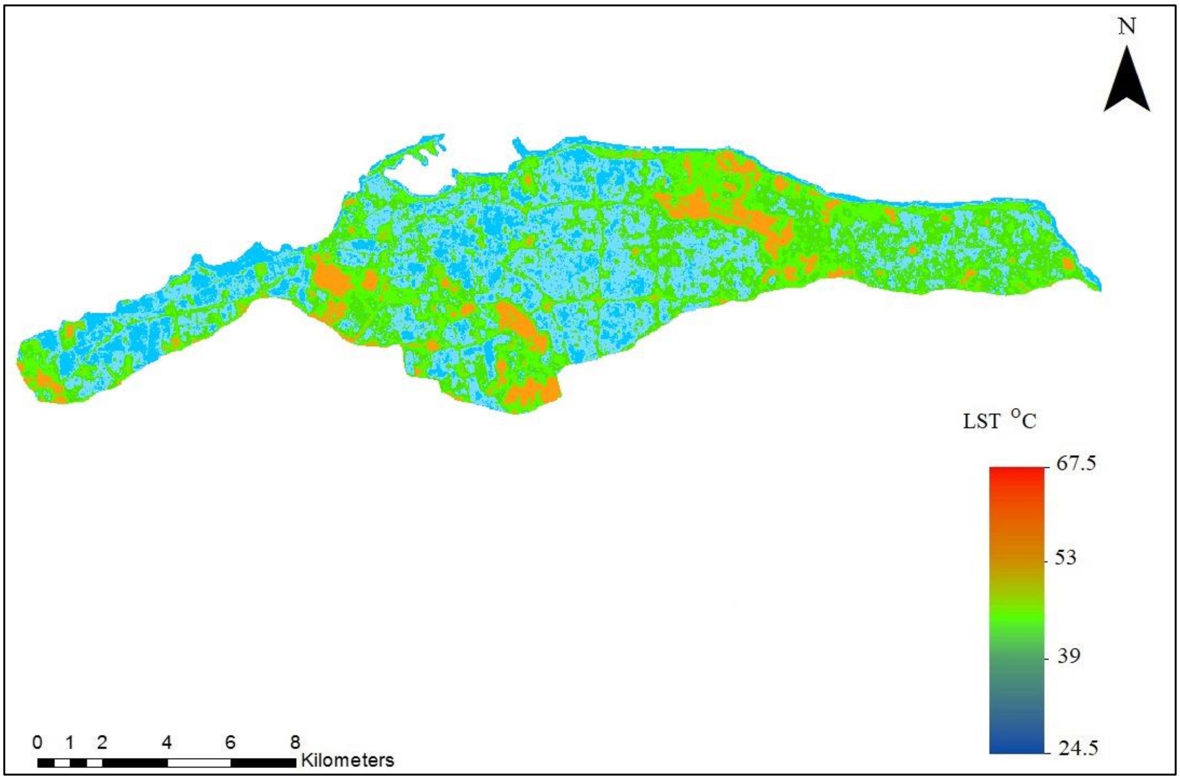

Figure 5-2: The estimated Landsat LST at peak temperature (1:15 pm) (10/9/2017)

5.5. Landsat LST image estimated during a peak temperature (1:15 pm) in the event of the lowest shadow effect for each pixel.

This is a hypothetical image extracted from the previous LST image (figure 5-2) in that all the homogenous pixels in terms of the properties should show similar LST values though this may not occur in reality, especially in urban areas, due to the shadow which effects the evenness of the amount of the incoming energy, creating disparities in the LST for this kind of pixel. The technique here considers the maximum LST within the bounds of certain types of land cover such as vegetation, buildings, paved roads or dry soil, and assumes a maximum absorption and emission of heat energy, in contrast to the lowest LST values which represent lower amounts and a maximum shadow effect. This image shows LST values for each pixel based on its property with the elimination or minimizing the effect of the shadow, which is achieved by using a maximum LST value for a particular pixel as it represents the lowest shadow effect, to make homogenous pixels that are unified within the maximum value that can be given based on their surface behaviour. Based on these considerations, this image can be extracted from the converted image (Figure 5-2) using the following expressions:

1. When (PV = 1): in this scenario, the highest LST value of the full vegetated pixels (↑LSTv) will be assigned
2. When (PV = 0): in this scenario, a pixel is considered to be composed of non-vegetative cover such as rocks, bare soil, paved roads, and therefore the following expression will be used.

$$(\uparrow LSTn \div LSEn \div LSAn) \times LSE \times LSA \tag{11}$$

3. When (PV > 0 and < 1): in this scenario, a pixel is considered to show partial vegetative cover, in which case the following expression will be applied.

$$((\uparrow LSTn \div LSEn \div LSAn) \times ((LSE - LSEv \times PV) \div (1- PV) \times ((LSA – LSAv \times PV) \div (1-PV) \times PV) + (\uparrow LSTv \times PV) \tag{12}$$

Where ↑LSTv is the highest LST value recorded on the full vegetative cover pixels, ↑LSTn is the highest LST value recorded on a non-vegetative cover pixels over a particular open space (dry soil), LSEn and LSAn are the emissivity and absorptivity of the non-vegetative cover pixel used in the expression as the highest LST, LSEv × LSAv are the emissivity and absorptivity of the full vegetative cover pixels. The LST values shown in this output image represent the maximum values for each land class under a particular weather condition (Figure 5-3).

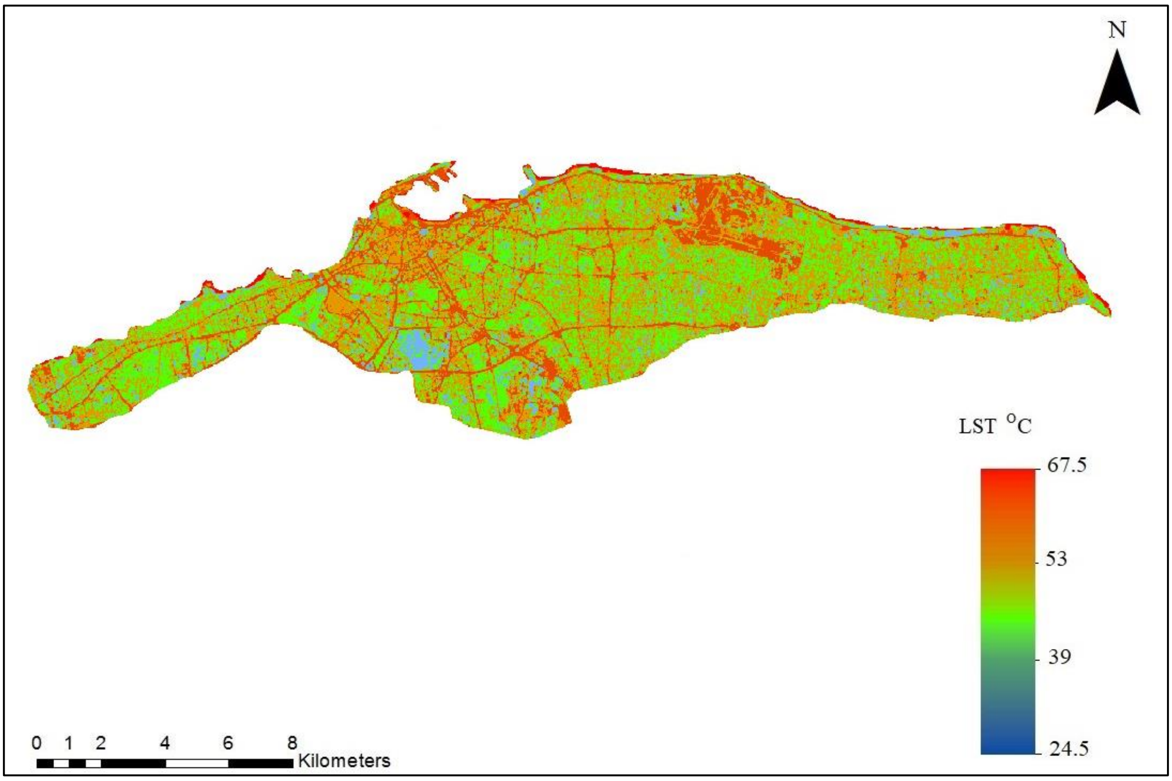

Figure (5-3). The estimated Landsat LST at around midday, as free of the shadow effect extracted from the converting image (1:15 pm).

5.6. The effect of time of day on the relationship between LST and urban land cover

The scatter plot model is performed in this chapter to analyse bivariate relationships. In addition, a sample of 80 LST points collected from equally different land cover (vegetation, buildings, asphalt roads, open land) will be used to identify the variation of LST among different classes.

5.7. Results

5.7.1. The effect of time of day on the relationship between LST and the density of vegetation

The result shows a significant different between the below three figures (5-4), which represent the relationship between LST and the density of the vegetation cover under three different conditions related to the time of day. The proportion of the vegetation (PV) image is plotted here with the three different LST images which could allow more linkages between LST values and the different proportions of vegetation to be obtained, making the effect of time of day on the shadow in the morning image more detectable. In other words, it can contribute to maximizing the correlation between LST and PV to make the effect of time of day on the LST spatial variation between the images more comparable. Figure (A) presents the relationship during the morning time (9:40 am), which clearly indicates a weak positive correlation ($y = 33.5x + 4.6$ and $R = 0.21$), where the LST values tended to increase with increased vegetative cover. Figure (B) uses the converted Landsat LST image (at 1:15 pm when temperature is around its peak) to be plotted with the proportion of vegetation, the relationship between the variables in this figure is clearly opposite to that in figure (A), where the line-trend of this figure shows an obvious negative relationship between LST and the density of the vegetative cover ($y = 44.9x + 0.092$ and $R= 0.12$), where the temperature decreased with an increased percentage of vegetative cover, and vice versa. Figure (C) shows this relationship with the lowest effect of shadow for every single pixel, where it becomes strongly negative ($y = 2.53x- 0.051$ and $R = 0.44$).

(A)

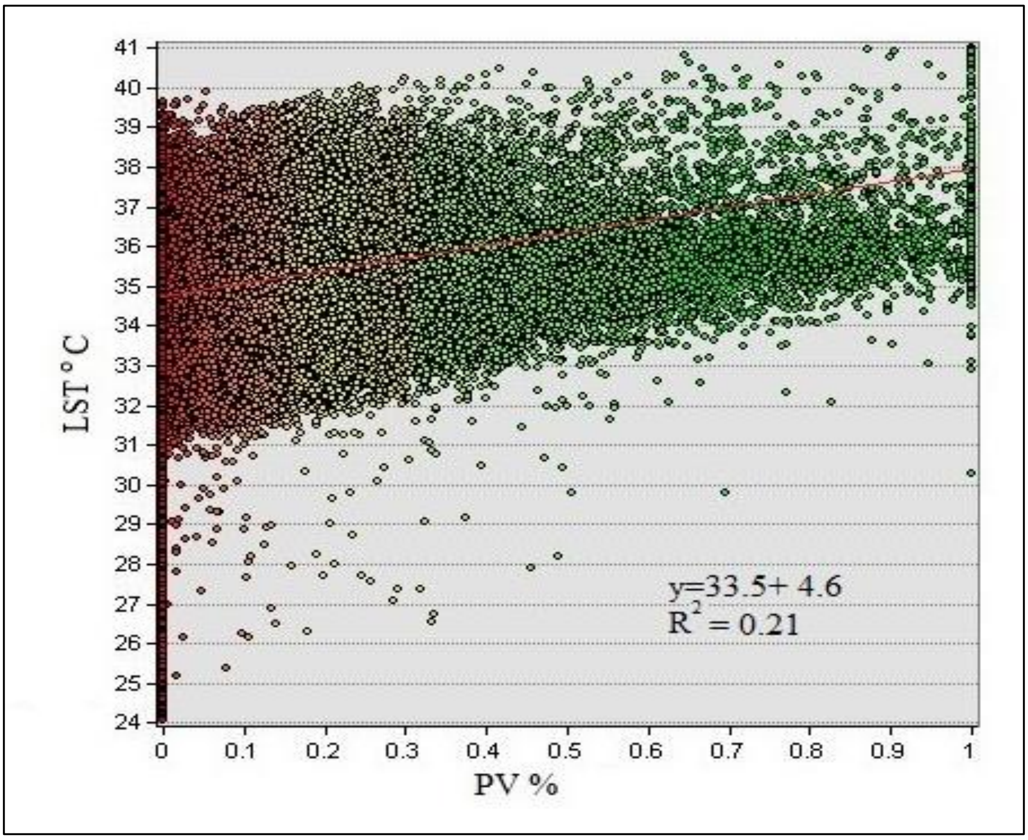

(B)

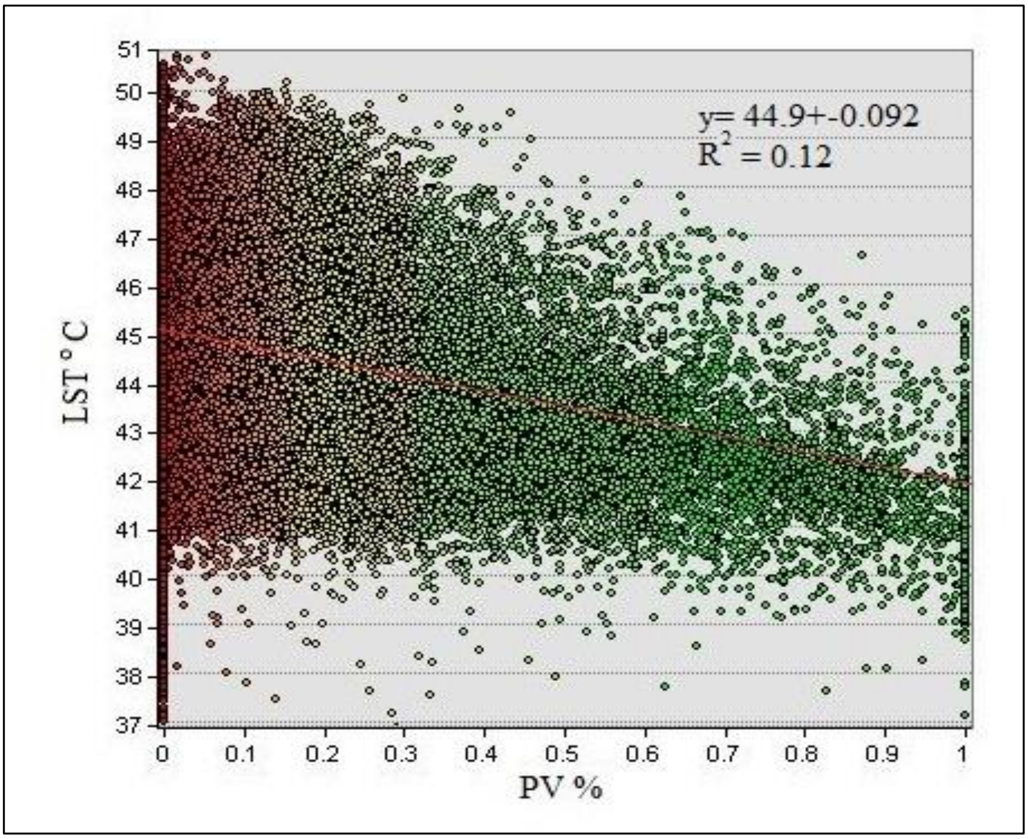

(C)

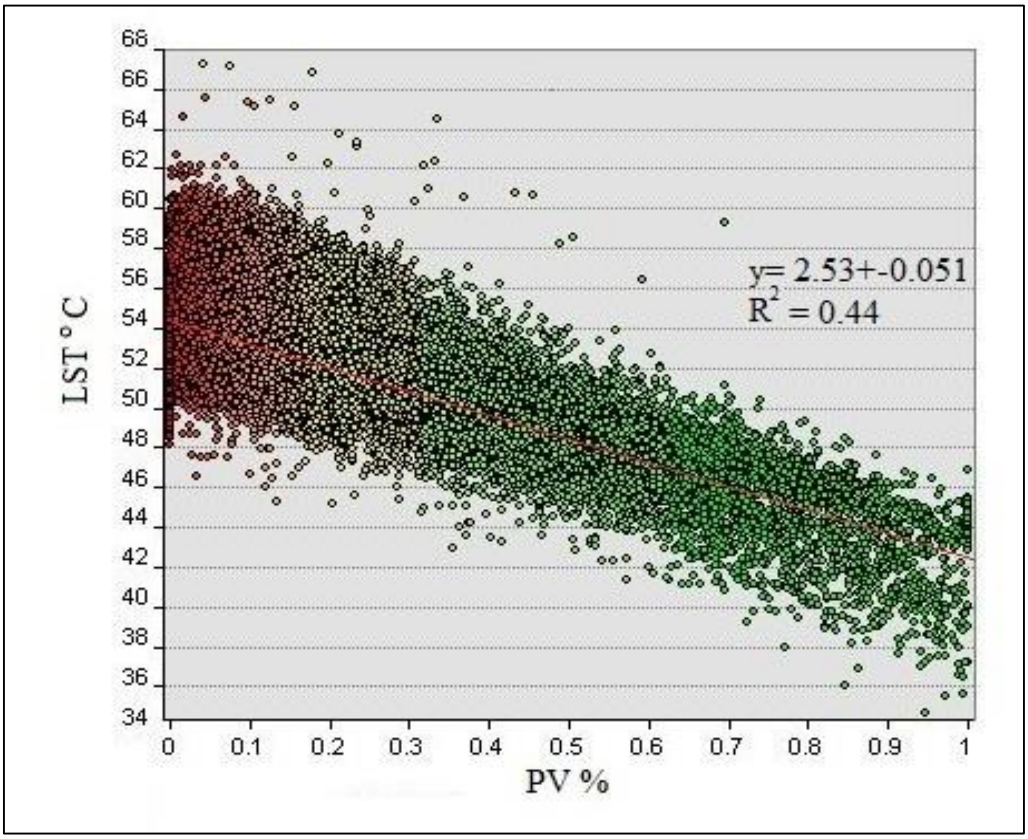

Figures 5-4: The relationship between LST and the proportion of vegetation under three different conditions: (A) represents morning time, (B) represents a local peak in temperature, and (C) represents the minimum effect of the shadow for all pixels.

5.7.2. The effect of time of day on the relationship between LST and different land cover classes

Figure (5-5) presents further information about the effect of the time of day on the relationship between LST and different forms of urban land cover (building areas, full vegetative cover, asphalt roads, and open land area), represented in a sample of 80 points (20 points for each class) collected randomly, including the minimum and the maximum values, to verify how these LST points are distributed and effected by changing land cover types at two different times of day (A represents 9:40 am and B represents 1:15 pm). Figure (A) shows there is an overlap between the boxes or classes, especially among those representing vegetation, buildings, and asphalt roads, which means there is a weak correlation between these forms of coverage and LST, while the open land area appeared more distinctive with regard to maximum levels of LST due to being exposed to a greater amount of incident radiation. In contrast, figure (B) gives significant different indications about the correlation between LST and these urban land during the peak in temperature (1:15 pm), which clearly shows the role or effect of different land classes on the spatial variation of LST, where the relationship between these land cover patterns and LST becomes more recognisable through the spaces between the boxes, especially the range of LST over vegetative cover which shows the minimum of LST.

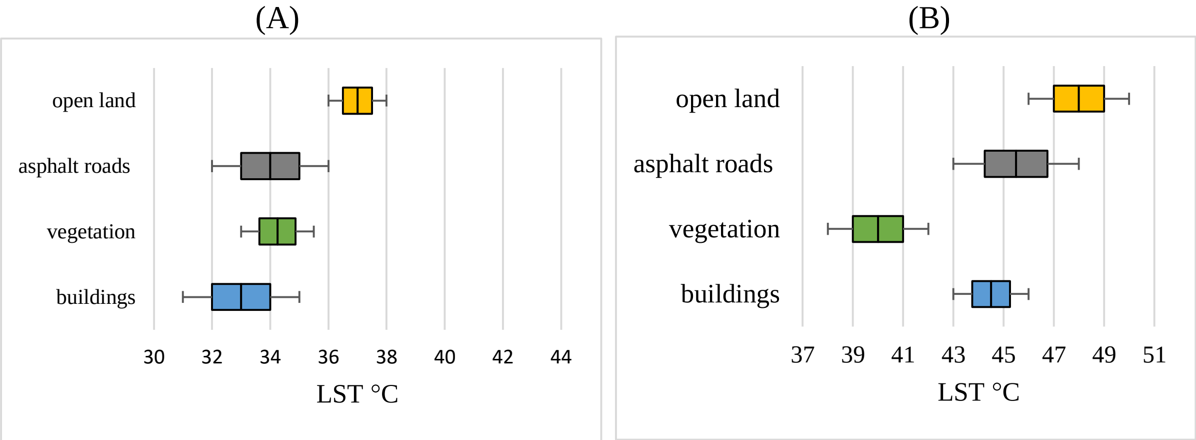

Figure 5-5: The spatial variation of LST including mean, min, and max values for different land cover classes (buildings, asphalt, barren land, and vegetation) during two different times of day; at 9:40 am the Landsat overpass time, and at 1:15 pm, the time estimated to represents a local peak in LST.

5.8. Discussion

This chapter is dedicated to the investigation of the impact of time of day on the spatial structure of LST by comparing the spatial variation of LST derived during the morning time when the Landsat satellite normally overpasses the study area (9:40 am local time), and the spatial variation in LST derived at the time when the temperature is expected to reach a maximum using the converted Landsat image (1:15 pm local time), contribute to identify the impact of the sun angle and associated factors such as the intensity of the incident radiation and building shadows on the relationship between LST and land cover, which in turn can cause a misconception of this relationship. This impact can be minimized by determining the ideal time at which to estimate LST and observe its relationship with urban land covers.

It was found that the spatial variation in the LST is affected significantly by the time of day, which is variable depending on the angle of the sun with the ground, so that LST variation can be shown to be more noticeable or at its greatest when temperature reaches a maximum and vice versa, supporting Mathew *et al.* (2018) and Zhou *et al.* (2013). Figure (5-4) shows the different LST images plotted with the proportion of the vegetation (PV) to reveal the extent of the effect of time of day on the relationship between these two variables, by influencing the amount of the incident solar radiation, which is normally more powerful during the morning due to the angle of the sun. During the morning, as per figure (5-4, A), the LST values are controlled less by the surface, resulting in an understandable variation in LST between vegetated and the non-vegetated pixels. By contrast, in figure (5-4, B), when the LST values are strongly distributed based on the surface patterns, the relationship between LST and PV became clear and sensible. For this reason, the relationship between the LST and the density of vegetation appeared to be clearly different between the morning (9:40 am) and during the peak in temperature (1:15 pm), where during the morning this can be shown to be slightly positive with density of vegetation, while this clearly became strongly negative during a local peak in temperature which also coincides with a reduced effect of shadow. Figure (5-4, C) illustrates the impact of the shadow according to time of day, as hypothesised by Weng *et al* (2004). Unlike the spatial variation in LST during peak temperatures, the distribution of LST during the morning time was not clearly associated with the spatial variation in the land surface patterns, where the LST for a particular pixel might be significantly lower or higher than others, are shown similar surface properties, essentially due to the unequal distribution of the incident solar radiation during the morning; in other words, the areas that are more open to the sun, whether they are in a natural form such as dry soil or in an unnatural form such as concrete surfaces (airport), show higher LST values of up to around 38°C regardless of their specific properties, which is in agreement with Coops *et al.* (2007) and Nichol (1998).

The absence of a clear correlation between LST and urban land cover patterns during the morning indicates the weak role of surface properties in distributing LST and being responsible for generating the heat. Shadow and other accompanying factors such as surface moisture have a strong influence on the control of the special variation of LST during this period, which affects the trend line in the relationship between the surface cover and LST, and thus was not consistent with the prevailing belief that built-up areas, such as urban centres, show the highest LST values. This results in the phenomenon known as urban heat islands (UHIs) in a relationship that is otherwise supposed to have a negative correlation with the density of vegetation and not the opposite, as shown in Figure (5-5).

The influence of land cover patterns on LST during the time estimated to represent a maximum in temperature was explored to be the highest, where LST values was clearly controlled by land coverage patterns. LST values were found to be similar across classes and pixels that were otherwise homogenous in their properties, and varied depending on the land surface type, whereby the sun being at a zenith and the minimal effect of shadow distribute the amount of the incident radiation more equally among the different classes than at earlier times. This effect was far more apparent over residential areas as these are affected to a greater extent by the angle of the sun compared with open areas, and it is therefore possible to say that when the majority of the surfaces in cities are covered by buildings, such as is the case for this study area, the sensitivity to the angle of the sun will be more obvious than for other areas. The open areas where there was no or a minimal shadow effect over a longer time showed the highest LST values, such as the airport runway and the surrounding grounds at around 49°C versus around 44°C in the city centre.

The above also showed that despite the diversity in the land surface cover, the LST variation during the morning was not recognisable. However, by measuring LST during peak temperature to minimize the effects related to time of day one can reduce scatter or noise, where the differences in LST among the homogeneous pixels is minimized, which means the distribution of the LST values are controlled more by the surface behaviour of each pixel. This is also demonstrated by Figure (5-5), where the effect of time of day on the spatial variation of LST is apparent. The distribution of LST over different urban land covers was dramatically changed between the morning and at estimated peak temperature. For example, the coolest class during the morning was over the built-up area, while during peak temperature the vegetation cover showed the lowest LST value. Despite the different patterns of land surface, the LST values during the morning appear similar or even intersect, while the variability between the different classes during peak temperature was greater than during the morning.

Studying LST during peak temperature can reduce – though not eliminate – any associated uncertainty because of the difference in the duration of exposure to sunlight, which is the reason for the differences even though they represent the same day and area. In addition, measuring LST during a local solar zenith time can gave an opportunity for those surfaces which are hidden from the sun to absorb and generate heat energy in proportion to the ability or properties of the associated classes, which contributes to the associated reduction in LST differences within the homogeneous classes or pixels and increase in LST differences between heterogeneous classes or pixels. Furthermore, this time is the most convenient during daytime for identifying the relationship between LST and different land cover.

Chaper 6. Assessment and enhancement of the temporal variation of LST over a time series

6.1. Introduction

Studying the spatial and temporal variation in LST using thermal remote sensing data allows for an assessment of the magnitude of the impact of human activities on change in temperature, and indeed on the climate in general. However, in some cases, such as this study area, the temperature is characterised by extreme values, resulting in exceptional conditions that would otherwise affect the accurate determination of change in LST as a time series; in addition, similar to the effect of time on the spatial variation of LST, the lack of high-resolution satellite thermal data to allow for an estimate of LST during the maximum in temperature can also provide questionable results when studying temporal variation of LST the due to shadow or weak solar irradiation during the morning, as compared to the peak period. Therefore, these two different aspects need to be investigated and taken into account when studying changes in LST over time.

This chapter seeks to improve the study of the change in multitemporal LST images by investigating two different expects: the difference between using a single image and more than one image in the form of an average representing each year; and a consideration of the effect of the time of day by examining the differences between the use of LST images recorded in the morning at the Landsat overpass time of around 9:40 am, and images estimated at peak temperature (1:15 pm, using the processes presented in chapter 4).

6.2. Data preparation and methods

This section presents the required data and the methods that are used to achieve the objective of this chapter.

6.2.1. Morning Landsat LST images (satellite overpass time)

12 multitemporal Landsat LST images were extracted from Landsat 5 and 8, as collected from the summer months (July, August and September) for the years 2005, 2009, 2013, and 2017, which were selected according to the start of the SEVIRI products and difficulties with using Landsat 7, so that three cloud-free satellite images from each year were collected, as provided by the United States Geological Survey (USGS) Earth Explorer website (http://earthexplorer.usgs.gov/). The processes presented in previous chapters for retrieving LST from Landsat and for obtaining estimated LST images during times of peak temperature are applied here to prepare the images required for this chapter, as shown in table (6-1). The Landsat LST images that are retrieved from both Landsat 5 and 8 will be considered later in this chapter.

Table 6-1: The LST images extracted from Landsat 5 and 8 for use in this chapter

Details / sensor	Time				clouds
	years	Number of images	Months	Local time	
Landsat 5	2005	3	July, August, and September	9:30 am to 9:40 am	0 % clouds
Landsat 5	2009	3	July, August, and September		
Landsat 8	2013	3	July, August, and September		
Landsat 8	2017	3	July, August, and September		

6.2.2. LST images estimated during times of peak temperature (images converted for estimate at 1:15 pm).

The processes used in Chapter 4 to convert Landsat LST from the satellite overpass time to one appropriate to the time of peak temperature are applied here to convert all the LST images reported in table (6-1).

6.2.3. Creating the average images for each year

Three images for each year (July, August, and September) at both times of day (morning and at peak temperature) will be combined to obtain one image for each year as an average.

6.2.4. Normalized differenced LST index (NDLI).

This chapter applies another method by which to identify changes in LST in terms of the changes of area covered by different LST rates, and further applies this to the LST values that need to be converted to a normalized LST index, which can be used to rearrange the LST values in the different images in the same template in order to make them range between 0 to 1. The index enables the extent of the LST values to be normalized to make them comparable and allows the investigation of how NDLI rates cover the study area (in units of area of km²), and then how the time of day influences the changes in this distribution over the years.

The averaged images at both times of day (morning and during peak temperature) are converted here to different normalized LST indexes using the following equation:

$$LST^{*} \frac{(LST - LST_{\circ})}{(LST_{s} + LST_{\circ})} \qquad (12)$$

Where LST* is the normalised LST. LST, LSTs and LST∘, represent the LST image, and the maximum and the minimum of the LST, respectively, for the study area of a particular image.

By preparing the required LST data estimated at different times and conditions, the temporal changes in LST can be investigated over these different cases.

As a first step, the effect of the extreme values of LST is examined in this chapter to identify and eliminate their effect when analysing the effect of time of day.

6.3. Investigating the effect of the extreme values of LST on its temporal changes

The changes in LST over the years, as represented across single seasonal images (August) as a mid-season measurement, are applied for comparison with the changes over these years using the averaged images for the three months of July, August and September to assess how well the use of a single image represents the year when analysing change in LST as a time series (6-2). This change will be investigated in terms of two different approaches, as follows:

6.4. Results

6.4.1. In terms of the three main levels of LST (minimum, maximum and mean).

Table 6-2: The three main levels of LST (minimum, maximum and mean) as single data (s) and as seasonal averaged from July, August and September (v) for several years (2005, 2009, 2013 and 2017), to assess the role of using seasonal averaged data in providing more representative images, through comparing the changes in these levels across the years (rate of change).

LST levels / Year	min	max	mean
2005s	23.0	35.0	30.0
2009s	23.0	36.0	30.0
2013s	29.5	41.0	35.0
2017s	24.0	41.0	34.0
Rate of change	0.24	0.57	0.42
2005v	25.0	41.0	35.0
2009v	22.5	38.0	32.0
2013v	25.0	38.0	32.5
2017v	26.0	42.5	35.0
Rate of change	0.13	0.11	0.01

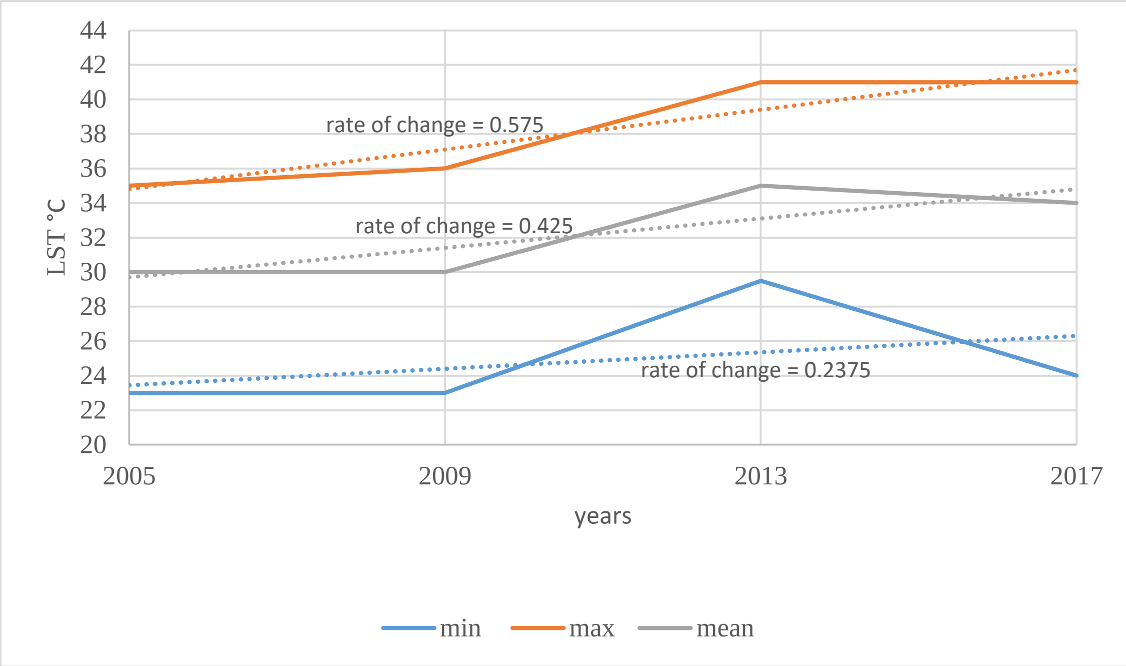

Figure 6-2: The changes in the three main measures of LST (minimum, maximum and mean) across the years when using a single image to represents each season.

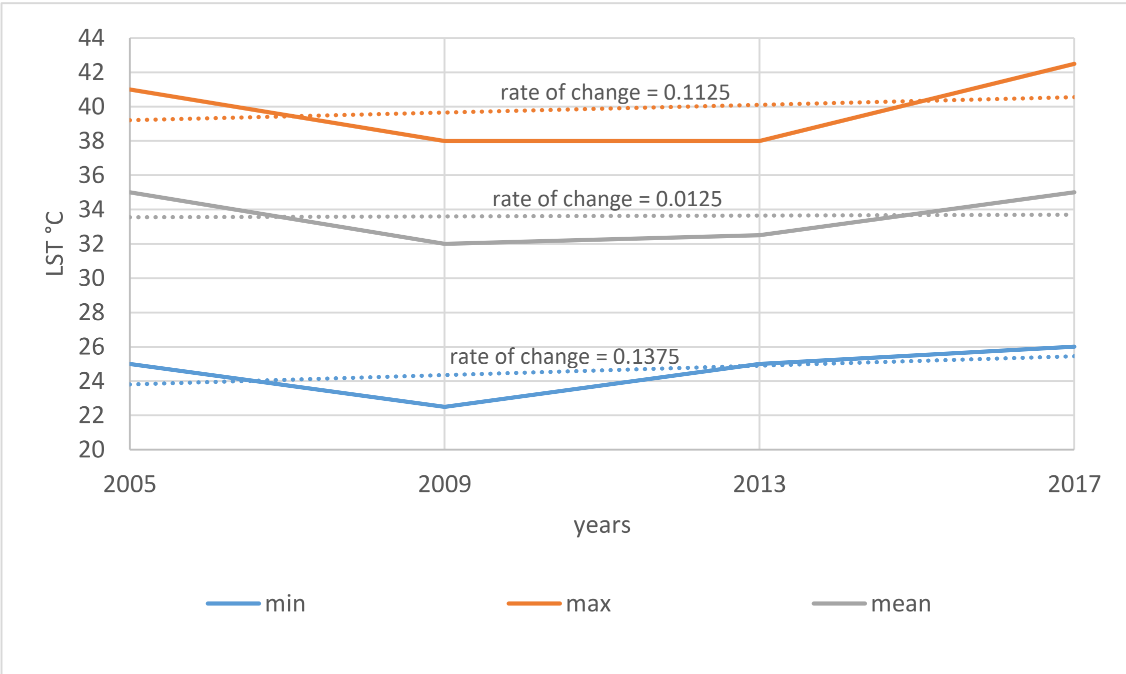

Figure 6-3: The changes in the three main measures of LST (minimum, maximum and mean) across the years when using seasonal averaged data from July, August, and September to represents each year.

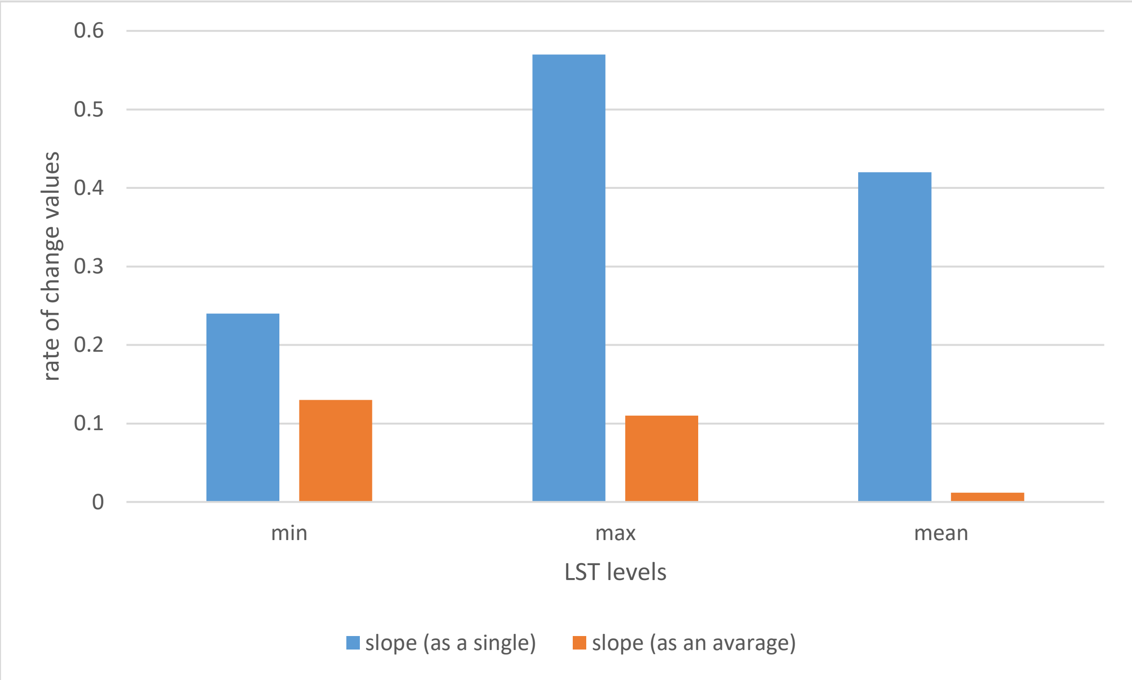

Figure 6-4: Comparing the change (rate of change) in the main measures of LST (minimum, maximum and mean) for the years 2005, 2009, 2013 and 2017, provided by using the two earlier approaches (single and averaged image).

By observing the details presented in Table (6-2) and Figures (6-2) to (6-4) it can be seen that there is a difference between using the single image and the average image method for studying LST changes over the years. The LST values, when using the single image method, show greater differences and more fluctuation over the years, as per Figure (6-2), compared to when using the average image mode which appeared more regular, as per Figure (6-3). Also, the first method showed that 2013 recorded the highest LST values, while in the second method these values were recorded in 2017; in addition, this difference was followed by a difference in the line trend for the years (gradient), so although both methods show an increase in LST values over the years, the single image method increases more obviously, especially for the maximum and the mean levels, as per Figure (6-4), which is not accurate where they showed an increase of several-fold compared to the increase shown by the average images method.

6.4.2. In terms of the spatial distribution using normalized LST difference LST* categories in an area unit (km²).

This demonstrates the effects of using the two earlier approaches (single and averaged image) on the changes in the spatial distribution of different 10 categories of normalized difference LST index (LST*) in an area unit (km²) over the four years (2005, 2009, 2013 and 2017) to assess the differences that may occur as result of using a single image to represent a season.

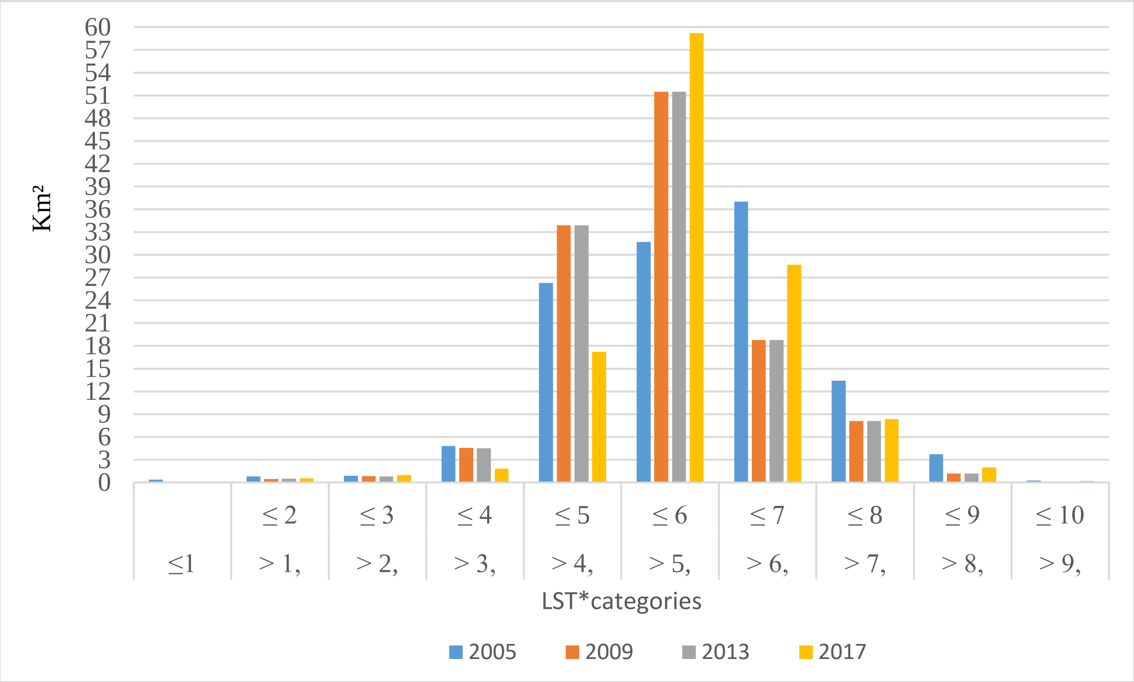

Figure 6-5: The changes in spatial distribution of 10 different categories of LST in km² when using a single image for representing each year of the four years (2005, 2009, 2013 and 2017).*

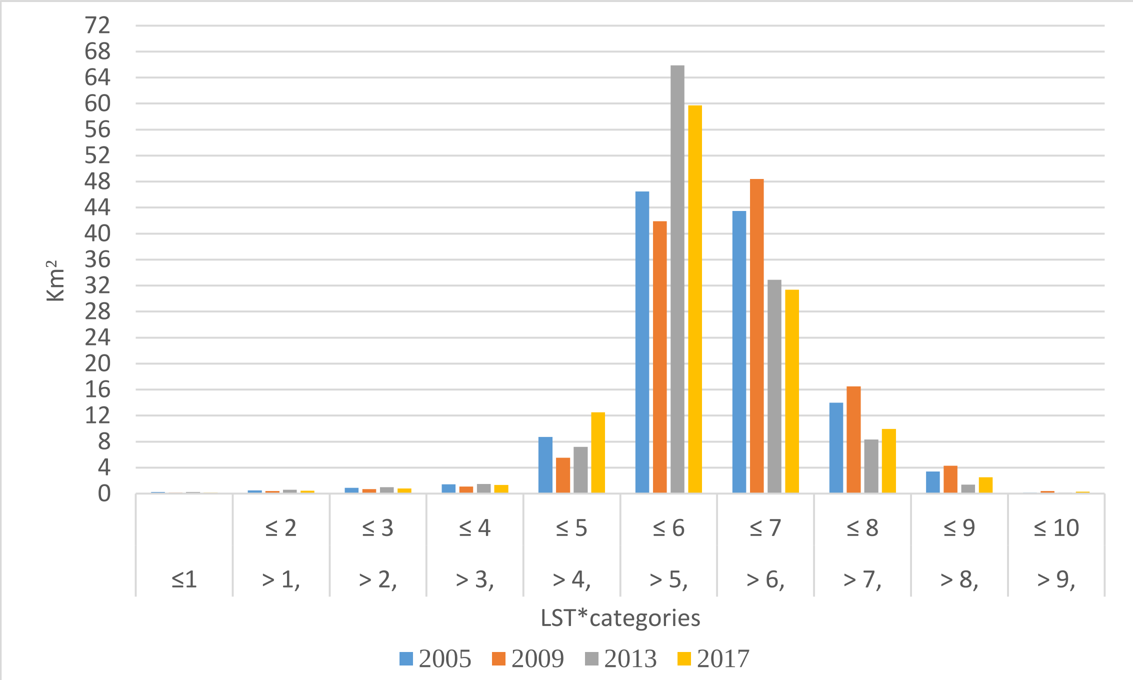

Figure 6-6: The changes in spatial distribution of 10 different categories of LST in km² when using when using seasonal averaged data from July, August, and September to represent each year.*

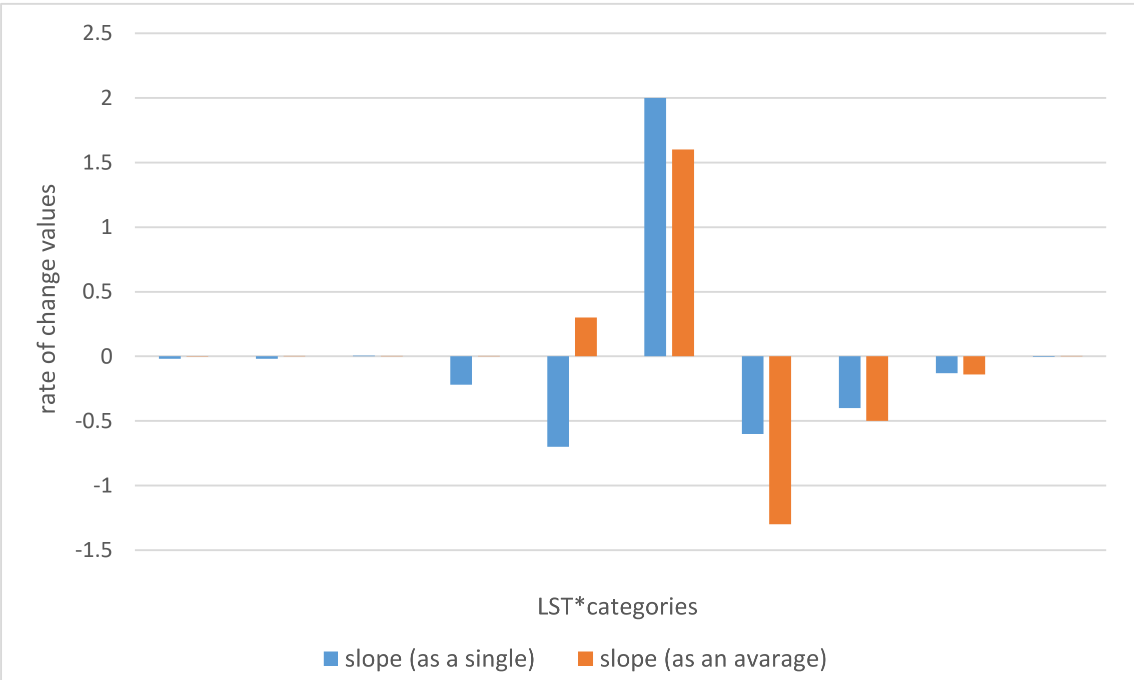

Figure 6-7: Comparing the changes in spatial distribution of 10 different categories of LST in km² for the years 2005, 2009, 2013 and 2017, provided by using the two earlier approaches (single and averaged image).*

Similarly, these differences were also clear in terms of the spatial distribution of the spaces covered by different LST categories via the LST* index, where the values were not compatible. Both methods showed that the medium LST* categories covered the largest areas, as per Figures (6-5) and (6-6), while the low and the high LST* categories covered the small spaces around the study area. However, Figure (6-7), which differentiates between the changes showed by these two methods, the coverage of LST* categories was unevenly changed, while some categories in the single image method showed increasingly large changes over these four years, while there were negative changes when using the averaging method, with some categories showing an increase but at a different pace.

6.5. Investigating the effect of the time of day on the temporal variation of LST over the years

The changes seen using the average images (July, August and September) for the years 2005, 2009, 2013 and 2017 in the morning (Landsat overpass time) were compared with the changes in the other average images that represented the peak temperature (converted images at 1:15 pm). This comparison is applied in terms of the two different ways that were used earlier.

6.6. Result

6.6.1. In terms of the effect on the three main measures of LST (min, max and mean)

Table 6-2 The three main levels of LST (minimum, maximum and mean) as seasonal averaged data during two different times of day for the years 2005, 2009, 2013 and 2017, to assess the effect of the time of day on the temporal variation (rate of change) of LST over the years.

year \ LST levels C°		min	max	mean
Morning time (9:40 am)	2005	25.0	41.0	35.0
	2009	22.5	38.0	32.0
	2013	25.0	38.0	32.5
	2017	26.0	42.5	35.0
	rate of change	0.13	0.11	0.012
Peak time (1:15 pm)	2005	35.0	53.0	45.0
	2009	32.0	49.0	42.0
	2013	35.5	47.0	41.0
	2017	38.5	53.0	46.0
	rate of change	0.35	-0.05	0.5

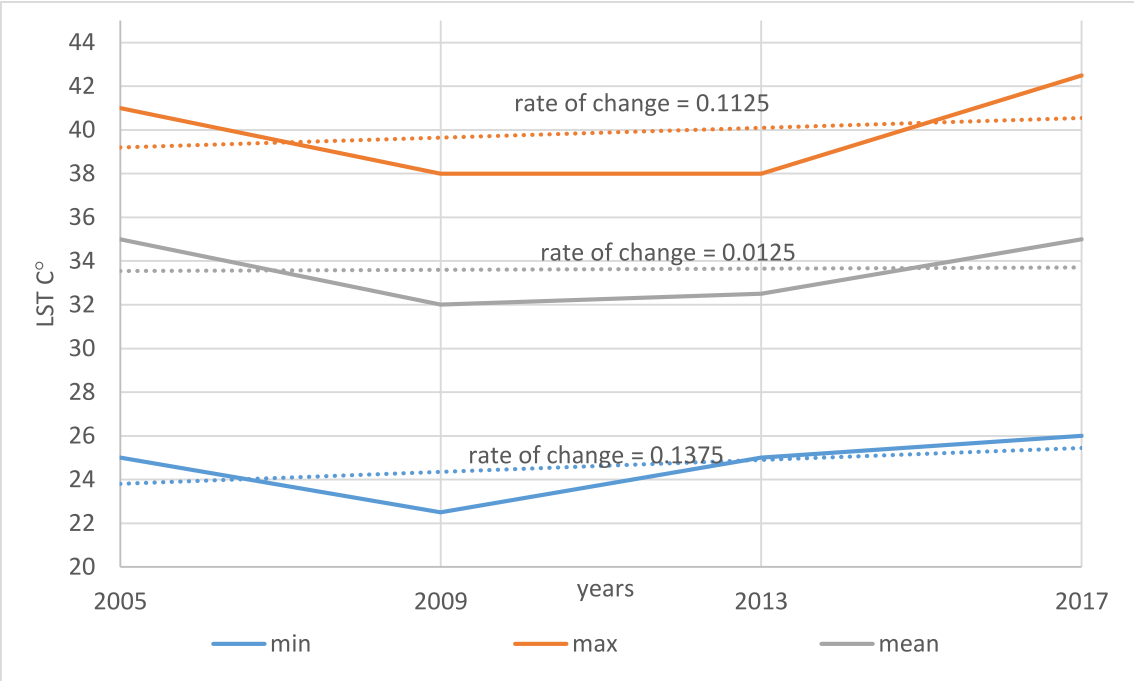

Figure 6-8: The temporal changes in the three main measures of LST (minimum, maximum and mean) across the four years 2005, 2009, 2013 and 2017 when using morning images (Landsat overpass time 9:40 am).

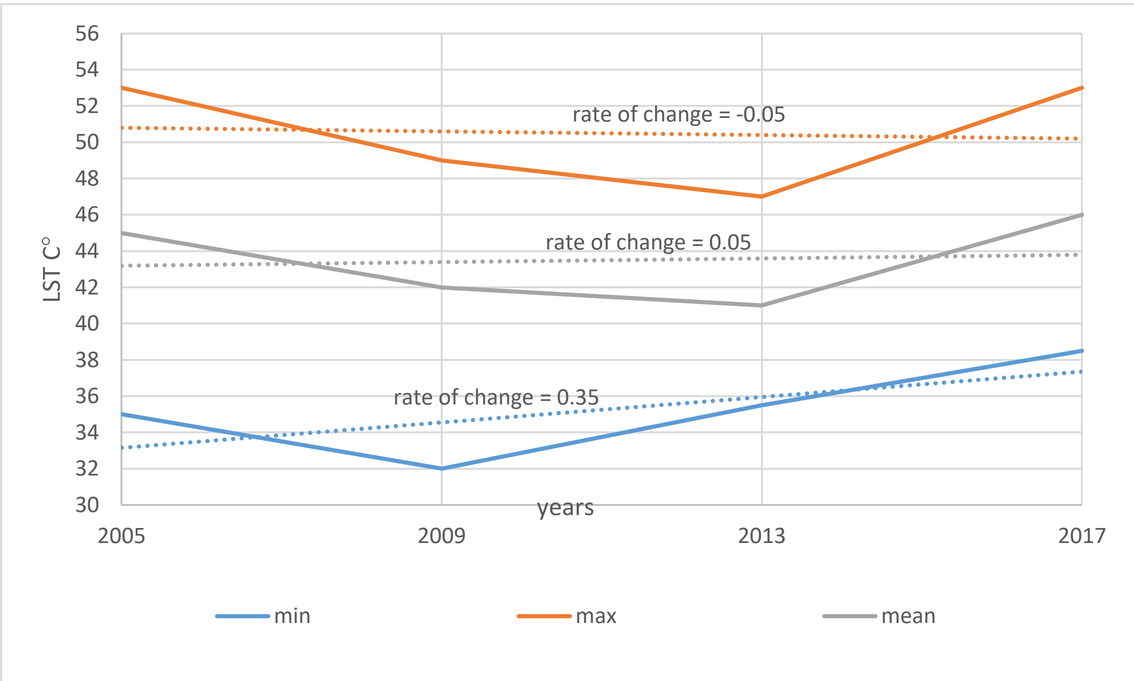

Figure 6-9: The temporal changes in the three main measures of LST (minimum, maximum and mean) across the four years 2005, 2009, 2013 and 2017, when using images estimated at a peak of temperature(1:15pm).

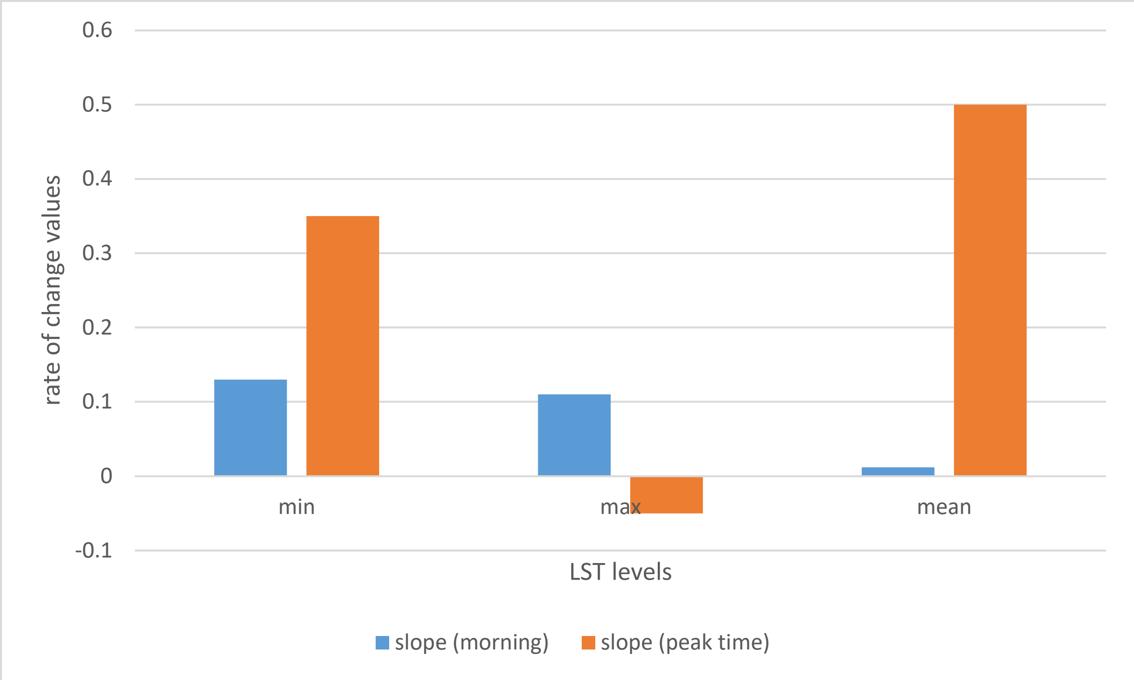

Figure 6-10: Comparing the temporal change in the main measures of LST (minimum, maximum and mean) across the years 2005, 2009, 2013 and 2017, provided by using images estimated during the morning and others estimated during the peak in temperature.

Tables (6-4) and Figures (6-8) to (6-10) show the effect of the time of day on studying change in LST over the years, where the results clearly show that there is a significant effect on the temporal variation of LST due to time of day through the differences shown by observing the figures representing the morning images (Landsat overpass time 9:40 am) and others for the images estimated during peak temperature. The overall change for the main measures of LST (minimum, maximum and mean) is one of a slight increase, and similarly when using the morning images, as per Figure (6-8), while these LST levels were changed differently, showing positive and negative changes when using the peak temperature images. For example, for the morning images, the maximum LST shows an increase over the years; however, for the estimated images for 1:15 pm, this level shows a tendency to decrease. Equally important, the minimum LST for the morning images shows a smaller increase than is shown by the estimated images for 1:15 pm, as per Figure (6-9). In addition, these differences were followed by a difference in the line tend over the years, so although both times show approximately similar line graphs, Figure (6-10) shows that the change when using the images for the peak time are greater and more obvious then when using morning images, especially with regard to the mean values.

6.6.2. In terms of the spatial distribution using normalized LST difference LST* categories in the area unit (km²).

This demonstrates the effect of time of day on the changes in the spatial distribution of different 10 categories of normalized difference LST index (LST*) in the area unit (km²) over the four years (2005, 2009, 2013 and 2017), to assess the differences that may occur between using the morning Landsat LST images and the images estimated to represent the peak of LST.

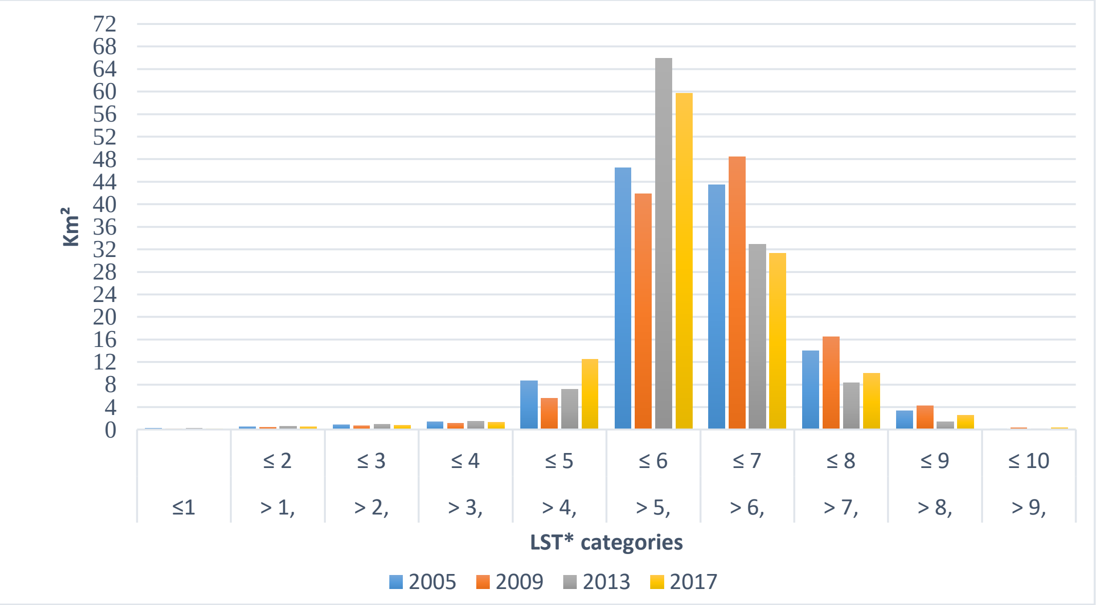

Figure 6-11: The changes in spatial distribution of 10 different categories of LST in km², across the four years 2005, 2009, 2013 and 2017 when using morning images (Landsat overpass time 9:40 am).*

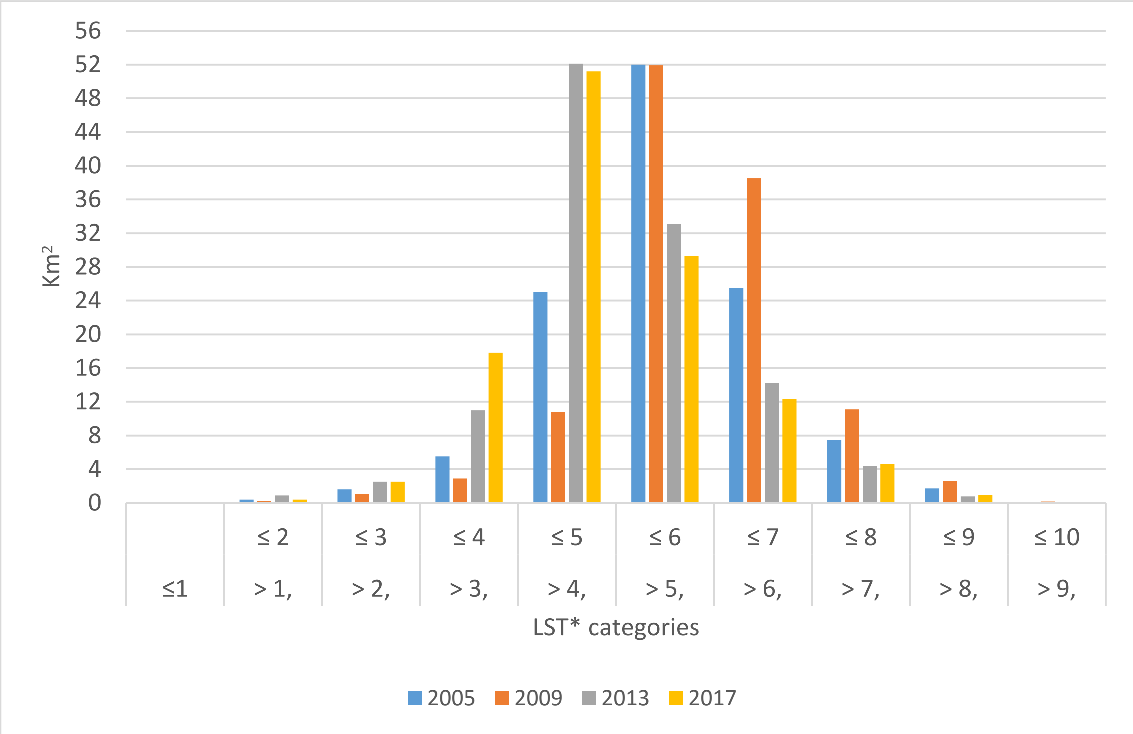

Figure 6-12: The changes in spatial distribution of 10 different categories of LST in km², across the four years 2005, 2009, 2013 and 2017, when using images estimated at a peak of temperature (1:15 pm).*

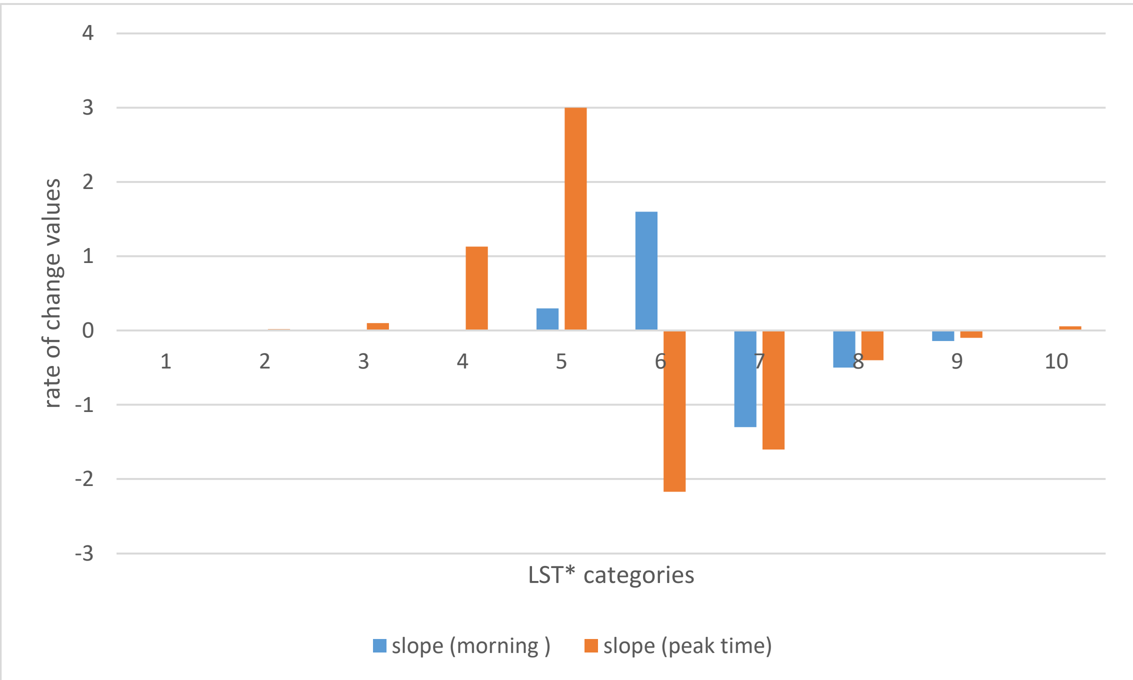

Figure 6-13: Comparing the changes in spatial distribution of 10 different categories of LST in km² for the years 2005, 2009, 2013 and 2017, provided by using images estimated during the morning and others estimated during the peak in temperature.*

Similarly, the effect of time of day was also clear in terms of the effect on the spatial distribution of the areas covered by the normalized different LST index LST* categories, which indicate that special distribution of LST was not compatible between the images in the morning and the others representing the peak in temperature. Both of these different times show that the medium LST* categories cover the largest areas, as pre Figures (6-11) and (6-12), while the low and the high LST* categories covered small spaces around the study area. However, Figure (6-13) shows that this distribution changed unevenly over the years for the two different times of day, as is clearly seen though category (6), where this category increased for the morning images and decreased for the images representing the peak temperature. The differences are similar to the other categories; whilst an increase was observed in some categories for both times of day, they were at a different pace.

6.7. Discussion

This chapter seeks to address certain controversial issues related to the study of the temporal variation of LST using satellite data, as represented in the investigation of the effect of time of day on the temporal change in LST that may result from the variability of the intensity of the incident sun radiation and the shadow, as achieved by comparing the changes in LST across the years 2005, 2009, 2013 and 2017 using two different time of day, the morning (the overpass time of Landsat 9:40 am locally) and the time when the temperature is estimated to be at its peak (Landsat images at 1:15 pm estimated by the presented conversion method). In addition to assessing the effect of the extreme in temperature on the dataset to represent seasons, by comparing the change in LST across the years 2005, 2009, 2013 and 2017 using one single image from each summer season of the year and the change by using the images in a form of average over the summer months. This analysis would examine and minimize the uncertainty caused by these issues and enhance the study of LST changes over years and identify its relationship with the changes in urban land cover.

It was found that there is a distinct difference between the change shown by using the single images and the averaged images with regard to representing seasons when studying LST changes across the years. The LST values when using the single image approach showed greater differences and greater fluctuation between years compared with the averaged image, where they appeared more regular. Also, using the single images showed that 2013 recorded the highest LST values while in the second method these values were recorded in 2017. This difference is followed by a difference in the overall trend of the years, where it was clearly seen that although both approaches showed an increase in LST over the years, the use of single images showed a greater increase, especially at the maximum and the mean levels of LST where they increased several times compared to the increase shown by the use of the average images. These differences can obviously explain the effects of the extreme values of LST on obtaining a representative dataset for studying temporal variation, which in turn could affect the validity of the findings. Studying temporal variation of LST needs to be conducted using the seasonal images in the form of averaged images rather than relying on single seasonal datasets to represent each year so as to minimize the uncertainty that can be caused by extreme values of LST.

In terms of the effect of time of day on the temporal variation of LST, it can be hypothesized that using LST data estimated during the morning might not be accurate enough as a result of the angle of the sun and associated factors such as shade. The results found that the comparison in both period; the morning time (the local overpass time of Landsat 9:40am) and the time when the temperature is expected to be reached a peak (Landsat images at 1:15 pm estimated by the presented conversion method) showed that the time of day can significantly effect on the temporal variation of LST over the years, the overall change for the three main LST levels (minimum, maximum and mean) increase slightly and similarly when using the morning images while these LST levels were changed differently as positive and negative change when using the images for the peak time. The variation when using the images representing the peak time were greater and more obvious then when using the morning images. In addition, these differences were followed by a difference in the spatial distribution of the areas covered by the normalized different LST index LST* categories, where the figures were not compatible between the images for the morning and those representing the peak in temperature.

The results prove whether there is a difference between using the single and the averaged image approach as well as using the morning images and the images estimated during the peak of temperature, it indicates to the inaccuracy that can be occurred in the results processed according to the available high spatial resolution thermal data and the approach used previously (single seasonal images), on the other hand the differences mean that the influencing factors can be minimized by enhancing the methods to achieve a minimum uncertainty in the results which is by using LST images estimated during the peak of temperature instead of being during morning time to reduce the effects associated to the sun angle, as it was clearly found in the figures (6-8) to (6-13), in addition to this the LST images of time series need to be used in a form of averaged seasonal images rather than being as single images, for the purpose of obtaining more representative images through minimising the extreme in temperature, which in turn would affect the correct trend line of the LST change over time series as it was clearly shown in the figures (6-2) to (6-7).

Chaper 7. General Discussion and Conclusions

This chapter is divided into four parts: The first section (1) gives an overall discussion, which presents the findings gained from the research questions addressed in Chapters 4, 5 and 6. The second section (2) identifies the contributions this research makes to current understanding. The third section (3) gives a set of concluding remarks to this study. Finally, the research presents directions for future research, which are recommended to build on the work from this study, as based on the present findings.

7.1. General discussion

This study focussed on addressing the Landsat LST data in terms of the time measurement of the satellite by creating a method to covert images taken in the morning (the satellite overpass time) to those representative of the local zenith to allow investigation of the effects of time of day on the study of the spatial and temporal variation of LST. The satellite sensors, which include the ability to detect thermal wavelengths, have facilitated the study of LST, especially those that provide high spatial resolution data such as Landsat, which is the most commonly used in this regard. However, the lack of high spatial resolution data from which one can estimate LST at a local zenith when the temperature is at a maximum results in maximizing some effects such as shadow and the weak concentration of the incident solar radiation which, in turn, can affect the amount of incoming and outgoing energy and thus the reliability of the analysis when studying spatial and temporal variation in LST (Petropoulos *et al.* 2009).

This research presented a method to improve the spatial and temporal study of LST derived by Landsat data across multiple years (2005, 2009, 2013 and 2017) in a large city setting in a southern Mediterranean climate system. The city of Tripoli in Libya was selected for this study. The research focussed on addressing two main issues which have long been weaknesses in the study of LST. The first is the impact of the time of image acquisition on modelling the spatial and temporal variations of LST. The second is to diagnose the effect of extreme values of temperature on the images representing seasons when studying LST changes over a time series. This method is based on converting Landsat LST data from the satellite overpass time (9:40 am) to a time estimated to be around a peak temperature (around 1:15 pm). Furthermore, each image in the time series is calculated in a form of an average of three images from the summer months (July, August, and September) with the aim of reaching more representative images which can minimize the effects of extreme values of temperature rather than images being used in a standalone manner.

The study used remote sensing data extracted from Landsat 5 and 8 (30 m resolution) and the Spinning Enhanced Visible and Infrared Imager LST products (SEVIRI 3 km resolution), in addition to LST-based measurements collected from the ground. The method is based on the use of an increasing difference between the morning and peak in temperature (ΔLST), which taken as the difference between the mean value from Landsat at the satellite overpass time (9:40 am) resampled to SEVIRI resolution, and SEVIRI at a time when the temperature is around a maximum (1:15 pm). This value then need to be processed as a black body value (absorptivity LSA = 1, emissivity LSE = 1) and then redistributed to the Landsat LST image based on the pixel properties (being absorptivity (LSA), emissivity (LSE) and the transpiration effect estimated from ground measurements). The results of this conversion method showed an accuracy in the standard error of 1.7°C, and R = 0.82 is achieved when compared with actual ground-based measurements. The study found that the spatial and temporal variation of surface temperature when derived from daily Landsat morning overpass images was significantly different to the modelled LST taken at 1:15 pm. These differences are higher as a result of the angle of the sun and associated factors such as shadows (Mathew *et al.*, 2018; Zhou *et al.*, 2013), which result in the LST in the high density of buildings being cooler in the morning images compared with other surface classes, including vegetation cover, while this picture was changed significantly when using LST images estimated at the local peak in temperature. It was also found that extreme temperatures can affect the trend of LST change across the years, which can be minimized by using the images in the form of the average of seasonal images of each year rather than images being used in a standalone manner. The results positively answered the research questions and supported the hypotheses stated at the beginning of the study, which would also provide an answer to the uncertainty that has sparked controversy among researchers, as represented in the effect of the time of day on the relationship between LST and urban land cover (Coops *et al.*, 2007; Nichol, 1998). Therefore, this research ascertained that the relationship between LST and urban land cover is significantly affected by time of day, and that studies during morning hours alone are not sufficient to identify this relationship as a result of the impact of the angle of the sun and associated factors such as shadows.

7.2. Research contributions

This thesis is considered an unprecedented piece of scientific research in the field of the study of land surface temperature (LST). It has developed methods for processing LST that are more reliable than in the current literature and presented associated new results. Different sources of LST data were used in this study including Landsat, SEVIRI, and ground-based measurements. The main chapters of the study have addressed issues regarding the available thermal remote sensing data which have long been controversial; Chapter 4 provides an alternative solution to addressing the lack of high-resolution thermal satellite data during the local solar zenith, which would allow an investigation to identify the relationship between LST and urban land cover during a local peak of temperature. This is considered more reliable than studying other times of day, such as the morning hours (the Landsat overpass time). Chapter 5 presented evidence regarding the effect of time of day on the spatial variation of LST as an important factor that has to be taken into account when studying the relationship between LST and land cover, which has long been a subject of controversy. It has also been ascertained that the ideal time for studying LST is when the temperature reaches a maximum in order to minimize the effect of factors related to the time of day such as shadow, hence achieving maximum certainty. Similar to Chapter 5, Chapter 6 demonstrated that time of day also can affect the study of temporal variation of LST, thus emphasizing the importance of conducting this study during the period when the temperature is at its diurnal peak, in addition to presenting an approach to minimizing the effects of extreme values of LST on the seasonal representation.

7.3. Conclusion

This thesis focusses on demonstrating and addressing important influencing factors in the study of spatial and temporal variation of LST in a semi-arid region, where the main research questions that were asked in the second chapter of this thesis can be answered as follows.

1- To what extent can the use of SEVIRI LST products (geostationary satellites) and the relevant pixel properties allow the accurate conversion of the LST retrieved by Landsat from that of morning time to that observed at zenith?

This study proposed a technique to estimate LST at Landsat resolutions during a local solar zenith period when the temperature is at its peak, where this method is based on the use of an increasing difference between morning and the peak temperature (ΔLST), which is taken as the difference between the mean value from Landsat at the satellite overpass time (9:40 am) when resampled to SEVIRI resolution, and SEVIRI at a time when the temperature is around its maximum (1:15 pm). This value then needs to be processed as a black body value (absorptivity LSA = 1, emissivity LSE = 1) and then redistributed to the Landsat LST image based on the appropriate pixel properties (absorptivity (LSA), emissivity (LSE) and transpiration effects, as estimated by ground measurements). The results showed that there are similar ratios for the role of the transpiration process in terms of reducing the increase of land surface temperature, ΔLST, for the vegetation on different days (Xiao *et al.*, 2007), where the actual increase in ΔLST of the vegetation is lower than the value which is supposed to be generated according to its absorptivity and emissivity (LSE, LSA) by around 50%. This gives an indication of the role of the transpiration process, which is also equivalent to around 44% of the value that which would otherwise be observed by a perfect black body (LSE = 1, LSA = 1) within the same area, at the same time, and under the same conditions. The output of this conversion process showed an accuracy with a standard error of 1.7°C, R = 0.82, when compared with simultaneously recorded ground-based measurements.

2- How is the relationship between LST and urban land cover influenced by the time of day?

LST studies have indicated that there is a strong correlation between the spatial variation of LST and changes in urban land cover. However, this relationship can also be affected by time of day as a result of the solar angle and the accompanying factors such as shade which can be more impactful during sunrise, thus this relationship needs to be studied at zenith rather than during the morning (Landsat overpass time) to minimise the effect of these factors, which has long been a controversial point that needs to be taken into account when conducting LST studies. This research used an LST Landsat image at the satellite overpass time (9:40 am) and a converted LST Landsat image during peak temperature (1:15 pm) to differentiate the spatial distribution of the LST at these two different times.

It was found that the relationship between LST and the urban land cover is variable depending on the time of day, where during the morning there was a weak positive correlation with the density of the vegetation cover, where the LST values are tend to increase with increasing proportion of vegetation cover, and indeed vice versa. The lowest LST values are centred over higher densities of buildings, especially the centre of the city, while the highest LST values were found in open areas, whether it is in natural forms such as dry soil or in unnatural forms such as concrete surfaces (e.g., airport runway). This relationship can explain the effect of the unequal distribution of the incident energy during the morning period when the sun is closer to the horizon or the ground and when there is more shadow and dispersion of solar radiation (Guillevic *et al.*, 2013). Therefore, there is an obvious correlation between solar angle and the line trend of the relationship between land cover and LST. In contrast, this relationship appeared different at peak temperature (1:15 pm) in comparison to the morning (9:40 am), which showed a strong negative correlation with the density of the vegetation cover, where the LST values decrease with increasing percentage of vegetation cover and vice versa for higher LST values. The lowest LST values were centred over higher densities of vegetation, while the highest were in open areas (e.g., the airport runway), which is an indication of a minimal effect of the angle of the sun and accompanying factors such as shadow and dispersion and weak sunlight on the spatial distribution of LST, which in turn can show a more accurate relationship between surface cover and LST.

3- To what extent does using a seasonal (July, August, and September) average temperature improvement rather than single data observations constitute a more representative dataset?

This research hypothesizes that when studying the temporal variation of LST over a number of years, the seasonal images used need to be in a form of an average rather than single data to minimise the possibility of the effects of extreme LST values, thus achieving a more representative image; where the temperature is a variable, it is often characterized by extreme values and exceptional conditions that might otherwise affect the representation of a season and that can then also affect the change of LST across a time series. This study used LST images derived by Landsat 5 and 8 for the summer seasons (July, August, and September) for the years 2005, 2009, 2013 and 2017 to investigate the difference between the temporal variation of LST over these years using a single image for each year and as an average of the above three months, which in turn can identify the effects of extreme values on the temporal variation of LST.

The results showed that there is a difference between using the single image and the average image for studying LST changes over the years. The LST, when using the single image method, showed greater differences and greater fluctuation between years compared with the average image method, which appeared more regular; also the single image method showed that 2013 recorded the highest LST values while in the second method the highest LST was in 2017. This difference was followed by a difference in the overall trend over the years (rate of change), so although both methods show an increase in LST over these years, the single image method showed a clearer increase, especially at maximum, and the mean levels of LST where they showed an increase several times compared to the increase shown by the average images method, these differences can obviously explain the effect of the extreme values of LST on the temporal variation analysis, which can be minimized by using averaged images.

4- To what extent does the time of day affect the temporal variation of LST?

Similar to the impact of the time of day on the spatial distribution of LST, this study assumed that the lack of high-resolution satellite data through which to estimate LST during a local zenith period can also cause issues when studying the temporal variation of LST over a number of years, considering that the spatial distribution of the LST using data estimated during the morning is likely to be inappropriate because of the effect of shade. Therefore, the study used LST images derived by Landsat 5 and 8 for the years 2005, 2009, 2013 and 2017 as an average for the three summer months (July, August and September) for each year during the satellite overpass time (9:40 am). It also converted images extracted from these merged images to estimate LST during the peak temperature (1:15 pm) to investigate the difference between the temporal variation of LST over these years during the morning time (9:40 am) and at the maximum in temperature (1:15 pm), which in turn can improve the ability to identify the effect of the time of day on the temporal variation of LST over the years.

The results showed that time of day significantly affects the temporal variation of LST over the years through the differences found between the changes in the images representing the morning (Landsat overpass time 9:40 am) and those representing the peak temperature (1:15 pm). The overall change for the three main measures of LST (minimum, maximum and mean) increase slightly and in a similar manner when using the morning images, while LST changed differently, showing both positive and negative changes, when using peak temperature images. The variation when using the images representing the peak time were greater and more obvious than for the morning images. In addition, these differences were followed by a difference in the spatial distribution of the areas covered by the normalized different LST index LST* categories, where the figures that represent the images in the morning time were not compatible with those representing the images during the peak in temperature

7.4. Limitations

This research is based on estimating data derived by remote sensing techniques with a relatively high thermal resolution of about 30 m, where the aim of the research is keen to achieve a high level of accuracy. However, this kind of data is not considered ground truth data, so that it cannot reflect the actual information on the ground surface, where the remote sensing data can be effected by noise, whether on the ground or in the atmosphere, which in turn affect the level of reliability of the data; for example, the spatial resolution of Landsat is not accurate enough to show detailed information about the land surface, especially in areas with mixed or heterogeneous land cover. The use of a manual thermal camera to collect readings for LST from the field may be more accurate than those provided by satellite, but this does not give the opportunity to collect a sufficient number of training points distributed over different classes within the study area during the same time. Although this study has been able to develop an expression to create LST images for the study area during a local peak temperature by converting Landsat data, it lacks accurate data and methods for conducting accuracy encasement processes for the images, whether with regard to the accuracy of the images used in the LST equations or the final LST images resulting from these equations.

7.5. Future work.

This research is a pioneering attempt to address important issues facing the study of LST; thus, it opens new horizons for future studies in this field. In general, it is recommended to consider the aforementioned limitations, which need to be addressed and improved. In addition, the study suggests verifying the applicability of the method suggested by this study for different areas with different properties, and investigating the impact of changes to an area's conditions to allow for the comparison between two or more different study areas. It is also recommended to use this method to conduct researches in cities have already been studied to examine the similarities and differences between the results have already been found, and those will be found by the new study within the same date and time. Moreover, this study recommends to improve the accuracy assessment method by allowing additional coverage to maximize the training points within the study area and this assessment process is not to be limited only in the final results, but to include the images used for processing the final image.

References

Aminou, D.M.A., 2002. MSG's SEVIRI instrument. *ESA Bulletin (0376-4265)*, (111), pp.15-17.

Arrau, C.P., and Pena, M.A., 2010. The Urban Heat Island (UHI) Effect. Available online at: http://www.urbanheatislands.com (accessed 20 October 2010).

Asgarian, A., Amiri, B. J. and Sakieh, Y. (2014) 'Assessing the effect of green cover spatial patterns on urban land surface temperature using landscape metrics approach', *Urban Ecosystems*, 18(1), pp. 209-222. doi: 10.1007/s11252-014-0387-7.

Avdan, U. and Jovanovska, G. (2016) 'Algorithm for Automated Mapping of Land Surface Temperature Using LANDSAT 8 Satellite Data', *Journal of Sensors*, 2016, pp. 1-8. doi: 10.1155/2016/1480307.

Biro, K., Pradhan, B., Buchroithner, M. and Makeschin, F. (2013) 'Land Use/Land Cover Change Analysis and Its Impact on Soil Properties in the Northern Part of Gadarif Region, Sudan', *Land Degradation & Development*, 24(1), pp. 90-102. doi: 10.1002/ldr.1116.

Bokaie, M., Zarkesh, M. K., Arasteh, P. D. and Hosseini, A. (2016) 'Assessment of Urban Heat Island based on the relationship between land surface temperature and Land Use/ Land Cover in Tehran', *Sustainable Cities and Society*, 23, pp. 94-104. doi: 10.1016/j.scs.2016.03.009.

Buyantuyev, A. (2010) 'Urban heat islands and landscape heterogeneity: linking spatiotemporal variations in surface temperatures to land-cover and socioeconomic patterns', doi: 10.1007/s10980-009-9402-4.

Cai, Y., Zhang, H., Zheng, P. and Pan, W. (2016) 'Quantifying the Impact of Land use/Land Cover Changes on the Urban Heat Island: A Case Study of the Natural Wetlands Distribution Area of Fuzhou City, China', *Wetlands*, 36(2), pp. 285-298. doi: 10.1007/s13157-016-0738-7.

Chakraborty, S. D., Kant, Y. and Mitra, D. (2015) 'Assessment of land surface temperature and heat fluxes over Delhi using remote sensing data', *J Environ Manage*, 148, pp. 143-152. doi: 10.1016/j.jenvman.2013.11.034.

Chaudhuri, G. and Mishra, N. B. (2016) 'Spatio-temporal dynamics of land cover and land surface temperature in Ganges-Brahmaputra delta: A comparative analysis between India and Bangladesh', *Applied Geography*, 68, pp. 68-83. doi: 10.1016/j.apgeog.2016.01.002.

Chuvieco, E. and Huete, A. (2010) *Fundamentals of satellite remote sensing.* CRC Press Inc. Boca Raton, FL 33487, USA.

Connors, J. P., Galletti, C. S. and Chow, W. T. L. (2012) 'Landscape configuration and urban heat island effects: assessing the relationship between landscape characteristics and land surface temperature in Phoenix, Arizona', *Landscape Ecology*, 28(2), pp. 271-283. doi: 10.1007/s10980-012-9833-1.

Coops, N. C., Duro, D. C., Wulder, M. A. and Han, T. (2007) 'Estimating afternoon MODIS land surface temperatures (LST) based on morning MODIS overpass, location and elevation information', *International Journal of Remote Sensing*, 28(10), pp. 2391-2396. doi: 10.1080/01431160701294653.

Dash, P., Gottsche, F., Olesen, F. & Fischer, H., 2002. Land Surface temperature and emissivity estimation from passive sensor data: theory and practice- current trends. *International Journal of Remote Sensing,* pp. 2563-2594.

Deng, C. and Wu, C. (2013) 'Examining the impacts of urban biophysical compositions on surface urban heat island: A spectral unmixing and thermal mixing approach', *Remote Sensing of Environment*, 131, pp. 262-274. doi: 10.1016/j.rse.2012.12.020.

Dewan, A. M. and Yamaguchi, Y. (2009) 'Land use and land cover change in Greater Dhaka, Bangladesh: Using remote sensing to promote sustainable urbanization', *Applied Geography*, 29(3), pp. 390-401. doi: 10.1016/j.apgeog.2008.12.005.

DiStasio Jr., R.J. & Resmini, R.G. (2010) 'Atmospheric compensation of thermal infrared hyperspectral imagery with the emissive empirical line method and the in-scene atmospheric compensation algorithms: a comparison', *SPIE - The International Society for Optical Engineering.* Orlando, FL, United States, 5-8 April.

EPA, 2009a. Reducing Urban Heat Islands: Compendium of Strategies – Urban Heat Island Basics; in Anonymous.

ESA, 2007. The AATSR Product User Guide. 2.2 ed. s.l.:ESA.

Feyisa, G. L., Meilby, H., Darrel Jenerette, G. and Pauliet, S. (2016) 'Locally optimized separability enhancement indices for urban land cover mapping: Exploring thermal environmental consequences of rapid urbanization in Addis Ababa, Ethiopia', *Remote Sensing of Environment*, 175, pp. 14-31. doi: 10.1016/j.rse.2015.12.026.

Fu, P. and Weng, Q. (2016) 'A time series analysis of urbanization induced land use and land cover change and its impact on land surface temperature with Landsat imagery', *Remote Sensing of Environment*, 175, pp. 205-214. doi: 10.1016/j.rse.2015.12.040.

Ghent, D., Kaduk, J., Remedios, J. & Balzter, H., 2011. Data Assimilation into Land Surface Model: The Implications for Climate Feedbacks. *International Journal of Remote Sensing,* 32(3), pp. 617-632.

Ghent, D., Kaduk, J., Remedios, J., Ardö, J. and Balzter, H. (2010) 'Assimilation of land surface temperature into the land surface model JULES with an ensemble Kalman filter', *Journal of Geophysical Research*, 115(D19), doi: 10.1029/2010jd014392.

Gibson, P., Gibson, P.J., Power, C. and Power, C.H., 2000. *Introductory remote sensing: Digital image processing and applications*. Psychology Press.

Gottsche, F.-M., Olesen, F.-S., Trigo, I., Bork-Unkelbach, A. and Martin, M. (2016) 'Long Term Validation of Land Surface Temperature Retrieved from MSG/SEVIRI with Continuous in-Situ Measurements in Africa', *Remote Sensing*, 8(5), p. 410. doi: 10.3390/rs8050410.

Guillevic, P.C., Bork-Unkelbach, A., Göttsche, F.M., Hulley, G., Gastellu-Etchegorry, J.P., Olesen, F.S. and Privette, J.L., 2013. Directional viewing effects on satellite land surface temperature products over sparse vegetation canopies-a multisensor analysis. *IEEE Geoscience and Remote Sensing Letters*, *10*(6), pp.1464-1468.

Guo, G., Wu, Z., Xiao, R., Chen, Y., Liu, X. and Zhang, X. (2015) 'Impacts of urban biophysical composition on land surface temperature in urban heat island clusters', *Landscape and Urban Planning*, 135, pp. 1-10. doi: 10.1016/j.landurbplan.2014.11.007.

Hanks, B.S., 1965. Reflection of radiant energy from soils. *Soil Sea*, *100*, pp.130-138.

Hansen, P.C. (1998) Rank-deficient and discrete ill-posed problems: numerical aspects of linear inversion. SIAM, Philadelphia, PA 19104-2688 USA.

Imhoff, M. L., Zhang, P., Wolfe, R. E. and Bounoua, L. (2010) 'Remote sensing of the urban heat island effect across biomes in the continental USA', *Remote Sensing of Environment*, 114(3), pp. 504-513. doi: 10.1016/j.rse.2009.10.008.

Isaya Ndossi, M. and Avdan, U. (2016) 'Application of Open Source Coding Technologies in the Production of Land Surface Temperature (LST) Maps from Landsat: A PyQGIS Plugin', *Remote Sensing*, 8(5), p. 413. doi: 10.3390/rs8050413.

Jiang, G. M. and Li, Z. L. (2008) 'Split-window algorithm for land surface temperature estimation from MSG1-SEVIRI data', *International Journal of Remote Sensing*, 29(20), pp. 6067-6074. doi: 10.1080/01431160802235860.

Jiang, J. and Tian, G. (2010) 'Analysis of the impact of Land use/Land cover change on Land Surface Temperature with Remote Sensing', *Procedia Environmental Sciences*, 2, pp. 571-575. doi: 10.1016/j.proenv.2010.10.062.

Jiang, Y., Fu, P. and Weng, Q. (2015) 'Assessing the Impacts of Urbanization-Associated Land Use/Cover Change on Land Surface Temperature and Surface Moisture: A Case Study in the Midwestern United States', *Remote Sensing*, 7(4), pp. 4880-4898. doi: 10.3390/rs70404880.

Jones, P. D., New, M., Parker, D. E., Martin, S. and Rigor, I. G. (1999) 'Surface air temperature and its changes over the past 150 years', *Reviews of Geophysics*, 37(2), pp. 173-199. doi: 10.1029/1999rg900002.

Kalkstein, L.S., 1991. A New Approach to Evaluate the Impact of Climate on Human Mortality. Environmental Health Perspectives, 96, 145-150.

Kalnay, E. and Cai, M. (2003) 'Impact of urbanization and land-use change on climate', *Nature*, 423(6939), pp. 528-531.

Karnieli, A., Agam, N., Pinker, R. T., Anderson, M., Imhoff, M. L., Gutman, G. G., Panov, N. and Goldberg, A. (2010) 'Use of NDVI and Land Surface Temperature for Drought Assessment: Merits and Limitations', *Journal of Climate*, 23(3), pp. 618-633. doi:

10.1175/2009jcli2900.1. 'Land-Surface Temperature and Thermal Infrared Emissivity' (2012), pp. 235-271. doi:10.1016/b978-0-12-385954-9.00008-

Krenzinger, A. and de Andrade, A. C. (2007) 'Accurate outdoor glass thermographic thermometry applied to solar energy devices', *Solar Energy,* 81(8),pp. 1025-1034. doi: 10.1016/j.solener.2006.11.014.

Landsat, NASA. 7, Science Data Users Handbook. 2011. http://landsathandbook.gsfc.nasa.gov

Zhu, Z., Fu, Y., Woodcock, C. E., Olofsson, P., Vogelmann, J. E., Holden, C., Wang, M., Dai, S. and Yu, Y. (2016) 'Including land cover change in analysis of greenness trends using all available Landsat 5, 7, and 8 images: A case study from Guangzhou, China (2000–2014)', *Remote Sensing of Environment*, doi: 10.1016/j.rse.2016.03.036

Li, J., Song, C., Cao, L., Zhu, F., Meng, X. and Wu, J. (2011) 'Impacts of landscape structure on surface urban heat islands: A case study of Shanghai, China', *Remote Sensing of Environment*, 115(12), pp. 3249-3263. doi: 10.1016/j.rse.2011.07.008.

Li, X., Li, W., Middel, A., Harlan, S. L., Brazel, A. J. and Turner, B. L. (2016) 'Remote sensing of the surface urban heat island and land architecture in Phoenix, Arizona: Combined effects of land composition and configuration and cadastral–demographic–economic factors', *Remote Sensing of Environment*, 174, pp. 233-243. doi: 10.1016/j.rse.2015.12.022.

Li, Z. and Becker, F. (1993) 'Feasibility of land surface temperature and emissivity determination from AVHRR data', *Remote Sensing of Environment,* 43(1), pp. 67-85.

Li, Z.-L., Tang, B.-H., Wu, H., Ren, H., Yan, G., Wan, Z., Trigo, I. F. and Sobrino, J. A. (2013) 'Satellite-derived land surface temperature: Current status and perspectives', *Remote Sensing of Environment*, 131, pp. 14-37. doi: 10.1016/j.rse.2012.12.008.

Liang, S., Li, X. and Wang, J. (2012) *Advanced remote sensing.* 1st edn. Amsterdam; Boston: Academic Press.

Liang, X., Wood, E. & Lettenmaier, D., 1999. Modelling ground heat flux in the land surface parameterization schemes. *Journal of Geophysical Research,* Volume 104, pp. 9581-9600.

Lin, C.-Y., Chen, F., Huang, J. C., Chen, W. C., Liou, Y. A., Chen, W. N. and Liu, S.-C. (2008) 'Urban heat island effect and its impact on boundary layer development and land–sea circulation over northern Taiwan', *Atmospheric Environment*, 42(22), pp. 5635-5649. doi: 10.1016/j.atmosenv.2008.03.015.

Lo, C. P., Quattrochi, D. A. and Luvall, J. C. (2010) 'Application of high-resolution thermal infrared remote sensing and GIS to assess the urban heat island effect', *International Journal of Remote Sensing*, 18(2), pp. 287-304. doi: 10.1080/014311697219079.

López, E., Bocco, G., Mendoza, M. and Duhau, E. (2001) 'Predicting land-cover and land-use change in the urban fringe: a case in Morelia city, Mexico', *Landscape and Urban Planning*, 55(4), pp. 271-285.

Maimaitiyiming, M., Ghulam, A., Tiyip, T., Pla, F., Latorre-Carmona, P., Halik, Ü. Sawut, M. and Caetano, M. (2014) 'Effects of green space spatial pattern on land surface temperature: Implications for sustainable urban planning and climate change adaptation', *ISPRS Journal of Photogrammetry and Remote Sensing*, 89, pp. 59-66. doi: 10.1016/j.isprsjprs.2013.12.010.

Martin, P., Baudouin, Y. and Gachon, P. (2015) 'An alternative method to characterize the surface urban heat island', *Int J Biometeorol*, 59(7), pp. 849-861. doi: 10.1007/s00484-014-09029.

Mathew, A., Khandelwal, S., Kaul, N. and Chauhan, S. (2018) 'Analyzing the diurnal variations of land surface temperatures for surface urban heat island studies: Is time of observation of remote sensing data important?' *Sustainable Cities and Society*, 40, pp. 194-213. doi: 10.1016/j.scs.2018.03.032.

Matsumoto, T., Koizumi, T., Kawakami, Y., Okamoto, K. and Tomita, M. (2013) 'Perfect blackbody radiation from a graphene nanostructure with application to high-temperature spectral emissivity measurements', *Opt Express*, 21(25), pp. 30964-30974. doi: 10.1364/OE.21.030964.

McMillin, L.M. (1975) 'Estimation of sea surface temperatures from two infrared window measurements with different absorption', *Journal of Geophysical Research*, 80(36), pp. 5113-5117.

Merchant, C., Le Borgne, P., Roquet, H. & Marsouin, A., 2009. Sea Surface Temperature from a Geostationary Satellite by Optimal Estimation. *Remote Sensing of Environment,* Volume 113, pp. 445-457.

Morabito, M., Crisci, A., Messeri, A., Orlandini, S., Raschi, A., Maracchi, G. and Munafo, M. (2016) 'The impact of built-up surfaces on land surface temperatures in Italian urban areas', *Sci Total Environ*, 551-552, pp. 317-326. doi: 10.1016/j.scitotenv.2016.02.029.

Nichol, J. E. (1998) 'Visualisation of urban surface temperatures derived from satellite images', *International Journal of Remote Sensing*, 19(9), pp. 1639-1649. doi: 10.1080/014311698215153.

Noyes, E.J., 2005. *An investigation into the accuracy of surface temperature retrievals from the AATSR* (Doctoral dissertation, Physics and Astronomy).

Peng, S., Piao, S., Ciais, P., Friedlingstein, P., Ottle, C., Bréon, F.M., Nan, H., Zhou, L. and Myneni, R.B., 2011. Surface urban heat island across 419 global big cities. *Environmental science & technology*, *46*(2), pp.696-703.

Peres, L. F. and DaCamara, C. C. (2004) 'Land surface temperature and emissivity estimation based on the two-temperature method: sensitivity analysis using simulated MSG/SEVIRI data', *Remote Sensing of Environment*, 91(3-4), pp. 377-389. doi: 10.1016/j.rse.2004.03.011.

Petropoulos, G., Carlson, T. N., Wooster, M. J. and Islam, S. (2009) 'A review of Ts/VI remote sensing based methods for the retrieval of land surface energy fluxes and soil surface moisture', *Progress in Physical Geography*, 33(2), pp. 224-250. doi: 10.1177/0309133309338997.

Qin, Z., Karnieli, A. and Berliner, P. (2001) 'A mono-window algorithm for retrieving land surface temperature from Landsat TM data and its application to the Israel-Egypt border region', *International Journal of Remote Sensing*, 22(18), pp. 3719-3746.

Rasul, A., Balzter, H. and Smith, C. (2015) 'Spatial variation of the daytime Surface Urban Cool Island during the dry season in Erbil, Iraqi Kurdistan, from Landsat 8', *Urban Climate*, 14,pp. 176-186. doi: 10.1016/j.uclim.2015.09.001.

R Core Team (2017). R: A language and environment for statistical computing. R Foundation for Statistical Computing, Vienna, Austria. URL https://www.R-project.org/.

Reichle, R. H., Kumar, S. V., Mahanama, S. P. P., Koster, R. D. and Liu, Q. (2010) 'Assimilation of Satellite-Derived Skin Temperature Observations into Land Surface Models', *Journal of Hydrometeorology*, 11(5), pp. 1103-1122. doi: 10.1175/2010jhm1262.1.

Rinner, C. and Hussain, M. (2011) 'Toronto’s Urban Heat Island-Exploring the Relationship between Land Use and Surface Temperature', *Remote Sensing*, 3(6), pp. 1251-1265. doi: 10.3390/rs3061251.

Rotem-Mindali, O., Michael, Y., Helman, D. and Lensky, I. M. (2015) 'The role of local land-use on the urban heat island effect of Tel Aviv as assessed from satellite remote sensing', *Applied Geography*, 56, pp. 145-153. doi: 10.1016/j.apgeog.2014.11.023.

Roth, M., Oke, T. and Emery, W. (1989) 'Satellite-derived urban heat islands from three coastal cities and the utilization of such data in urban climatology', *International Journal of Remote Sensing*, 10(11), pp. 1699-1720.

Rozenstein, O., Qin, Z., Derimian, Y. and Karnieli, A. (2014) 'Derivation of land surface temperature for Landsat-8 TIRS using a split window algorithm', *Sensors (Basel)*, 14(4), pp. 5768-5780. doi: 10.3390/s140405768.

Santana, L.M., 2007. Landsat ETM+ image applications to extract information for environmental planning in a Colombian city. International Journal of Remote Sensing, 28, 4225-4242.

Seto, K. C., Guneralp, B. and Hutyra, L. R. (2012) 'Global forecasts of urban expansion to 2030 and direct impacts on biodiversity and carbon pools', *Proc Natl Acad Sci U S A*, 109(40), pp. 16083-16088. doi: 10.1073/pnas.1211658109.

Shen, G., Ibrahim, A. N., Wang, Z., Ma, C. and Gong, J. (2015) 'Spatial–temporal land-use/land-cover dynamics and their impacts on surface temperature in Chongming Island of Shanghai, China', *International Journal of Remote Sensing*, 36(15), pp. 4037-4053. doi: 10.1080/01431161.2015.1043404.

Shen, H., Huang, L., Zhang, L., Wu, P. and Zeng, C. (2016) 'Long-term and fine-scale satellite monitoring of the urban heat island effect by the fusion of multi-temporal and multisensor remote sensed data: A 26-year case study of the city of Wuhan in China', *Remote Sensing of Environment*, 172, pp. 109-125. doi: 10.1016/j.rse.2015.11.005.

Sobrino, J. A. and Raissouni, N. (2000) 'Toward remote sensing methods for land cover dynamic monitoring: Application to Morocco', *International Journal of Remote Sensing*, 21(2), pp. 353-366. doi: 10.1080/014311600210876.

Song, C., Woodcock, C.E. and Li, X. (2002) 'the spectral/temporal manifestation of forest succession in optical imagery: The potential of multitemporal imagery', *Remote Sensing of Environment,* 82(2), pp. 285-302.

Srivanit, M. and Hokao, K. (2012) 'Thermal Infrared Remote Sensing for Urban Climate and Environmental Studies: An Application for the City of Bangkok, Thailand', *JARS Journal of Architectural/Planning Research and Studies,* 9(1), pp. 83-100.

Tempfli, K., Huurneman, G., Bakker, W., Janssen, L., Bakker, W., Feringa, W., Gieske, A., Grabmaier, K., Hecker, C. and Horn, J. (2009) *Principles of remote sensing: an introductory textbook.* 4th Edition edn. Enschede, Netherlands: ITC.

Trenberth, K.E., Fasullo, J.T. and Kiehl, J., 2009. Earth's global energy budget. Bulletin of the American Meteorological Society, 90(3), pp.311-324. Weng, Q. (2009) 'Thermal infrared remote sensing for urban climate and environmental studies: Methods, applications, and trends', *ISPRS Journal of Photogrammetry and Remote Sensing*, 64(4), pp. 335-344. doi: 10.1016/j.isprsjprs.2009.03.007.

Tupin, F., Inglada, J. and Nicolas, J.M. eds., 2014. *Remote Sensing Imagery*. ISTE.

Veal, K.L., Corlett, G.K., Ghent, D., Llewellyn-Jones, D.T. and Remedios, J.J., 2013. A time series of mean global skin SST anomaly using data from ATSR-2 and AATSR. *Remote sensing of environment*, *135*, pp.64-76.

Von Schuckmann, K., Palmer, M. D., Trenberth, K. E., Cazenave, A., Chambers, D., Champollion, N., Hansen, J., Josey, S. A., Loeb, N., Mathieu, P. P., Meyssignac, B. and Wild, M. (2016) 'An imperative to monitor Earth's energy imbalance', *Nature Climate Change*, 6(2), pp. 138-144. doi: 10.1038/nclimate2876.

Voogt, J. A. and Oke, T. R. (2003) 'Thermal remote sensing of urban climates', *Remote Sensing of Environment*, 86(3), pp. 370-384. doi: 10.1016/s0034-4257(03)00079-8.

Voogt, J.A., 2004. Urban heat islands: hotter cities. *America Institute of Biological Sciences*.

Wan, Z. and Li, Z. (1997) 'A physics-based algorithm for retrieving land-surface emissivity and temperature from EOS/MODIS data', *IEEE Transactions on Geoscience and Remote Sensing*, 35(4), pp. 980-996.

Weng, Q. (2009) 'Thermal infrared remote sensing for urban climate and environmental studies: Methods, applications, and trends', *ISPRS Journal of Photogrammetry and Remote Sensing*, 64(4), pp. 335-344. doi: 10.1016/j.isprsjprs.2009.03.007.

Weng, Q. and Fu, P. (2014) 'Modeling annual parameters of clear-sky land surface temperature variations and evaluating the impact of cloud cover using time series of Landsat TIR data', *Remote Sensing of Environment*, 140, pp. 267-278. doi: 10.1016/j.rse.2013.09.002.

Weng, Q. and Lu, D. (2008) 'A sub-pixel analysis of urbanization effect on land surface temperature and its interplay with impervious surface and vegetation coverage in Indianapolis, United States', *International journal of applied earth observation and geoinformation*, 10(1), pp. 68-83. doi: 10.1016/j.jag.2007.05.002.

Weng, Q., Fu, P. and Gao, F. (2014) 'Generating daily land surface temperature at Landsat resolution by fusing Landsat and MODIS data', *Remote Sensing of Environment*, 145, pp. 55-67. doi: 10.1016/j.rse.2014.02.003.

Weng, Q., Lu, D. and Schubring, J. (2004) 'Estimation of land surface temperature–vegetation abundance relationship for urban heat island studies', *Remote Sensing of Environment*, 89(4),pp. 467-483. doi: 10.1016/j.rse.2003.11.005.

Westermann, S., Langer, M. & Boike, J., 2011. Spatial and temporal variations of summer surface temperatures of high-arctic tundra on Svalbard — Implications for MODIS LST based permafrost monitoring. *Remote Sensing of Environment*, 115(3), pp. 908-922.

Wu, H., Ye, L.-P., Shi, W.-Z. and Clarke, K. C. (2014) 'Assessing the effects of land use spatial structure on urban heat islands using HJ-1B remote sensing imagery in Wuhan, China', *International journal of applied earth observation and geoinformation*, 32, pp. 67-78. doi: 10.1016/j.jag.2014.03.019.

WWF, 2010. Natural Resources. (World Wildlife Fund). Available online at: http://wwf.panda.org/about_our_earth/teacher_resources/webfieldtrips/natural_resources/ (accessed 4 December 2010).

Xiao, R.-b., Ouyang, Z.-y., Zheng, H., Li, W.-f., Schienke, E. W. and Wang, X.-k. (2007) 'Spatial pattern of impervious surfaces and their impacts on land surface temperature in Beijing, China', *Journal of Environmental Sciences*, 19(2), pp. 250-256. doi: 10.1016/s1001-0742(07)60041-2.

Xiaoma Li, W. Z., Zhiyun Ouyang. (2013) 'Relationship between land surface temperature and spatial pattern of green space: What are the effects of spatial resolution?' p.doi: 10.1016/j.landurbplan.2013.02.005.

Xiong, Y., Huang, S., Chen, F., Ye, H., Wang, C. and Zhu, C. (2012) 'the Impacts of Rapid Urbanization on the Thermal Environment: A Remote Sensing Study of Guangzhou, South China', *Remote Sensing*, 4(12), pp. 2033-2056. doi: 10.3390/rs4072033.

Zhang, H., Qi, Z.-f., Ye, X.-y., Cai, Y.-b., Ma, W.-c. And Chen, M.-n. (2013) 'Analysis of land use/land cover change, population shift, and their effects on spatiotemporal patterns of urban heat islands in metropolitan Shanghai, China', *Applied Geography*, 44, pp. 121-133. doi: 10.1016/j.apgeog.2013.07.021.

Zhou, W., Huang, G. and Cadenasso, M. L. (2011) 'Does spatial configuration matter? Understanding the effects of land cover pattern on land surface temperature in urban landscapes', *Landscape and Urban Planning*, 102(1), pp. 54-63. doi: 10.1016/j.landurbplan.2011.03.009.

Zhou, W., Qian, Y., Li, X., Li, W. and Han, L. (2013) 'Relationships between land cover and the surface urban heat island: seasonal variability and effects of spatial and thematic resolution of land cover data on predicting land surface temperatures', *Landscape Ecology*, 29(1),pp. 153-167. doi: 10.1007/s10980-013-9950-5.